Universität für Bodenkultur Wien
University of Natural Resources
and Life Sciences, Vienna

Master Thesis

Evaluation of soil-specific infiltration capacity in dependence on soil moisture and precipitation intensity

submitted by

Katharina SANTNER, BSc

in partial fulfilment of the requirements for the academic degree

Diplom-Ingenieurin

Vienna, July 2021

Supervisor:

Univ.Prof.in Dr.in Christine Stumpp
Institute for Soil Physics and Rural Water Management (SoPhy)

Abstract

Heavy rainfall events, in connection with infiltration exceedance, can lead to pluvial floods. In Austria, the trend of the occurrence of pluvial floods is increasing, due to excessive land sealing (anthropogenic forces) and a rising number of extreme weather events caused by climate change. In the National Flood Risk Management Plan, pluvial floods are addressed to the extent that possible flow paths are identified through a topographical analysis. Infiltration properties of different soils are not considered. Characteristics of pluvial floods should be further investigated by means of modern 1D as well as 2D simulation programmes and also consider the infiltration capacity of the soil, which plays a crucial role in flood generation. Therefore, the objective of this master thesis was to evaluate soil-specific infiltration capacity in dependence on initial soil moisture, precipitation intensity and slope. The sensitivity of overland flow generation regarding different input variables was analysed. This analysis is based on soil and hydraulic characteristics of 14 measuring stations in Austria covering different climatic conditions and soil types. The water retention and saturated conductivity according to van Genuchten and Mualem, have already been inversely calibrated using the simulation program HYDRUS-1D. Furthermore, different climate scenarios for the years 2050-2100 were modelled. The sensitivity analysis was carried out for two measurement profiles that already showed strong pluvial floods over the recorded period. The surface runoff coefficient (φ) was used for the direct comparison of the evaluation output. It was found that (i) φ increases significantly with increasing initial water content if the stratification of different materials shows an increasing or constant hydraulic conductivity with depth. If the hydraulic conductivity decreases with depth, φ decreases again after a certain degree of saturation in the upper layers. (ii) With increasing precipitation intensity, φ increases. At high precipitation intensities overland flow generation is independent on soil water content and stratification. (iii) The influence of slope could not be satisfactorily represented using HYDRUS-1D. (iv) The trend for overland flow generation at both tested stations (Salzburg and Styria) increased. Therefore, the inclusion of climate change forecasts in pluvial flood simulations and mitigation measurement plans is suggested. Overall, the simulations indicate that the initial water content plays a crucial role in overland flow simulations, but not with higher precipitation intensities. Initial conditions therefore often have a decisive influence on surface runoff generation and should be included in an area-wide representation. Furthermore, attention should be paid to the temporal and spatial resolution of the data, as the temporal resolution can produce strong deviations, especially in the case of rainfall intensities.

Zusammenfassung

Starkregenereignisse, in Verbindung mit Infiltrationsüberschreitungen, können zu pluvialen Hochwässern führen. In Österreich nimmt die Tendenz des Auftretens von pluvialen Hochwässern zu, sowohl in Verbindung mit wachsender Flächenversiegelung (anthropogener Einfluss), also auch mit steigenden Zahlen an Extremwetterereignissen, verschuldet durch den Klimawandel. Im nationalen Hochwasserrisikomanagementplan werden pluviale Hochwässer durch eine topografische Analyse möglicher Fließwege gekennzeichnet. Infiltrationseigenschaften verschiedener Böden werden hier nicht berücksichtigt. Durch moderne 1D- sowie 2D-Simulationsprogramme sollen Charakteristiken von pluvialen Hochwässern weiterführend untersucht werden. Die Infiltrationskapazität der Böden spielt hier eine ausschlaggebende Rolle. Ziel dieser Masterarbeit war es daher, die bodenspezifische Infiltrationskapazität in Abhängigkeit von Bodenfeuchte, Niederschlagsintensität und Hangneigung zu untersuchen. Für diesen Zweck wurde eine Sensitivitätsanalyse durchgeführt. Diese Analyse basiert auf den bodenhydraulischen Eigenschaften von 14 Messstationen in Österreich, die unterschiedliche klimatische Bedingungen und Bodentypen abdecken. Die Wasserretention und gesättigte Leitfähigkeit nach van Genuchten und Mualem, wurden bereits mittels dem Simulationsprogram HYDRUS-1D inverse kalibriert Des Weiteren wurden verschiedenen Klimaszenarien für die Jahre 2050-2100 modelliert. Die Sensitivitätsanalyse wurde an zwei Messprofilen durchgeführt, die über die Aufzeichnungsperiode bereits starke pluviale Hochwässer aufwiesen. Der Oberflächenabflusskoeffizient (φ) wurde für den direkten Vergleich der Auswertungsergebnisse herangezogen. Es konnte herausgefunden werden, dass (i) φ mit zunehmendem Anfangswassergehalt signifikant ansteigt, wenn die Schichtung der verschiedenen Materialien eine mit der Tiefe zunehmende oder konstante hydraulische Leitfähigkeit aufweist. Nimmt die hydraulische Leitfähigkeit mit der Tiefe ab, nimmt φ ab einem gewissen Sättigungsgrad in den oberen Schichten ebenfalls ab. (ii) Mit zunehmender Niederschlagsintensität nimmt φ zu. Bei hohen Niederschlagsintensitäten ist die Entstehung von Oberflächenabfluss unabhängig vom Bodenwassergehalt und der Schichtung. (iii) Der Einfluss der Hangneigung konnte mittels HYDRUS-1D nicht zufriedenstellend dargestellt werden. (iv) Der Trend für Oberflächenabflussgenerierung an beiden Stationen (Salzburg und Steiermark) ist steigend. Daher wird der Einbezug von Klimawandelprognosen in pluviale Hochwassersimulationen empfohlen. Insgesamt zeigen die Simulationen, dass der Anfangswassergehalt eine entscheidende Rolle spielt, jedoch nicht bei höheren Niederschlagsintensitäten. Anfangsbedingungen haben demnach einen oftmals maßgebenden Einfluss auf die Oberflächenabflussgenerierung und sollten bei einer flächendeckenden Darstellung miteinbezogen werden. Des Weiteren ist auf die zeitliche und räumliche Auflösung der Daten zu achten, da vor allem bei Regenintensitäten die zeitliche Auflösung starke Abweichungen hervorbringen kann.

Ich versichere hiermit, dass ich die Arbeit selbstständig und nur mit den angegebenen Quellen und Hilfsmitteln angefertigt habe und, dass ich alle Stellen der Arbeit, die aus anderen Werken dem Wortlaut oder dem Sinne nach entnommen sind, kenntlich gemacht habe.

_____

Ort, Datum und Unterschrift

Contents

List of Figures

List of Tables

1. Introduction

Pluvial floods are a possible consequence of extreme weather events with high precipitation intensity and short duration combined with an exceedance of infiltration capacity (Glade et al., 2020). Unlike fluvial floods, which are a temporary but widespread overflowing of river banks resulting from torrent, precipitation or snowmelt, pluvial floods are not directly related to water bodies and only occur locally due to precipitation (Bundesministerium für Nachhaltigkeit und Tourismus, 2019, Paprotny *et al.*, 2021, Chen *et al.*, 2010). Therefore, fluvial flood protection measures do not provide sufficient mitigation. While the severity of fluvial floods is addressed in many studies over the last centuries, pluvial floods have only moved into focus in the last decade (Glade et al., 2020). However, in Austria the damage caused by pluvial floods equates with that of fluvial flooding (Glade et al., 2020). The severity of pluvial floods lies in the damage which overland flow can cause to properties, infrastructure, agriculture and especially to persons. Because of their dependence on heavy precipitation events, pluvial floods have a limited warning and reaction time. As meteorological processes undergo a continuous change due to climate conditions, heavy precipitation events have also moved into focus concerning climate change studies. Seasonal changes, as well as changes in intensity and duration are considered. The trend implicates extended thunderstorm seasons (ÖWAV-Forum Klimawandel, 2020) and precipitation events with higher rain intensities and shorter duration (Becker, 2019). Furthermore, anthropogenic causes, such as soil sealing and soil compaction due to intensive agriculture and land use, can aggravate overland flow events. In Austria, the risks of pluvial and fluvial floods are described and evaluated in the National Flood Risk Management Plan. To establish these risk plans, which describe the basin and flow paths of potential pluvial floods, only topographical data is used (Chimani *et al.*, 2016). Other parameters, such as soil hydraulic properties, are not considered. These properties, however, have a huge impact on the flow accumulation of pluvial floods as the overland flow does not only depend on topographical properties of the basin, but also on the infiltration capacity of the soil (Rosenzweig *et al.*, 2018). Therefore, beside precipitation properties, soil hydraulic properties and their influence on overland flow generation should be considered.

The amount of infiltration into the soil depends on interdependent soil hydraulic properties of the vadose zone environment, defined as the unsaturated layer between the soil surface and the groundwater body (Holden and Fierer, 2005). The infiltration capacity describes the water flux, which can be absorbed from the soil. To understand the water movement trough the vadose zone, the storage ability and hydraulic conductivity are fundamental parameters to incorporate (Tuller and Or, 2004). The former can be described with the water retention curve (WRC), the latter with the hydraulic conductivity curve (HCC). Within these curves, the correlation of matric potential, water content and hydraulic conductivity can be expressed (van Genuchten, 1980).

Meteorological conditions, referring to precipitation intensity and duration, soil hydraulic properties, with regard to antecedent soil moisture, and topographical properties, such as slope, are decisive parameters for the generation of pluvial floods. Combining those parameters, soil-hydrological simulations imply interdependent model functions to generate sufficient descriptions about their interconnections and effects on overland flow generation. The degree of complexity rises with increasing number of dimensions and decreasing scale, whereas the acquisition or availability of data are the limiting factors.

In Austria, there are different approaches to simulate overland flow events, whether in 1D or combined with 2D. The simple code of practice (Markart et al., 2011) is based on more than 700 rain simulation experiments, focusing on alpine catchments, whereas the infiltration capacity is expressed in a total runoff coefficient. To avoid the influence of initial conditions within the soil profile, e.g., water content, hydrophobic effects or retention due to surface roughness differences, a mean value of the coefficient is used. Surface runoff coefficient maps for different site characteristics (e.g., vegetation, soil type and land use) are generated covering violent precipitation events. Another map source, conducted as data for geoinformation system (GIS) applications, is provided by HYDROBOD II (Sotier et al., 2017). By using Pedotransfer Functions (PTF) and the Soil Conservation Service Curve Number (SCS-CN) method coupled with the infiltration model of KINEROS (Woolhiser et al., 1990), infiltration capacities are displayed, including four different antecedent soil moisture conditions. The data is confined for the state of Lower Austria. The project RAINMAN (Achleitner *et al.*, 2020) was established to conduct testing concerning different simulation software, including 2D simulations of event-related water levels, flood elevations and flow velocities, for the area of Upper Austria. Infiltration deficit is included by the SCS-CN method and simplified net precipitation models. In order to apply a regionalization of the model HYDROBOD II to the whole of Austria, the infiltration capacity is derived from area-wide soil data (eBOD). As part of the project Infiltration Capacity Austria (InfCapAT), module one focuses on the generation of nationwide data for infiltration capacities, as well as its significance and quality. Module two is based on 14 measurement stations, which represent typical soils in Austria, with focus on the analysis of soil hydraulic properties and the input of initial conditions on overland flow generation. Module two is thus intended to reduce uncertainties in Module one.

Focusing on Module two, the aim of this master thesis is to analyze soil hydraulic parameters of the vadose zone environment as well as state variables, such as initial water content and slope, coupled with precipitation intensity and their influence on the initiation of pluvial floods at 14 additional long-term measuring stations. Furthermore a climate change analysis will be included, as it is not yet considered in HYDROBOD II.

The focus of this master thesis is (i) to analyse the different sites in the measurement period to screen out possible overland flow events, (ii) to conduct a sensitivity analysis of the influence of different

initial conditions, e.g., rain intensity, antecedent water content and slope, on the generation of overland flow and (iii) to include climate change in a forecast simulation for the years 2070-2100.

The following research questions are addressed:

1. How sensitive is the overland flow generation process, concerning the different input parameters mentioned above?
2. Is it possible to establish a connection between these deviations and soil specific properties (humus content, distribution of soil materials etc.)?
3. How do the different sites react to the introduced climate scenarios?

By means of a simulation software, it will be possible to conduct a sensitivity analysis on these input parameters, for different soil profiles in Austria. The monitoring project of the Federal Ministry of Agriculture, Regions and Tourism in Austria was established to collect data about soil hydraulic properties. Using the available data, the simulation approach will be based on 14 monitoring sites, representing typical soils and climates across Austria. In situ measurements of soil water content, matric potential and temperature were taken to collect enough data for further soil analysis (Albert *et al.*, 2020). The main variables influencing the generation of pluvial floods are hydraulic conductivity, the initial water content, slope and precipitation intensity. Working with the in-situ measurement data within the project RechAUT, PhD candidate MSc. Marleen Ambrosia Schübl inversely calibrated soil hydraulic parameters for each profile by using the software HYDRUS 1D. Thus, 14 models were generated and are available for further analysis. The sensitivity analysis is part of the project Infiltration Capacity Austria (InfCapAT).

The lack of sufficient incorporation of pluvial floods in flood protection measurement plans, indicates the necessity of further analysis, especially with respect to soil hydraulic parameters. This master thesis will provide a first assessment for the sites concerning those parameters and their influence on overland flow generation additionally regarding climate change scenarios.

2. Theoretical Background

To further understand the dependency of overland flow (OF) formation processes and the infiltration capacity of the soil, it is necessary to understand the soil hydraulic properties in the vadose zone environment. Interdependent properties such as initial water content, hydraulic conductivity and matric potential are decisive for the water movement and subsequently for the initiation of OF. In this chapter, the most important parameters and state variables necessary for this master thesis, as well as governing equations, are described. Additionally, pluvial floods in consequence of extreme precipitation events will be explained.

2.1 Vadose Zone Environment

In the hydrological cycle, the vadose zone environment builds the link between the soil surface and the groundwater body (aquifer) (Figure 1). It is described as the soil layer situated below the surface and above the groundwater table including the capillary fringe and the root zone (Holden and Fierer, 2005). As it is directly connected to the atmosphere, the vadose zone environment is highly influenced by meteorological parameters and therefore also by climate change. It contributes to following processes within the hydrological cycle (Simůnek *et al.*, 2009):

- **Evaporation** is the vaporization of water on the soil surface or the surface of leaves. The used unit is length per time (L/T)
- **Transpiration** is the absorption of water via plant roots and the consecutive water release in form of water vapor via plant leaves. The unit is length per time (L/T). Together evaporation and transpiration form evapotranspiration.
- **Overland flow** is water flow on the soil surface, which is not in connection with a stream channel (Steenhuis *et al.*, 2005)(L/T).
- **Infiltration** is the rate at which the soil can absorb surface water (mainly precipitation and irrigation). It is measured in length per time (L/T).

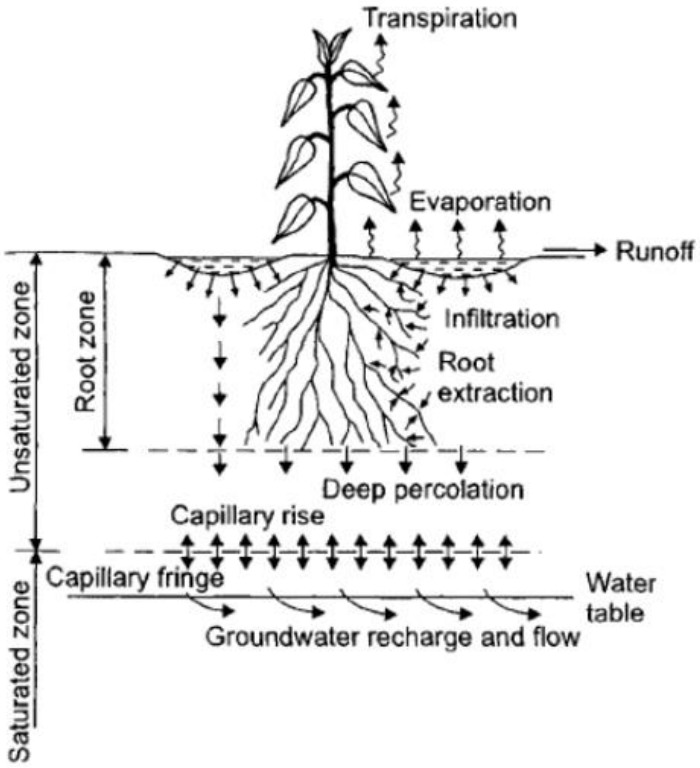

Figure 1: Soil water fluxes described by Hillel, 1998.

2.1.1 Water Flow in the Vadose Zone

The water flow in the vadose zone environment is strongly dependent on the soil matrix, since the water movement only takes place in the soil pores (Kammerer, 2020). The physical approach to describe the low-velocity flow in a porous medium uses the theory of potentials. The potential theory states, that the potential energy of water is equivalent to the work done to remove a unit water from the soil pores under certain gas phase pressure and temperature conditions from each elevation (Bolt *et al.*, 1976). The water flow is always in direction from the higher to the lower potential. The total water potential consists of:

$$\psi_t = \psi_g + \psi_o + \psi_p \qquad \textbf{(2.1)}$$

With:

- ψ_t **the total potential in** volume in unit aera per time (VL^2T^{-2}).
- ψ_g **the gravitational potential**, which is the energy to hold the water against gravitational forces inside a porous medium (VL^2T^{-2}).
- ψ_o **the osmotic potential**, which is the energy to equalize differences in concentration in a liquid medium (VL^2T^{-2}).
- ψ_p **the pressure potential**, which includes the matric potential, gas phase pressure potential, the load potential, and the hydrostatic potential (VL^2T^{-2})(Romano, 1999). **The matric potential** ψ_m is the energy needed to move water due to adhesion and capillary forces. The gas phase pressure potential occurs when additional gas pressure is applied, for example when an infiltrating wetting front collides with entrapped air in the soil column(Stumpp, 2020). Load and hydrostatic potential can be caused by the weight of additional materials on the surface or water in the pores under saturated conditions.

Under saturated conditions the matric potential is always 0, resulting in a positive total potential. As the water content decreases, capillary forces and adhesion become predominant. Thus, the matric potential is negative. The total potential can be expressed in **pressure head** (L), which is derived by the total potential multiplied with the weight of the fluid.

The **water content** of the vadose zone can be split up into residual, saturated and soil volumetric water content. The soil volumetric water content θ is calculated as the quotient of the water volume and the volume of the whole soil probe. The residual water content θ_r indicates a very dry soil, where remaining water is in dead-end pores or highly influenced by adsorptive forces (Kammerer, 2020). The saturated water content θ_s is reached when the whole pore volume is filled up with water.

To physically describe water flow in a porous medium, Darcy's law (2.2) forms the foundation for water flow under saturated conditions. The water flux (v_f) is described as the proportionality factor(k) multiplied with the quotient of the elevation difference (ΔH) and the
length of the flow path (L).

$$v_f = k\frac{\Delta H}{L} \qquad \textbf{(2.2)}$$

The proportionality factor can be referred to as the **saturated hydraulic conductivity (k_s)**. It is the water flow through a saturated porous medium due to a hydraulic gradient. It is influenced by the pore volume, tortuosity, water content and viscosity of the liquid.

There are some modifications to be made when changing to unsaturated conditions:

1. The geohydraulic potential ($\psi_{g+}\psi_p$) must be changed to the soil physical potential (($\psi_{g+}\psi_m$).
2. The matric potential is regarded as a function of the water content. The more negative the matric potential the smaller the water content. The interdependency of the matric potential and the water content are composed as the **water retention curve θ(ψ)** (WRC) which defines the water storage capacity of the soil matric and is strongly dependant on the pore size distribution (Kammerer, 2020).
3. The unsaturated hydraulic conductivity (k_u) is a function of the volumetric water content and in turn of the matric potential. This can be expressed in the **unsaturated hydraulic conductivity curve K(ψ)** (HCC). When unsaturated conditions occur, the hydraulic conductivity changes due to a decrease of the cross-sectional area of water flow in the soil matric, an increase of tortuosity and an increase of drag forces.

The water flow in unsaturated conditions is considered as unsteady. To completely describe water flow in a porous medium the impulse equation of Darcy has been modified by Buckingham. As a partially differential equation, the Buckingham-Darcy law (2.3) is a function of time and space and reads as follows:

$$q = -K(\theta)\frac{d(\varphi_p + \varphi_g)}{dz} \quad \textbf{(2.3)}$$

where q is the water flux (LT^{-1}), K(θ) shows the hydraulic conductivity K (LT^{-1}) depending on the soil volumetric water content θ (L^3L^{-3}) and d (ψp + ψg)/dz the gradient of the total water potential, which consists of ψg, the gravitational potential and ψp, the matric potential in vertical direction (z).
Additionally, to the impulse equation, the water movement needs to be described in terms of continuity. Under steady state conditions, regarding a certain soil volume, the water inflow is equal to the outflow. Under unsteady state conditions the flow rate is volatile, expressed in the difference in water storage (Δθ) over time (t):

$$\frac{\partial\theta}{\partial t} = -\frac{\partial q}{\partial z} \quad \textbf{(2.4)}$$

where Δq is the difference of water flux along the vertical direction z (Δz). The Richards equation (2.5) combines equation (2.3) and (2.4) for the one-dimensional uniform water movement in the vadose zone environment by the soil water content over time (Richards, 1931)

$$\frac{\partial \theta}{\partial t} = \frac{\partial}{\partial x}\left[K\left(\frac{\partial h}{\partial x} + \cos\alpha\right)\right] - S \qquad \textbf{(2.5)}$$

where h is the water pressure head (L), θ is the volumetric water content (L^3L^{-3}), t is time (T), x is the spatial coordinate (L), S is the sink term ($L^3L^{-3}T^{-1}$), α is the angle between the flow direction and the vertical axis (for vertical flow cos α = 1) and K is the unsaturated hydraulic conductivity function (LT^{-1}). To solve the Richards equation, the WRC and HCC must be established.

2.1.2 Water Retention Curve and Hydraulic Conductivity Curve

Model of Van-Genuchten and Mualem

To define the unsaturated soil hydraulic properties, θ(ψ) and K(ψ), the analytical model of Van Genuchten and Mualem can be used. By using the statistical pore-size distribution model of Mualem (2.8) to define the unsaturated hydraulic conductivity, van Genuchten established a mathematical solution of the WRC (2.6), showing the relation between effective saturation (2.7) and the matric potential (van Genuchten, 1980 and MUALEM, 1976)

$$\Theta = \begin{cases} \dfrac{1}{\left(\left(1 + (\alpha|\varphi|)\right)^n\right)^{1-\frac{1}{n}}} & \text{if } \psi \leq 0 \\ 1 & \text{if } \psi > 0 \end{cases} \qquad \textbf{(2.6)}$$

$$\Theta = \frac{\theta - \theta_r}{\theta_s - \theta_r} \qquad \textbf{(2.7)}$$

$$K = \begin{cases} K_s \Theta^l \left[\left(1 - \left(1 - \Theta \dfrac{n}{n-1}\right)\right)^{1-\frac{1}{n}}\right]^2 & \text{if } \psi < 0 \\ K_s & \text{if } \psi > 0 \end{cases} \qquad \textbf{(2.8)}$$

where Θ is the effective saturation (L^3L^{-3}), describing a scaled value between θ_s and θ_r.(Brooks and Corey, 1964). α is a shape parameter (L^{-1}), which is inversely related to the air-entry point (van Genuchten, 1980). n is a pore-size distribution index (–), which describes the curvature of the WRC and the interdependence of capillary forces and pore size distribution (Kosugi, 1994). The steeper the

curve, the higher is the value for n. Ks is the saturated hydraulic conductivity (LT^{-1}), K the hydraulic conductivity function and l is the tortuosity and pore-connectivity parameter (–).

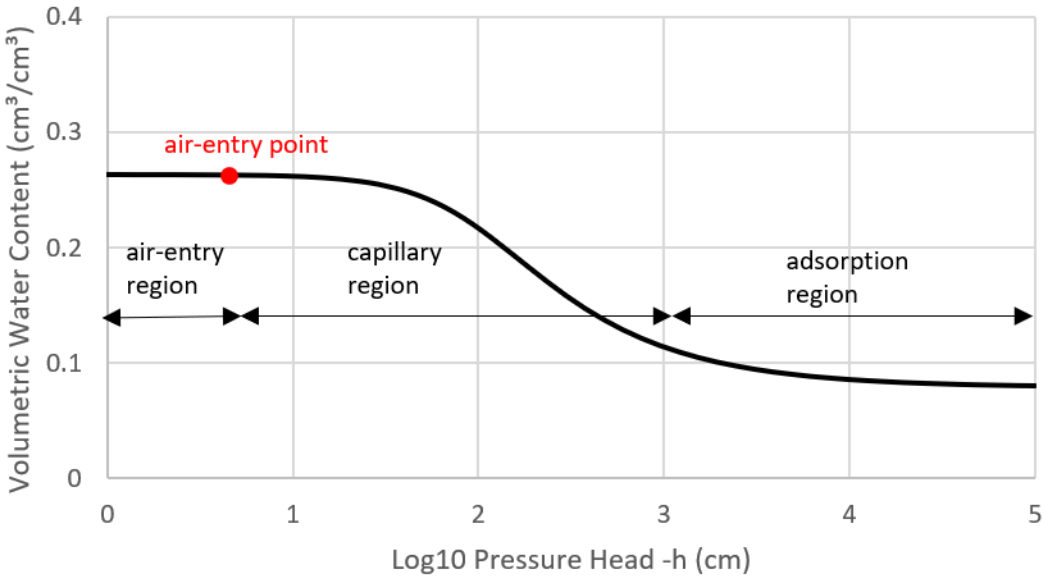

Figure 2: Water retention curve of the material sandy loam. Describing the different regions and the air-entry point in red

In Figure 2, the model of Van-Genuchten and Mualem shows a WRC for the material sandy loam. The typical characterizations are:

- At a pressure head of 0 cm the soil column is saturated. A decrease of pressure head only shows an effect on the volumetric water content when the air-entry point is reached. To that point, the water retention is highly dependent on larger soil pores (Romano, 1999).
- A further decrease in pressure head (between the air-entry point and values near θr) shows a stronger decrease in water content. Capillary forces are predominant.
- When nearly reaching θr adsorptive forces take precedence.

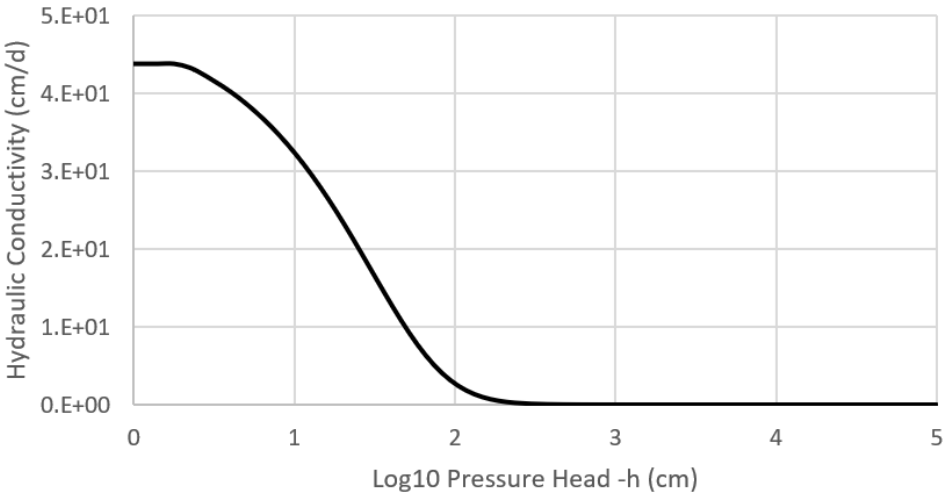

Figure 3: Hydraulic conductivity curve for the material sandy loam.

Figure 3 shows the related HCC for sandy loam. The typical characterizations are:

- At a pressure head of 0 cm, the slope of the HCC is 0. Thus, the hydraulic conductivity is highest when the soil is saturated.
- After a steep decline, the hydraulic conductivity reaches 0, when the WRC indicates its turning point and approaches θr.

Plant Available Water

The WRC does not only show the storage capacity of water in a porous medium, but also indicates the availability of water for plants. The plant available water is referred to as the usable field capacity and is defined as $\theta(\psi)$ between the permanent wilting point (PWP) and the field capacity (FC). The PWP describes the point at which a plant is no longer able to absorb water via its roots due to a very low water content in the soil matric. Irreversible plant damages occur. The FC is the water content which can be stored against gravity, measured 2 to 3 days after complete saturation.

2.2 Pluvial Floods

Precipitation events with a high intensity and a short duration can cause rapidly rising OF in small catchment areas (Glade, Mergili and Sattler, 2020), so-called pluvial floods. OF generation processes are a function of precipitation characteristics and soil hydraulic properties of the vadose zone as well as the soil surface. The contributing processes are nonlinear, and their time scale can differ, for example OF is faster than infiltration (Brunetti, Šimůnek and Bautista, 2018). There are multiple approaches to mathematically describe their interconnection. These processes as well as expedient modelling approaches are presented on the following pages.

2.2.1 Initiation Characteristics

The knowledge of possible hydrological responses of the vadose zone during a high intensity precipitation event is crucial for pluvial and fluvial hazard mitigation measurements (Krammer *et al.*, 2016). In simple terms, the generated OF (LT^{-1}) results from precipitation (LT^{-1}) minus the infiltration flux (LT^{-1}). The OF again can be separated into two different types: the Hortonian Overland Flow (HOF), which is characterized by infiltration excess (Horton, 1945) and the Saturated Overland Flow (SOF), which is characterized by saturation excess (Dunne and Black, 1970). Furthermore, the initiation of OF is highly dependent on the following site and physical characteristics:

- **The characteristics of precipitation events**: precipitation intensity (L/T) and duration (T).
- **The vadose zone properties**: Infiltration capacity in combination with antecedent soil moisture.
- **The properties of soil surface and its morphology:** Slope, vegetation LAI and land use.

The interdependency of these characteristics forms the main challenge for the generation of rainfall-runoff models.

Characteristics of Precipitation

The main characteristics of precipitation events are the rain intensity R_i (LT^{-1}), the duration D (T) and the shape of the event. The Hyetograph, which plots the rain intensity over time, provides important information about the temporal distribution and the position of the peak. Heavy precipitation events are categorized in (i) large-scale events, with consistent precipitation over hours to a few days and (ii) convective events, which occur locally with a short duration and high rain intensity (Glade, Mergili and Sattler, 2020). Although high R_i are decisive for the initiation of overland flow (HOF) most of the time, the interaction between those two is significant as light-intensity events can lead to saturated conditions and hence to overland flow (SOF). The precipitation distribution over the year is characterised by seasonal changes (Cerdà, 1997). Climate change, as a considerable factor in forecast

simulation, has an impact on seasonal changes, including thunderstorm season beginning much earlier and ending later in the year (ÖWAV-Forum Klimawandel, 2020).

Vadose Zone Properties

The infiltration capacity (I_c) can be described as the water flux (LT^{-1}) into the soil and along the vertical direction z (L). The infiltration at the soil surface forms an important boundary condition, separating precipitation into infiltrating water and OF. It is influenced by soil texture, soil structure, vegetation, temperature, preferential flow paths, water content and surface condition (moist to dry) (Horton, 1945). Under unsaturated conditions:

if $\mathbf{R_i < I_c}$ Precipitation is absorbed entirely

if $\mathbf{R_i > I_c}$ Precipitation leads to OF

If the soil is saturated I_c is equated to k_s. If the soil is unsaturated I_c depends on the HCC and therefore on the water content throughout the precipitation event. Horton describes i (=I_c) as follows (Horton, 1932):

$$i = i_f + (i_0 - i_f)e^{(-\beta t)} \quad \textbf{(2.9)}$$

Where i_0 is the initial infiltration capacity (LT^{-1}), i_f the final infiltration capacity at steady state (LT^{-1}) and β a variable that describes the decrease of i_0 throughout the rain event. The equation can be explained by Figure 4.

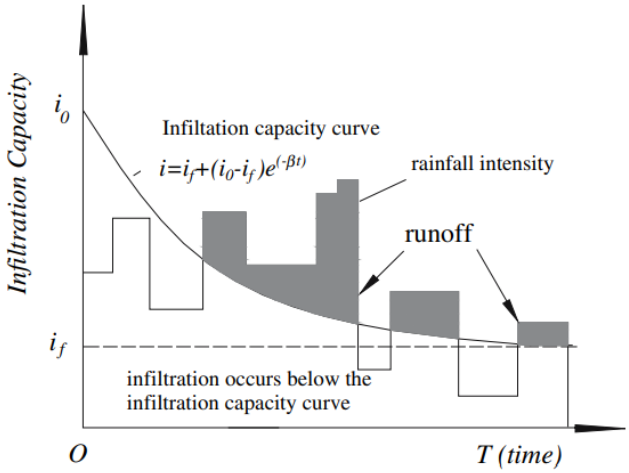

Figure 4: Infiltration capacity curve for HOF ((Xue and Gavin, 2008 and Viessman, L.Lewis and Knapp, 1996)

The infiltration capacity decreases as the energy of precipitation causes compression of the soil surface, variation of the crumb structure and leaching of fine material (Horton, 1945). Horton states that because of surface alterations, the infiltration at the soil surface is lower than in underlying layers. Thus, the soil stays unsaturated. Dunne and Black, 1970 developed a different empirical approach, where OF is generated under saturated conditions. By defining the boundary conditions for the Richards-equation (2.5), Neuman et al. (1974), describe the infiltration capacity as follows:

$$\left|-\mathrm{K}\frac{\partial \mathrm{h}}{\partial \mathrm{x}}-\mathrm{K}\right| \leq \mathrm{E} \quad \text{at } \mathrm{x}=\mathrm{L} \tag{2.10}$$

$$\mathrm{h_A} \leq \mathrm{h} \leq \mathrm{h_S} \quad \text{at } \mathrm{x}=\mathrm{L} \tag{2.11}$$

where E is the maximum potential rate of infiltration (LT^{-1}), K is the unsaturated hydraulic conductivity (LT^{-1}), $\Delta h/\Delta x$ the difference of pressure head along the vertical direction x, h_A is the minimum pressure head and h_S the maximum pressure head allowed at the soil surface. h_A is limited by the water vapour pressure. h_S is equal to 0, except water ponding at the surface is allowed ($h_S > 0$).

Surface Properties

The slope of the soil surface can range from a horizontal orientation to the maximum orientation, which is limited by the angle of repose. The angle of repose (γ) is defined as the maximum angle of slope, where the soil can stay without sliding (Carter, 1950). The slope can alter the infiltration capacity as gravitational forces decrease normal to the hillslope by a factor of cos(γ) (Morbidelli *et al.*, 2018). Furthermore, vegetation can influence infiltration, as the roots build preferential flow paths, the transpiration reduces the water content, the leaves intercept precipitation and the plant coverage can decrease OF velocity. The interception of precipitation is influenced by vegetation properties, and in particular from the Leaf Area Index (LAI), where the total area of leaves over a unit of surface can hinder the water to reach the soil. Another decrease of infiltration capacity can be caused by different types of land use and cultivation. Typical examples are (1) sealing of the soil by building impermeable top layers, (2) compressing the soil surface by strongly cultivated fields and (3) altering the contents of the soil and thus their soil physical properties. Once again, these characteristics are highly dependent on seasonal changes. Differences in plant coverage, content of organic matter or cultivation types occur over the year (Markart *et al.*, 2011).

Overland Flow Description

The one-dimensional OF can be described by the Saint-Venant equation. Modified by Yen (Yen, Te Chow and Akan, 1977) it is written as follows:

$$\frac{\partial \mathrm{h}}{\partial \mathrm{t}} + \frac{\partial(\mathrm{uh})}{\partial \mathrm{x}} = \mathrm{r} - \mathrm{f} \qquad \textbf{(2.12)}$$

where h (=h_s) is the mean overland flow depth (L), u (=U_s) the average flow velocity (LT^{-1}), t is time (T), x is the distance at the soil surface (L), r is precipitation (LT^{-1}) and f the infiltration rate (LT^{-1}).

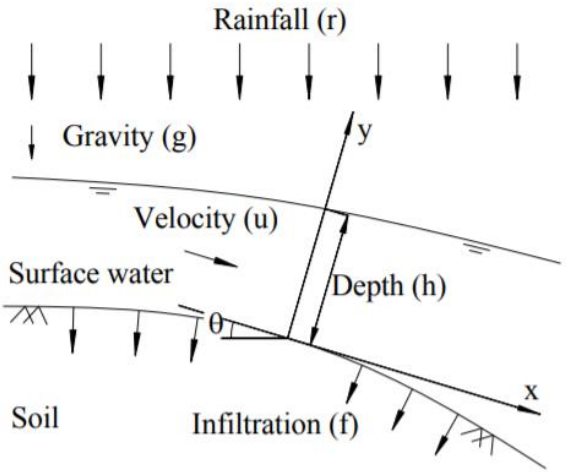

Figure 5: Schematic illustration of De Saint Venant variables ((Zhang *et al.*, 2015))

Equation 13 indicates rapid varied unsteady flow conditions. However, for simplification, OF is considered uniform. This implicates that (1) the depth, water area, velocity, and discharge on the soil surface are constant and that (2) the energy line, water surface and soil surface are parallel (Chow, 1959). The Manning-Strickler formula (2.13) describes the uniform flow velocity as follows (Chow, 1959):

$$U_S = \frac{h^{2/3}}{n}\sqrt{S_f} \tag{2.13}$$

where S_f is the friction slope and n is the Manning`s roughness coefficient (-). n describes the retardation of flow, influenced by surface roughness, vegetation, channel irregularity, channel alignment, silting and scouring, obstruction, size and shape of channel and stage and discharge (Chow, 1959). The mass balance equation (2.12) combined with the momentum equation (2.13) builds the OF equation (2.15) using the diffusion wave approximation.

$$\text{with} \quad S = \frac{\partial(h_s + z_l)}{\partial x} \tag{2.14}$$

$$\frac{\partial h_s}{\partial t} = \frac{\partial}{\partial x}\left[\frac{k h_s^{5/3}}{n\sqrt{S}}\frac{\partial(h_s + z_l)}{\partial x}\right] + q_s \tag{2.15}$$

where k is the Unit conversion factor, which can be neglected, z_l is the land surface elevation (L), S is the mean local slope (-) and q_s is the rate of local input (LT^{-1}) (= r-f). OF is a discontinuous process, happening only throughout a precipitation event. In contrast, infiltration processes are continuous as they are not dependent on the precipitation period (Brunetti, Šimůnek and Bautista, 2018). To enable a statement on the operative effect of precipitation event to generate overland flow, the runoff coefficient (φ) can be used. It is defined as (Markart *et al.*, 2011):

$$\varphi = \frac{total\ runoff}{total\ precipitation}$$

(2.16)

2.2.2 Data Acquisition and Rainfall-Runoff Models

Deterministic models are based on a detailed definition of physical correlations, whereas empirical models are mostly unbiased by physical properties (Krammer *et al.*, 2016). While the former uses physically based relationships (e.g., Darcy equation) to simulate the process, the latter is obtained from data (e.g., linear regression). Rainfall-runoff models are generally deterministic. The presented data and related sources especially for Austria are based on the collected information of Glade, Mergili and Sattler, (2020) The two main required data series for OF modelling, are (1) precipitation data and throughout the event (2) predominant boundary condition data (e.g., infiltration capacity).

Precipitation Data

The 'Zentralanstalt für Meteorologie und Geodynamik' (ZAMG at http://www.zamg.ac.at/incaanalyse/) and the 'Hydrographischer Dienst' (eHYD at https://ehyd.gv.at/) are the main operators for high quality measurement stations. While ZAMG provides precipitation data in a 1 km grid for every 15 minutes, eHYD has 940 measurement stations in total (Eybl, Godina and Weilguni, 2018) with daily data and partly one-minute data. It is possible to receive additional data from ZAMG, with a higher temporal resolution if available. Another important value, accessible in ehyd, is the design depth of precipitation. Existing in a 6 km grid, the precipitation is categorised by a certain annuality and duration. The duration can vary between 5 minutes and 6 days and the annuality is up to 100 years. This design depth of precipitation is often used as a basis for rainfall-runoff models and mitigation measurements for floods. It should be noted that convective precipitation events occur mostly on a local scale and can cause problems with accurate measurements. Thus, the grid size of monitoring stations is of utmost importance.

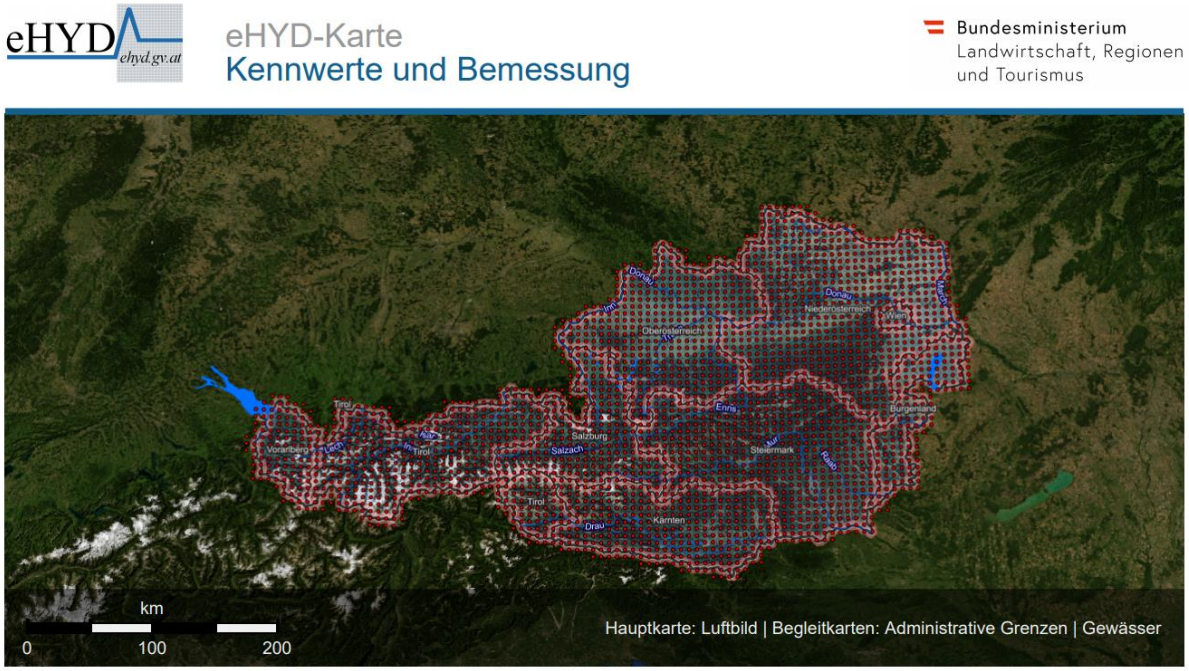

Figure 6: Grid points (red) for the design depth of precipitation (Bundesministerium für Landwirtschaf, 2020)

Physicochemical Characteristics

As mentioned before, the infiltration capacity is highly dependent on land use, vegetation, soil type and antecedent water content. For the attributes land use and vegetation, the program CORINE (Coordination of Information on the Environment), which is a project of the European Environment Agency implemented in Austria by the Umweltbundesamt, delivers high resolution data for geographic information systems. The soil type, humus content, bulk density or soil texture can be seen in the 'digitale Bodenkarte Österreichs' (eBOD at https://bodenkarte.at/), which results from the methodical implementation of ÖNORM L 1076 (Austrian Standards Institute, 2013b). In addition, the Code of Practice (Markart *et al.*, 2011) provides surface runoff coefficients resulting from more than 700 rain simulation experiments. However, the previously mentioned data systems only include soil properties, and do not provide soil hydraulic properties. The runoff coefficient or the infiltration capacity can only be estimated for typical soil types. For this reason, HYDROBOD I and II was established. It includes the following parameters in a 50-meter grid for the Province of Lower Austria: k_s, k_u, pore size volume, usable field capacity and storage capacity. Using these parameters as a basis, OF could be derived for five different precipitation scenarios under saturated and unsaturated conditions. The data was then regionalized over Lower Austria.

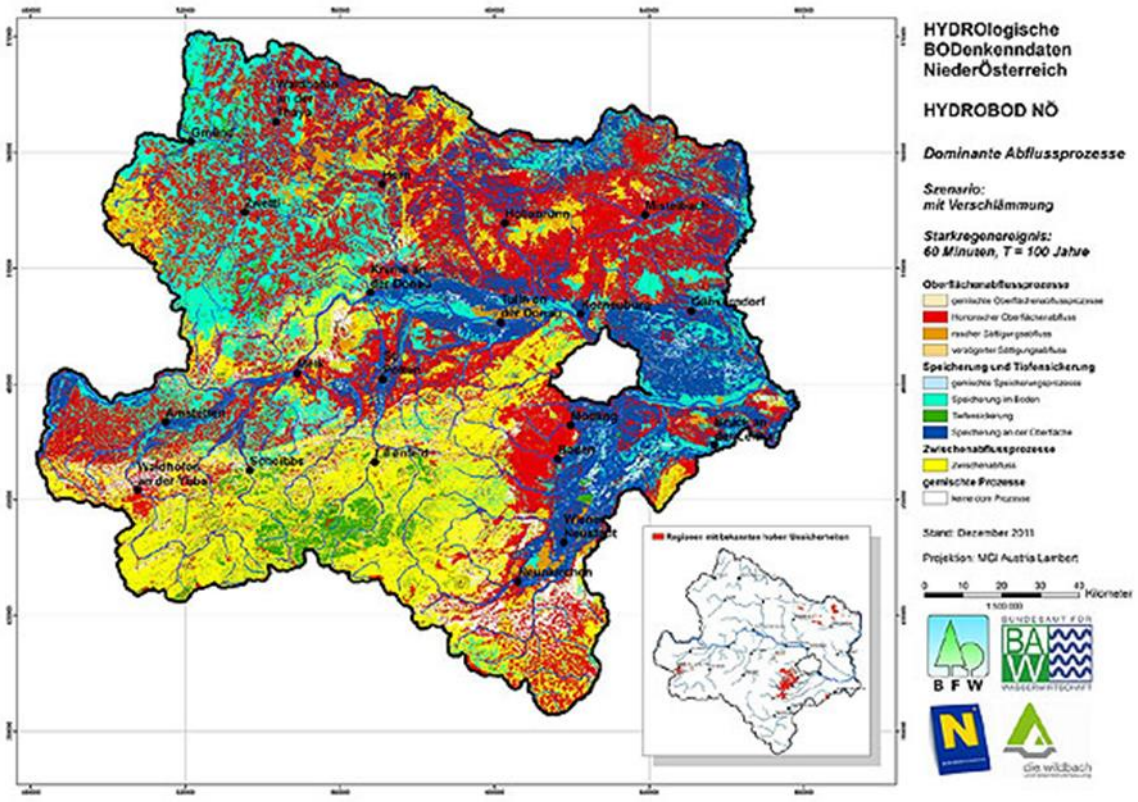

Figure 7: Map of HYDRBOD 2 showing the dominant runoff processes in Lower Austria for a design depth of precipitation for a event of 60 minutes and a return period of 100 years (Land Niederösterreich, 2017).

2.2.3 InfCapAT

In order to expand the data of soil physical properties, especially the infiltration capacity for all of Austria, the project Infiltration Capacity Austria (InfCapAT) was established by the Federal Ministry of Agriculture, Regions and Tourism (BMLRT) . Module 1 focuses on the derivation of soil physical properties from already existing data sets of eBOD and HYDROBOD I and II. The outcome will include nationwide information on the infiltration capacity and their quality and uncertainties (Schulz, 2020). To reduce these uncertainties, Module 2 is based on 14 soil water monitoring sites established by the BMLRT and situated all over Austria. These sites represent typical climate and soil types for the selected region. The initiation of pluvial floods will be analysed regarding to the infiltration capacity and initial conditions, such as soil water content and rain intensity.

3. Methods

The model HYDRUS-1D is used to analyse the influence of different initial conditions such as antecedent soil moisture, slope, and precipitation intensity and their input on the initiation of overland flow. The focus lies on the computational modelling of subsurface flow, whereas overland flow will be expressed as a boundary condition. It is an explanatory modelling approach to show the sensitivity of various parameters on the output function. The functional analysis will be based on 14 measurement stations situated in Austria. Selected overland flow events will be additionally simulated in a 2D approach. To include the factor of climate change, four different climate scenarios for the years 2050 ununtil 2100 will be implemented in the analysis. The output of the functional model is further analysed by statistical methods.

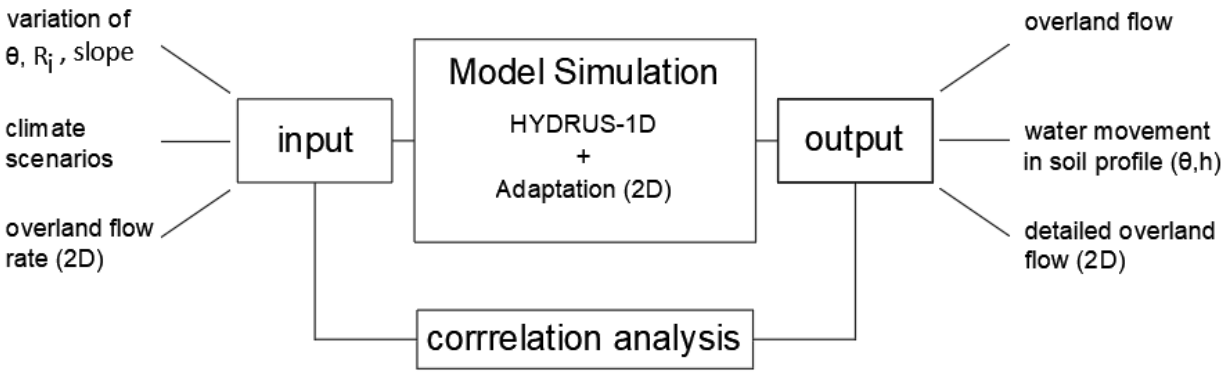

Figure 8: Schematic concept of the individual analysis steps.

3.1 Data Basis

14 monitoring sites, distributed over Austria (Figure 9) were used as a data resource. At all 14 sites in-situ measurements of soil hydraulic properties, such as soil water content, matric potential and soil temperature in four to seven depths, were taken over the last 20 years (Albert *et al.*, 2020). Besides field measurements, an additional laboratory analysis of the soil probes was performed. Statutory provisions based on the 'Wasserrechtsgesetz 1959 idF BGBI. I Nr.82/2003' and the Wasserkreislauferhebungsverordnung (Österreichische Bundesrepublik, 2006) determine the monitoring of the vadose zone environment.

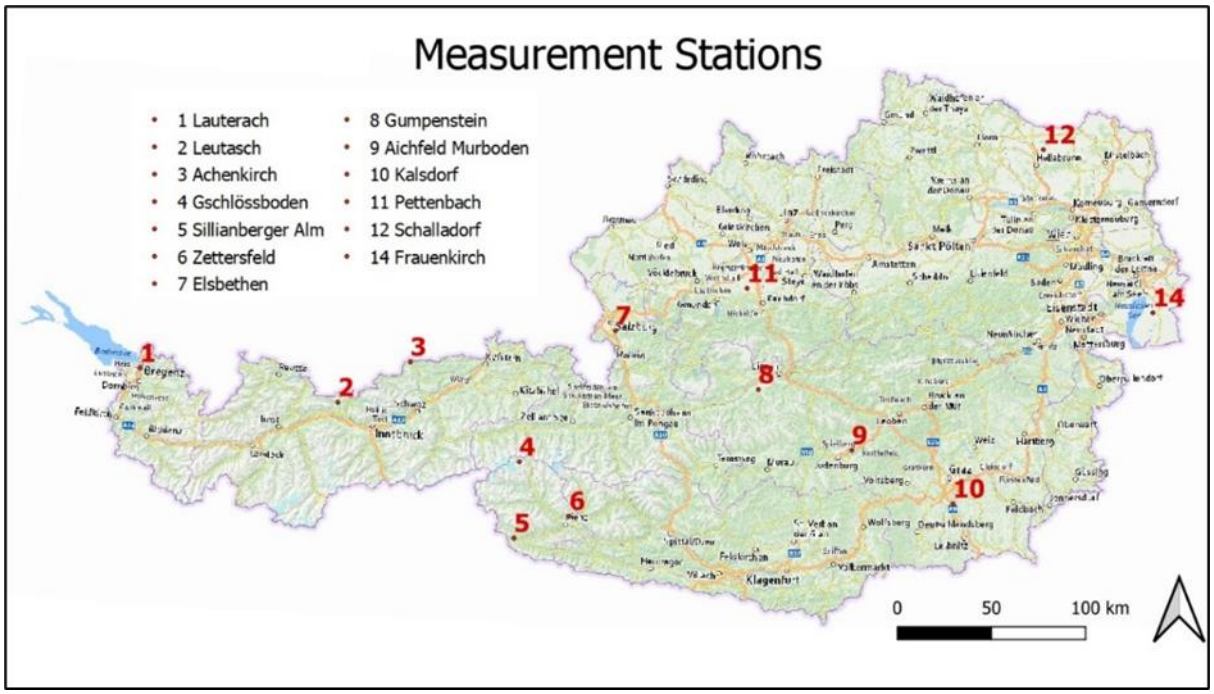

Figure 9: Map of the different measurement sites in Austria

3.1.1 Field Measurements

To fully analyse the heterogeneity of the soil most sites have two profiles at which measurement devices are installed. The most common devices to measure soil water content are the TDR (Time Domain Reflectometry) and FDR (Frequency Domain Reflectometry). The former is more frequently used. Measurement devices for the matric potential are Tensiometers, as well as gypsum blocks and MPS sensors. Tensiometers with a measurement range of $\psi_m > -800$ hPa, can have a low degree of coverage concerning dry conditions, therefore MPS sensors (-100 hPa $< \psi_m < 1.5$ MPa) are widely used (Bundesministerium für Nachhaltigkeit und Tourismus, 2019). MPS sensors cover the whole spectrum of plant available water. At five sites Lysimeters are installed additionally. As their measurement scope covers all the parameters of the water balance equation, they are often used for validation purposes.

3.1.2 Laboratory Measurements

Due to the fact that some soil properties cannot be measured in the field, soil samplings are taken and analysed in soil physical laboratories. The grain size distribution is determined by sieving and the pipette method according to ÖNORM L 1061 (Austrian Standards Institute, 2013a).The grain friction of sand (grain diameter from 0.063-2.0 mm), silt (grain diameter from 0.063-0.002 mm) and clay (grain diameter ≤ 0.002 mm) can be illustrated in the texture triangle according to ÖNORM L 1050 (Austrian Standards Institute, 2016). Bulk density, pore volume and FC are determined by using undisturbed soil probes according to ÖNORM L 1055 (Austrian Standards Institute, 2004a) and L1056 (Austrian

Standards Institute, 2004b). The WRC and the HCC can be defined by a vaporization process (Bundesministerium für Nachhaltigkeit und Tourismus, 2019).

3.1.3 Inverse Calibration

The field measurements for each profile have already been processed within the project Recharge Austria (RechAUT), where the focus lies on groundwater recharge studies. MSc. Marleen Ambrosia Schübl inversely calibrated and validated the Van Genuchten and Mualem parameters by using the software HYDRUS-1D. To calibrate a functioning model, she used geometric data (e.g., depth of profile and root zone), meteorological data (e.g., daily precipitation, radiation, minimum temperature, maximum temperature, humidity, wind etc.), crop data (e.g., LAI, crop height etc.) and in-situ measurement data (e.g., water content and matric potential) as input. The calibration is based on the Bayesian approach, where the probability of the posterior outcome is based on the prior knowledge of related conditions (Foreman-Mackey *et al.*, 2013). Adapted to the requirements of the PhD thesis the Bayes theorem goes as follows:

$$\mathrm{P}(\theta|\mathrm{D},\mathrm{M}) = \frac{\mathrm{P}(\mathrm{D}|\mathrm{M},\theta)\ \mathrm{P}(\theta|\mathrm{M})}{\mathrm{P}(\mathrm{D}|\mathrm{M})} \tag{3.1}$$

where the posterior parameter distribution of the θ is determined by its prior distribution resulting from the input data D and the given model M. Soil texture data and bulk density from the modelling program ROSETTA v3 are used as prior parameters. The Markov chain-Monte-Carlo (MCMC) algorithm was used to numerically solve the Bayesian theorem (Foreman-Mackey *et al.*, 2013). As a result, soil hydraulic properties and associated uncertainties could be described for 13 out of 14 sites (Example Lauterach Table 1). Site 13, situated in Lobau, does not provide sufficient results due to the influence of groundwater within the soil profile.

Table 1: Van Genuchten and Mualem parameters for a profile within the RechAUT project and the PHD Thesis of Marleen Ambrosia Schübl.

	depth (cm)	**θ_r (-)**	**θ_s (-)**	**α (1/cm)**	**n (-)**	**K_s (cm/day)**
Median	**0-80**	**0.069**	**0.414**	**0.235**	**1.181**	**50.325**
2.50%		0.061	0.410	0.191	1.144	34.792
97.50%		0.076	0.426	0.521	1.204	235.270

3.2 Functional Analysis

3.2.1 HYDRUS-1D

The one-dimensional finite element model HYDRUS-1D is a modelling tool for the analysis of water, heat and solute movement in variably saturated porous media (Simůnek *et al.*, 2009).To run the model, input values of profile geometry, crop properties and water flow are required. Figure 10 shows an example soil profile with leading processes. The outcome of the simulation will provide one dimensional data of overland flow initiated throughout the simulation time. The overland flow is described in mm per day or cumulated over the whole time period. Furthermore, the WRC and the HCC are displayed. By adding observation points along the soil profile, θ, pressure head and water flux can be observed in the desired depth.

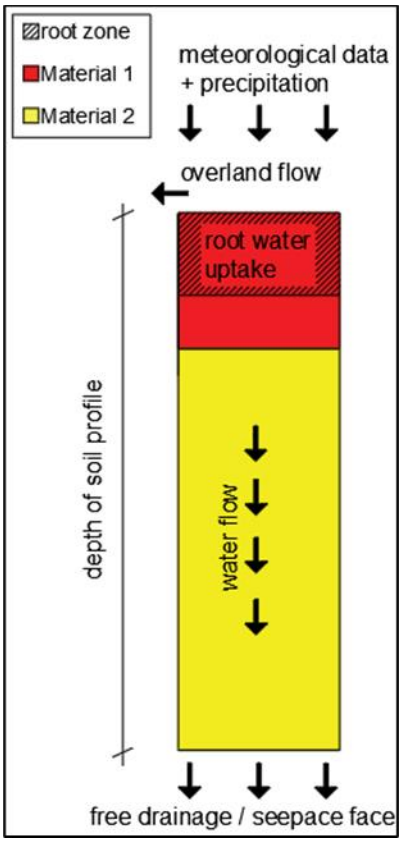

Figure 10: Water fluxes and boundary conditions of a soil profile as input parameters for the software HYDRUS-1D

Time variable boundary conditions are restricted by the availability of in-situ measurements. Precipitation data is expressed in (LT^{-1}). The time resolution varies from daily totals to the precipitation height per minute. Meteorological parameters are required to calculate the potential evapotranspiration using the FAO standard Penman Monteith equation (Allen *et al.*, 1998):

$$ET_0 = \frac{0.408\Delta(R_n - G) + \gamma \frac{900}{T+273} u_2 (e_a - e_d)}{\Delta + \gamma(1 + 0.34u_2)} \quad \textbf{(3.2)}$$

where ET_0 is the reference evapotranspiration (LT^{-1}), R_n is the net radiation at crop surface ($WL^{-2}T^{-1}$), G is the soil heat flux density ($WL^{-2}T^{-1}$), T is the mean daily air temperature at 2 m height (°C), u_2 is the wind speed at 2 m height (LT^{-1}), e_s is the saturation vapour pressure (P), e_a is the actual vapour pressure (P), e_s- e_a is the saturation vapour pressure deficit (P), Δ is the slope of the vapour pressure curve ($P°C^{-1}$) and γ is the psychrometric constant ($P°C^{-1}$). Meteorological conditions include information about daily radiation, temperature differences, humidity, wind, and sunshine hours.

Water flow is described by the Richards equation (2.5) and the water retention model of Van Genuchten and Mualem (see equations 2.6, 2.7, 2.8). Whereas the effect of hysteresis is neglected. The water flow boundary condition at the upper boundary is defined as atmospheric BC with surface runoff (=overland flow). The lower boundary it is defined as free drainage or seepage face. Former indicates a groundwater table far below the soil profile. The latter indicates the possible installation of a Lysimeter. It states that the boundary flux is zero when the pressure head is negative (Simůnek *et al.*, 2009).

Root water uptake is described by the function of Feddes (Feddes, 1980). The extraction of water is nearly 0 when the soil is saturated (P0) or the PWP is reached (P3). The different pressure head parameters provide information on the range to which roots can withdraw water from the soil (P0 to P3) as well as, the optimal withdrawal rate (POpt) and the withdrawal rate at two different potential transpiration rates (P2H at r2H and P2L at r2L). Most profiles are covered with grass or pasture.

Adaptation of HYDRUS 1D

To not only analyse soil hydraulic parameters throughout the overland flow event, a more detailed presentation of the overland flow will be introduced by using an adaptation of HYDRUS-1D (Šimůnek, 2015). The time variable boundary condition is changed as this module simulates water flow over impervious surfaces. The outcome for overland flow of the first simulation, where the infiltration is already subtracted, serves as new input. The overland flow is implemented by the equation 2.14, whereas the surface slope (S) and the surface roughness (n) must be defined.

Numerical Solution

The numerical solution of the model is based on an iterative process. Current time or iteration levels and current positions in the finite difference mesh are based on their previous value (Simůnek *et al.*, 2009). As the iterative process implies a certain degree of complexity, convergence problems can occur.

These errors can be circumvented by:

1) Increasing the space discretization near the soil surface, as higher pressure heads are expected.
2) Changing the water flow boundary condition from surface runoff to surface layer, where nearly zero ponding is allowed (h=0.1 cm). The 1 mm ponding height can be neglected.
3) Using the Van Genuchten and Mualem Model with an air entry point at -2 cm.

The calculation of the water balance is implemented and can be used as a plausibility check for the model. The water balance error should not exceed 1 %.

3.2.2 Precipitation Event Analysis

The time resolution of the precipitation input used by MSc. Marleen Ambrosia Schübl is per day. Additional data in a one-minute resolution is required to analyse overland flow events, which are mainly caused by convective precipitation events. The data, provided by ZAMG, spans over a period of 1996 until 2018 for the monitoring sites of Elsbethen and Aichfeld-Murboden. Due to the large number of values, a python script is used for the separation of specific precipitation events. A certain limit for the precipitation event volume and the minimum interevent time (MIT) is determined. As precipitation is described as falling in events, the MIT defines the dry period in between (Dunkerley, 2008). The MIT should be selected, so that the water content in the soil profile is almost not influenced by a previous precipitation event and thus has no influence on overland flow generation (Lázaro, Arnau and Calvo-Cases, 2016).

3.2.3 Sensitivity Analysis

There are three different approaches for the sensitivity analysis concerning antecedent soil moisture, precipitation intensity and slope. The sensitivity analysis is conducted for the sites Elsbethen and Aichfeld-Murboden. The profile in Elsbethen (Salzburg) is separated into two materials. Both can be characterized as sandy silt. The ks of material one is 20.21 cm/day of material 2 0.28 cm/day. The upper layer of Aichfeld-Murboden consist of sandy loamy silt with a ks of 3.07 cm/day, the lower layer of poor sandy loam and a ks of 43.93 cm/day. For both profiles, ten different precipitation events are selected.

Influence of Initial Water Content

The range of the initial water content is between θ_r and θ_s. The selected θ values are inclined towards the water content classes of HYDROBOD II (Sotier *et al.*, 2017). Under **(1) saturated conditions** the θ equals θ_s. **(2) Wet conditions** are determined as the value that is exceeded by 25 % of the measured values. **(3) The median** is exceeded by 50 % of the measured values. **(4) Moderate conditions** imply

that 25 % and **(5) dry conditions** that 0.01 % of the measured values fall below this θ. And **(6) very dry conditions** describe a value when 44 % of the possible water content (= θ_s-θ_r) is reached. The water content is varied, whereas the precipitation event stays the same. Ten different events are determined for each site.

Influence of Precipitation Intensity

The different R_i is divided into following classes (Weather and Environmental Monitroing Directorate, 2013):

Table 2: Classes of different Ri selected as input variables.

classes	rain intensity	
light	<0.04	mm/min
moderate	0.04-0.125	mm/min
heavy	0.125-0.83	mm/min
violent	>0.83	mm/min

To avoid a possible impact of different precipitation hydrographs on the output function, three events (Figure 11) are determined. For each event one light, two moderate, two heavy and one violent R_i is simulated. The illustrated events are scaled to reach the defined R_i.

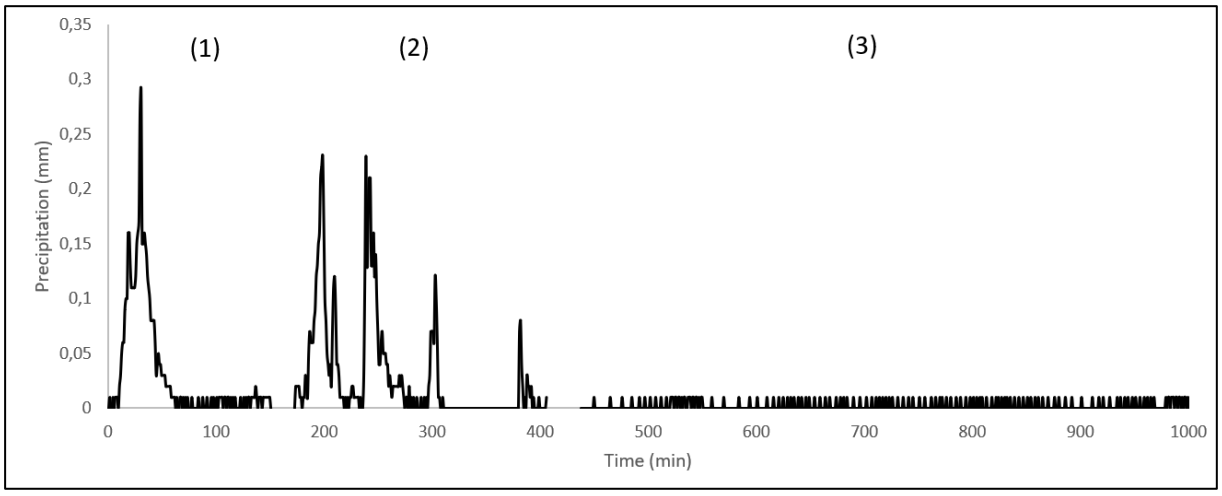

Figure 11: Hydrograph of different precipitation events. (1) A uniform Hydrograph, (2) a multi peak Hydrograph and (3) an even Hydrograph

Influence of Slope

The slope will be differed from a horizontal orientation to the maximum possible orientation, depending on the different soil type. The maximum slope is defined by the angle of repose, which describes the steepest angle between the horizontal axis and the soil surface at which a material can

stay without sliding (Morbidelli *et al.*, 2018). For sandy silt and sandy loam, the angle of repose is approximately 35°. For a sufficient analysis, the angle is set as follows: 0°,7°,21°,28°and 35°.

3.2.4 Comparison of Sites

To analyse the possible impact of different time resolutions within the boundary conditions, a precipitation event with a R_i of 0.12 mm/min for all 13 profiles is simulated. The initial water content is set to the median for each site. Furthermore, because not all profiles have moderate precipitation events, a possible increase of overland flow due to climate change can be presented.

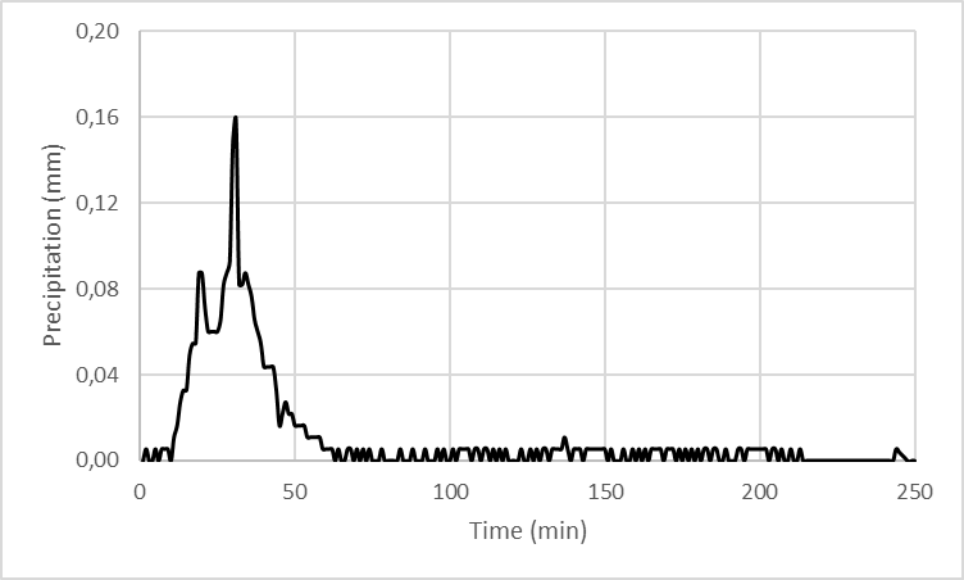

Figure 12: Precipitation event as boundary condition for all 13 profiles.

3.2.5 Climate Scenarios

To include the factor of climate change within the simulation, four different climate scenarios (2071-2100) from the project 'ÖKS15-Klimaszenarien für Österreich' are used. The project was established as a cooperation between ZAMG, the Wegener Centre for Climate and Global Change of the University of Graz and the department of geoinformatics of the Paris London University of Linz. The aim of the project was to analyse climate change in the past as well as in the future influenced by two different greenhouse gas scenarios(Chimani *et al.*, 2016). The first scenario considers a pathway, where mitigation measurements for climate change are conducted. The second scenario represents a pathway, where an unabated emission of greenhouse gases is assumed (business-as-usual). The latter is based on a representative concentration pathway, where the climate is influenced by a change of radiative forcing of 8.5 W/m². The data is based on the global model ICHEC-EC-EARTH and the regional model KNMI-RACMO22E. The temporal resolution is daily and the spatial resolution 1km. The available time period is from 1980 until 2100. Each data point contains information about the sum of global

radiation, the minimum daily temperature, the maximum daily temperature, the sum of precipitation per day, the relative humidity, and the average wind speed per day. The four climate scenarios are based on the Master Thesis of Marion Wallner (Wallner, 2021).

Dry

The data point for the dry scenario is situated in Burgenland near the measurement site of Frauenkirchen (grid cell 57829, 122 m.ü.A.). It represents the Pannonian climate with dry summers and cold but snowless winters. The average annual precipitation is 589 mm and the average annual temperature 14°C (Wallner, 2021).

Moderate

The data point for the moderate scenario is in Upper Austria near Freistadt (grid cell 77396, 562 m.ü.A.). It represents a Central European climate with little fluctuations in temperature and precipitation throughout the year. The average annual precipitation is 796 mm and the average annual temperature 12°C (Wallner, 2021).

Wet

The data point for the wet scenario is in Styria, at the measurement station of Gumpenstein (grid cell 42528, 690 m.ü.A.). It represents a moderate alpine climate. The average annual precipitation is 1127 mm and the average annual temperature 11°C (Wallner, 2021).

Very wet

The data point for the very wet scenario is in Vorarlberg, near Bludenz (grid cell 26029, 1120 m.ü.A.). It represents an alpine climate with warm summers and possible cold air entrapments in the valley overnight. The average annual precipitation is 1702 mm and the average annual temperature 10°C (Wallner, 2021).

Climate at Station

The climate scenario RCP 8.5 is also taken for the measurement stations Elsbethen and Aichfeld-Murboden. Elsbethen is situated in Salzburg, close to the capital Salzburg (grid cell 52961, 493 m.ü.A.). The climate can be described as Central European Climate. The average annual precipitation is 1477 mm and the average annual temperature 13°C. Aichfeld-Murboden is in Styria, near Zeltweg (grid cell 26934, 645 m.ü.A.). The climate is alpine. The average annual precipitation is 840 mm and the average annual temperature 11°C.

3.3 Statistical Analysis

The effect of the initial parameter deviation on the overland flow function is shown by means of a correlation analysis. The Pearson Correlation analysis describes a linear relation between two variables (x, y) and is expressed as follows (Siebertz, Van Bebber and Hochkirchen, 2017):

$$r = \frac{\sum_{i=1}^{n}(x_i - \bar{x})(y_i - \bar{y})}{\sqrt{\sum_{i=1}^{n}(x_i - \bar{x})^2}\sqrt{\sum_{i=1}^{n}(y_i - \bar{y})^2}}$$

(3.3)

where x resembles the input variables, y the output variables and $\bar{x}$ and $\bar{y}$ their mean values. It is preconditioned that the variables x and y are normally distributed and have a linear relation. The coefficient of determination (r), or R^2 if the relation is squared, indicates the proportion of variables that are predictable from the input data to variables that are not predictable. If r=0, there is no relation between x and y. If r=1, it resembles a perfect linear relation.

4. Results

4.1 Input Data

For sites with sufficient data on their grain size distribution, Figure 13 shows their distribution in the texture triangle. The data originates from the laboratory analysis of the soil probe. Therefore, the results of the functional analysis apply to the laboratory measurements, as the eBOD data does not always resemble the state of the site itself.

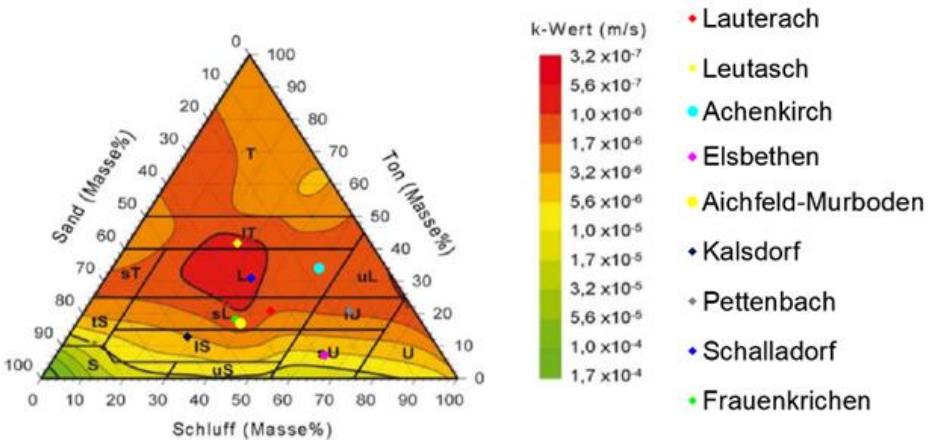

Figure 13: Texture triangle with the saturated hydraulic conductivity (Kammerer, 2012).

The k_s value for each soil type was implemented in the texture triangle by Kammerer, 2012. The values are compared to the inversely calibrated VGM data (Appendix A.4). The results show that the range expected from the texture triangle vary widely from those of the calibrated function. Only the station in Frauenkirchen shows a compliance for both k_s values. A possible influence of the humus content on the alteration of the k_s can be seen in Figure 14. The coefficient of determination is 0.6., whereas the largest values of humus content (21 % for Leutasch and 31 % for Achenkirch) are not considered. The range of humus content from 0 to 4 % is taken into account.

Table 3: The saturated hydraulic conductivity generated from the texture triangle (tt) and the Van Genuchten Mualem parameters (VGM) for each profile.

Measurement Sites	k_s tt (cm/day)	k_s VGM (cm/day)
Lauterach	8.6-14.7	50.32
Leutasch	4.8-8.6	23.47
Achenkirch	8.6-14.7	21.6
Elsbethen	48.4-86.4	20.21
Aichfeld-Murboden	8.6-14.7	3.07
Kalsdorf	27.6-48.4	2.20
Pettenbach	8.6-14.7	37.96
Schalladorf	4.8-8.6	2.20
Frauenkirchen	8.6-14.7	11.70

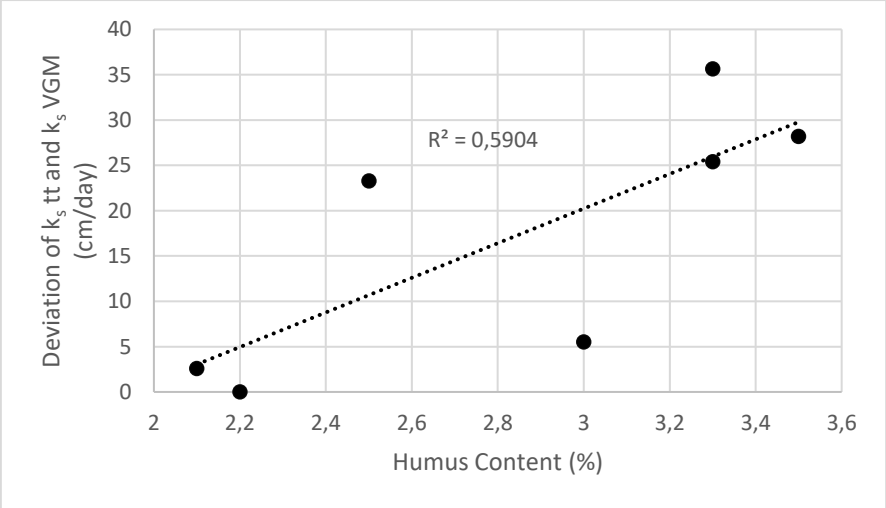

Figure 14: Comparison of the ks values of the texture triangle and the Van Genuchten Mualem parameters and their relation to the humus content (%) of the upper layer

4.2 HYDRUS-1D

The results, within the general simulation of the calibrated profiles show that 10 out of 13 profiles generate OF, whereby considerable differences in the cumulative amount are visible.

Table 4: Cumulated overland flow output of the general simulation at the different sites and their simulated time period in a daily resolution.

Station Nr.	Name	cum. Overland Flow (cm)	Time Period (days)
3	Achenkirch	7	730
5	Sillianberger Alm	37	8035
6	Zettersfeld	22	8401
7	Elsbethen	1257	8401
8	Gumpendorf	19	8401
9	Aichfeld-Murboden	105	8401
10	Kalsdorf	166	8401
11	Pettenbach	5	8401
12	Schalladorf	8	8401
14	Frauenkrichen	3	8401

The by far largest amount of OF is reached at the measurement site of Elsbethen with 1257 cm in 23 years (Figure 15). The annual cumulative OF in EL reaches a maximum in 2016 (109 cm) and its minimum in 2003 (29 cm). Its maximum daily OF is 12.87 cm. The OF events are relatively evenly distributed over the year, whereas the peak is in September (Appendix B.1). At the site Aichfeld-Murboden the maximum annual OF is in 2011 and 2017 (9 cm). The distribution over the year resembles a unimodal distribution with its peak in August (Appendix B.1). Although the cumulated percentage of precipitation for the 50 % and 95 % benchmark is nearly the same for both profiles, the differences in cumulated OF are decisive. Further results focus on the profiles in Elsbethen (EL) and Aichfeld-Murboden (AM). The sites show notable OF accumulation, as well as differences in their soil hydraulic parameters. Therefore, varied responses concerning their infiltration capacity can be expected.

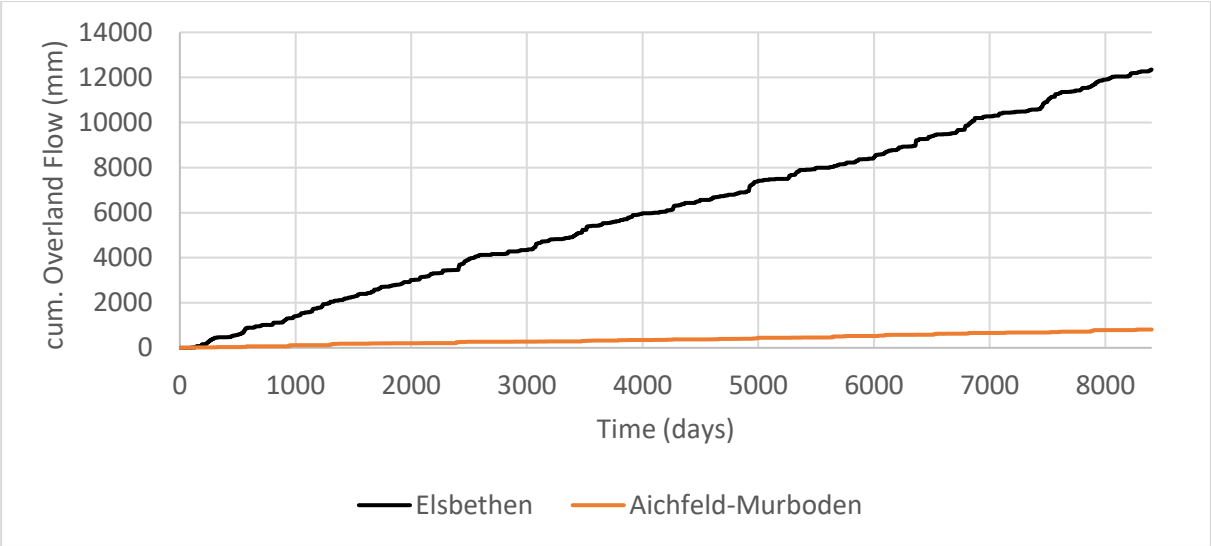

Figure 15: Cumulated overland flow for Elsbethen (black) and Aichfeld-Murboden (orange)

4.3 Precipitation Event Analysis

For the separation of the individual precipitation events for EL and AM, the MIT is set to 12 hours and a precipitation volume of 2 cm (AM) and 4 cm (EL). The required volume derives from the minimum volume of the daily OF events. Thus 198 events for EL and 282 events for AM can be separated.

Table 5: Precipitation events for Elsbethen and Aichfeld-Murboden separated by a certain MIT and volume. In a one-minute time resolution.

Rain Intensity (mm/min)	Elsbethen	Aichfeld-Murboden
light <0.04	180	228
moderat 0.04-0.125	15	48
heavy 0.125-0.83	3	6
violent >0.83	0	0

Both profiles show that after 6 hours of no precipitation, the water content can still have a not negligible effect on the next event. Even though some studies determine the maximum MIT at 24 hours (Dunkerley, 2008 and Lázaro, Arnau and Calvo-Cases, 2016), Bracken, Cox and Shannon, 2008, used a MIT of 12 hours between OF events which showed a sufficient effect on OF generation processes. Figure 16 and Figure 17 illustrate that even if the initial water content is not reached after a 12-hours dry period, it is assumed that (1) the initial condition would still not be attained after 24 hours (EL) and (2) that the decrease is sufficient for this simulation as the events are considered separately (AM).

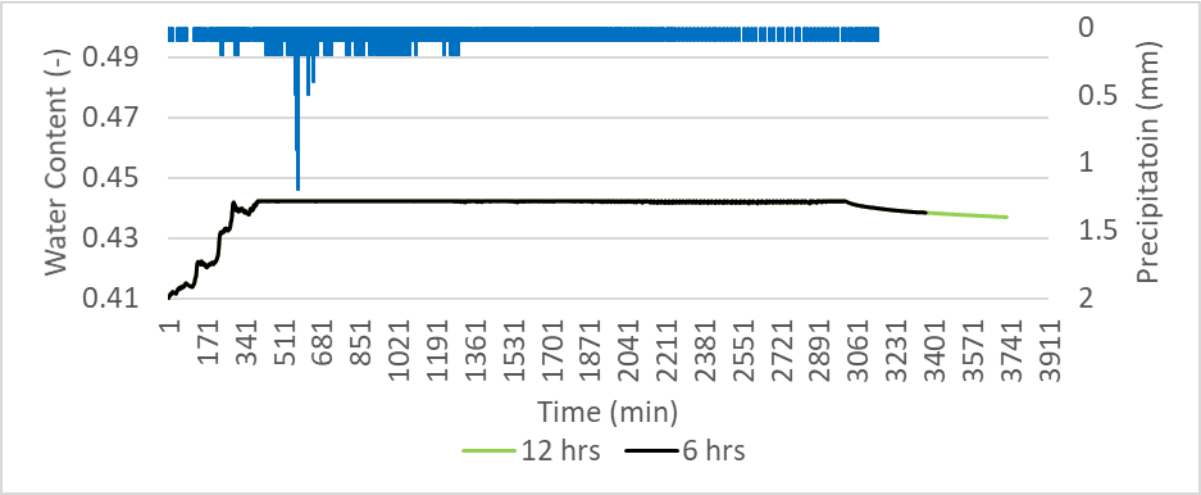

Figure 16: The water content is displayed resulting of a MIT in green (12 hrs) and black (6 hrs) for a precipitation event (blue) for the site Elsbethen.

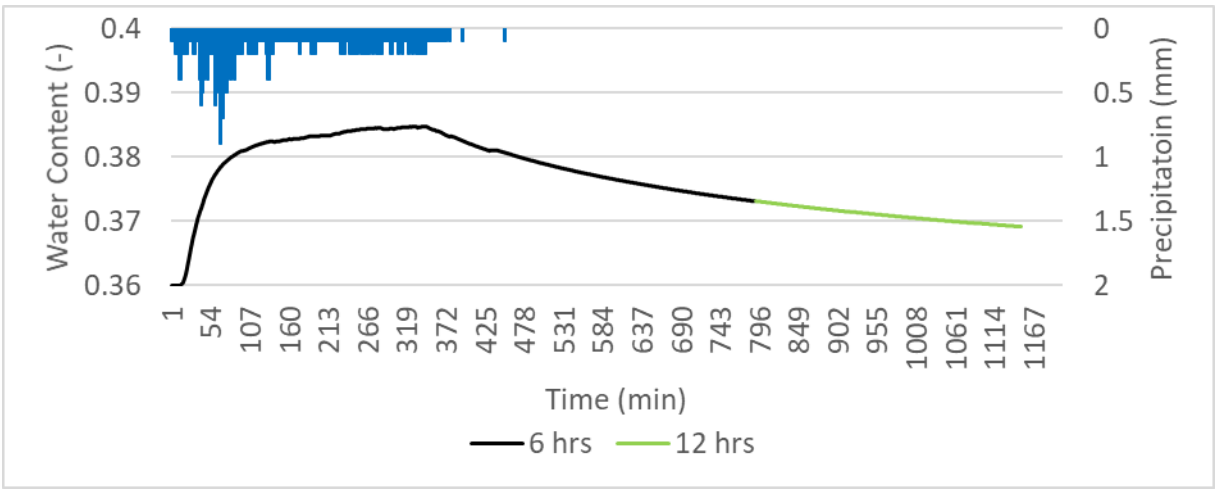

Figure 17: The water content is displayed resulting of a MIT in green (12 hrs) and black (6 hrs) for a precipitation event (blue) for the site Aichfeld-Murboden.

The MIT of 12 hours led to an increase of precipitation duration in 90 % and an increase of cumulated OF in 80 % of the events in EL (Figure 18). In AM, the event duration is reduced by 80 % and the cumulated OF increased by again 80 %. In both cases the higher temporal granularity of the input data, increased the generation of OF significantly, however, it showed differences concerning the deviation of event duration.

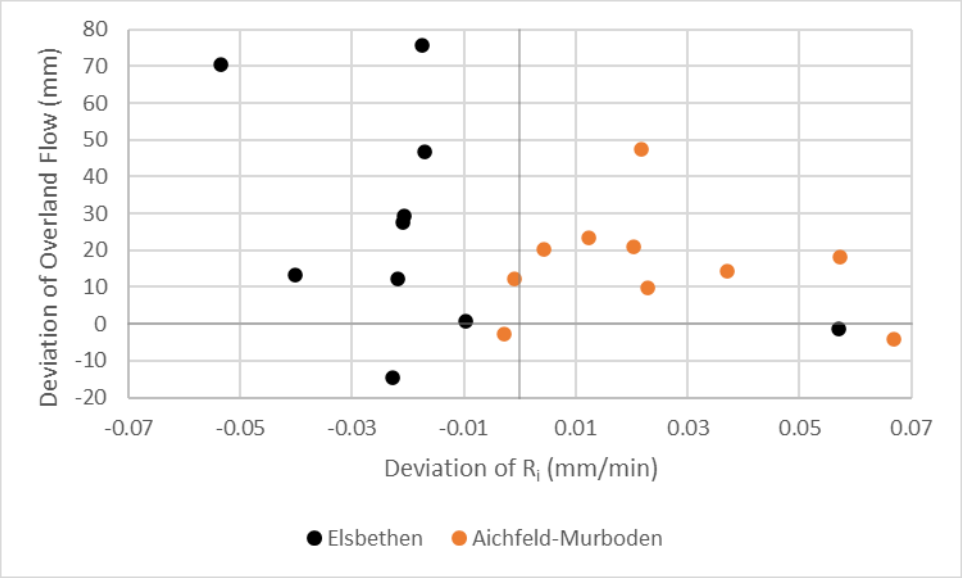

Figure 18: Deviation of overland flow compared with the deviation of Ri for Elsbethen (black) and Aichfeld-Murboden (orange).

4.4 Sensitivity Analysis

The sensitivity analysis is conducted for the profiles EL and AM. For each profile 10 individual precipitation events have been selected. As the Richards equation does not always provide satisfactory results under saturated conditions, convergence problems occurred. However they could be solved by applying the solution options introduced before.

4.4.1 Influence of Initial Water Content

Elsbethen

The influence of the initial water content on the initiation of OF is shown in Figure 19. The initial water content is differed for each precipitation event and is compared with the resulting cumulative OF. Furthermore, the mean value for all events is displayed. For EL, the mean value shows an increase of OF with rising initial conditions, until a θ of 0.415 is reached. This resembles a state, where 95% of the pore volume of the upper layer is filled with water. After this value, the mean curve falls until θ_s is attained. Compared with Figure 20, it is possible to describe the rise and subsequent fall of the curve in combination with the infiltrating waterfront over time when the initial water content is 0.164 for material 1 (M1) and 0.154 for material 2 (M2). Figure 20. is based on the 9th precipitation event (Appendix 7.1B.1.1), whereas the time period is separated into 10 equal sections. It is evident, that at a very low θ in both materials, M1 absorbs the water until a certain degree of saturation is reached. At the same time, M2 remains at its initial θ. As the k_s of M1 (20.21 cm/day) is much higher than in M2 (0.28 cm/day) the water movement is hindered, accumulates at the border, and increases the

hydraulic gradient to M2. When the θ of approximately 0.415 (M1) is reached, the infiltrating waterfront starts descending towards M2. As the waterfront overcomes the hydraulic gradient, the saturation of M1 also devolves into a saturation in M2 (Figure 20 at time step 2544 minutes). It can be said that the increase of the initial water content increases the contribution of M2 to the water absorption. The cumulative OF decreases if both materials reach a certain degree of saturation. In the first section (θ of 0.164-0.415) the OF generation depends on the soil hydraulic parameters of M1 and the impound properties of M2, whereas in section 2 it depends on M2. The boxplot (Figure 21) shows that the range between the first and third quartile concerning the runoff coefficient, is very low. With the initiation of deeper infiltration into M2, the range starts to increase. Outliers indicate the shift in infiltration, as the waterfront is hindered and the necessary hydraulic gradient is not yet reached (e.g., at a water content of 0.435).

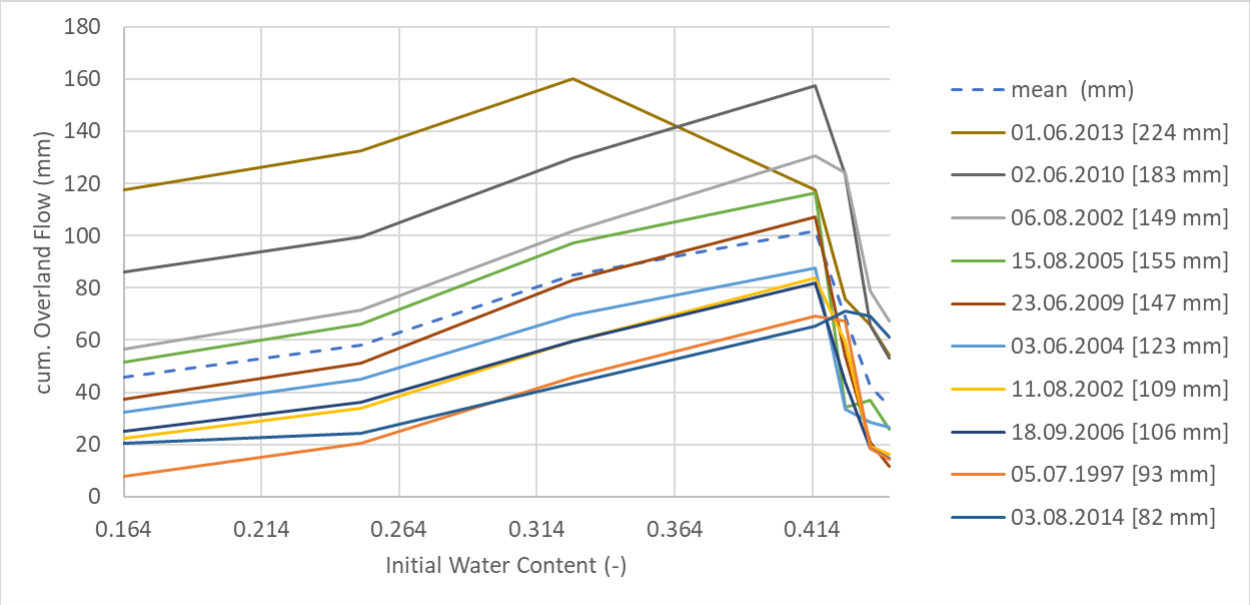

Figure 19: Cumulated overland flow generated with different initial water contents for the site Elsbethen. 10 different precipitation events are shown with each volume in brackets. The mean value is displayed by the dashed line.

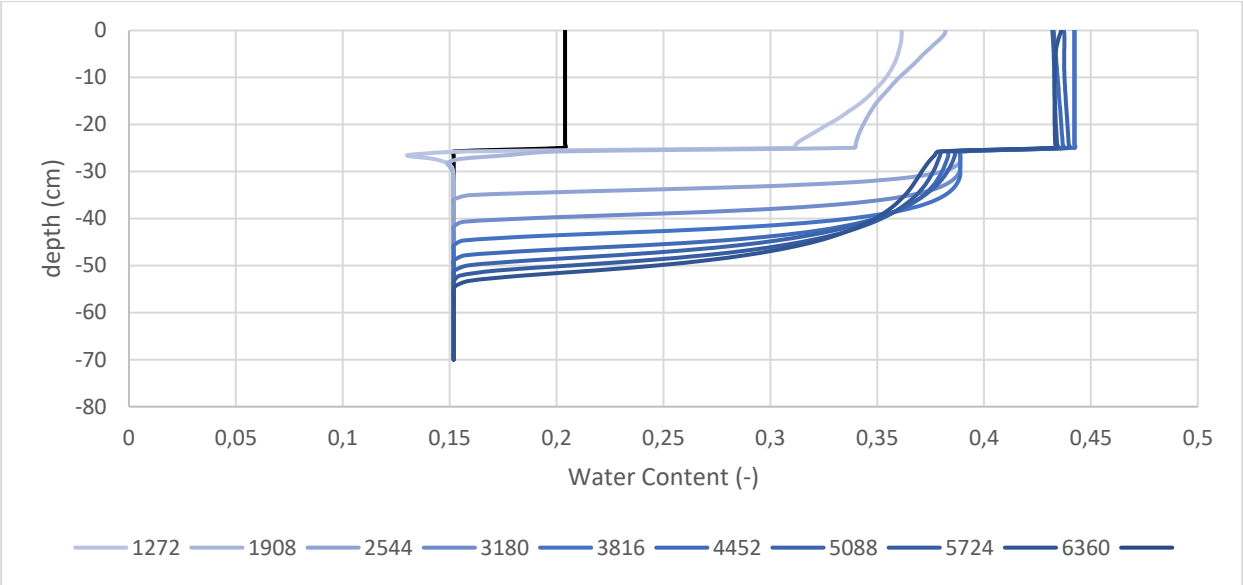

Figure 20: The water content displayed over the depth of the profile in 10-time steps. The initial water content is 0.164 for material 1 and 0.154 for material 2.

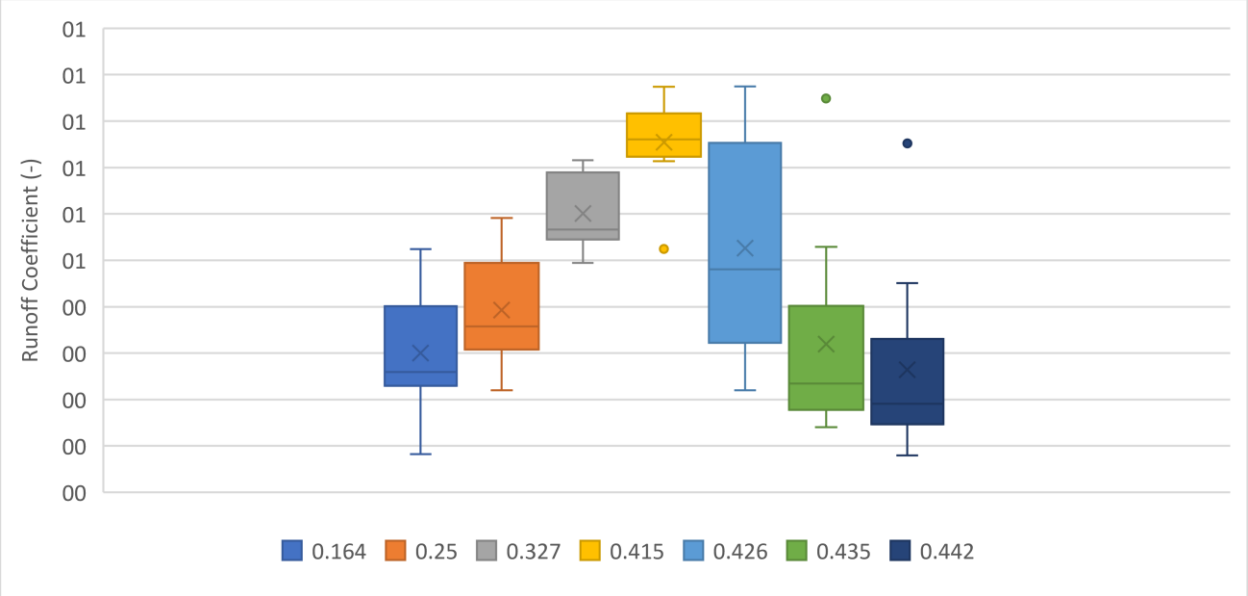

Figure 21: Box plot of the runoff coefficient with changing initial water content for Elsbethen

Aichfeld-Murboden

In contrast to EL the k_s for the upper layer is 3.07 cm/day and for the lower layer 43.93 cm/day. The increase of the initial conditions also shows an increase in OF (Figure 22). However, the slope of the individual lines starts flat and increases when a θ of approximately 0.242 is reached. In drier conditions, the simulation for the 24.07.2017 did not converge a satisfactory result and is therefore excluded. As stated in Figure 23 the infiltrating waterfront, starting at a very low initial θ, is only seen in M1, as the water infiltrates further into M2 does not rise the θ. The water is drained faster than it descends from M1. Figure 24 shows the infiltrating waterfront if the simulation is started under saturated conditions. As the initial condition in M2 is set to a maximum θ and still drains faster than it replenishes, the θ

decreases with progressing time. The overland flow generation is still dependent on M1 as the k_s determines the infiltration velocity.

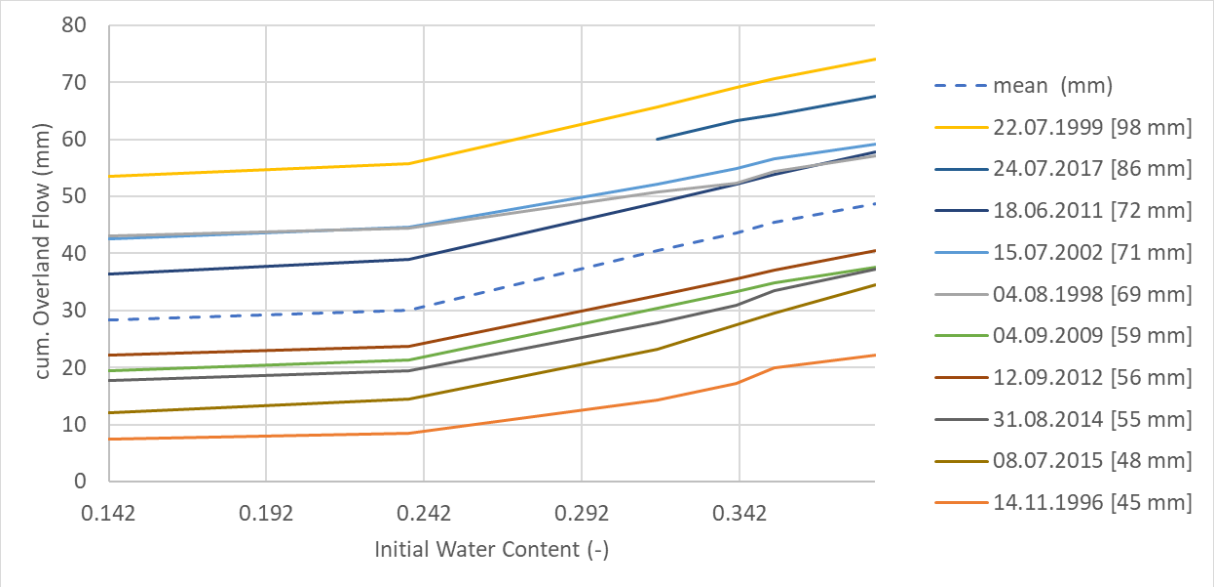

Figure 22: Cumulated overland flow generated with different initial water contents for the site Aichfeld-Murboden. 10 different precipitation events are shown with each volume in brackets. The mean value is displayed by the dashed line.

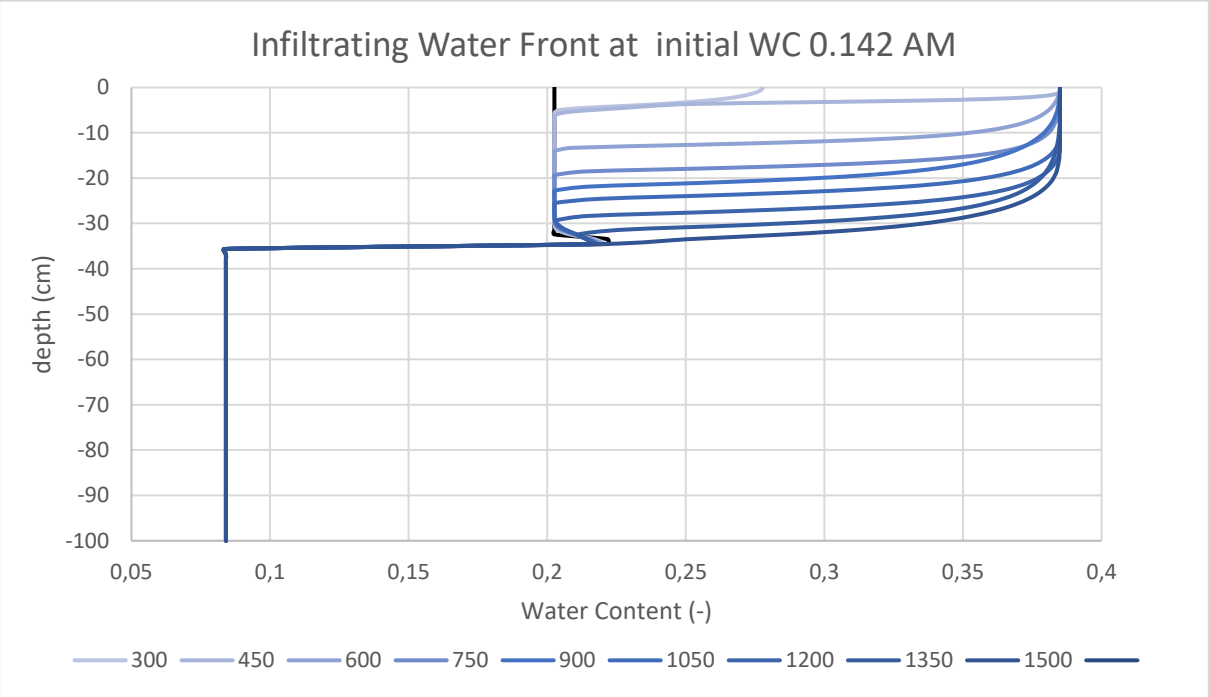

Figure 23: The water content displayed over the depth of the profile in 10-time steps. The initial water content is displayed under dry conditions.

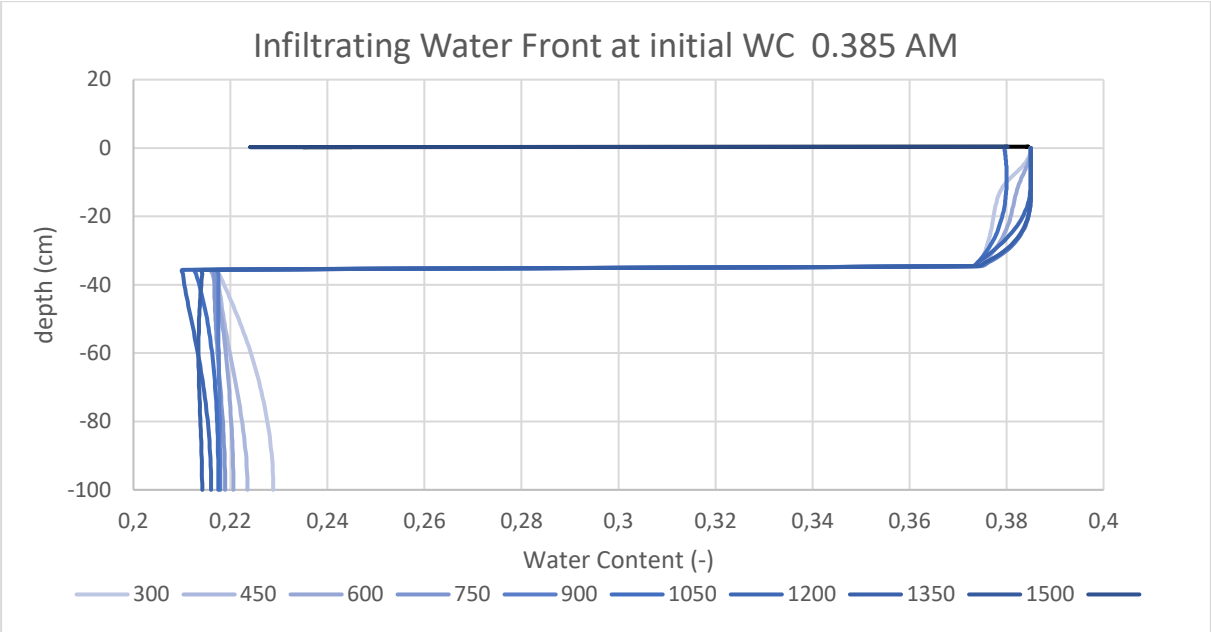

Figure 24.: The water content displayed over the depth of the profile in 10-time steps. The initial water content is displayed under saturated conditions.

The comparison of the runoff coefficient shows that with increasing initial water content, the deviation of φ decreases within the first and third quartile. The range of φ is very high for the initial values of 0.142 and 0.237. It can be said, that with increasing initial water content, the runoff coefficient gains significance.

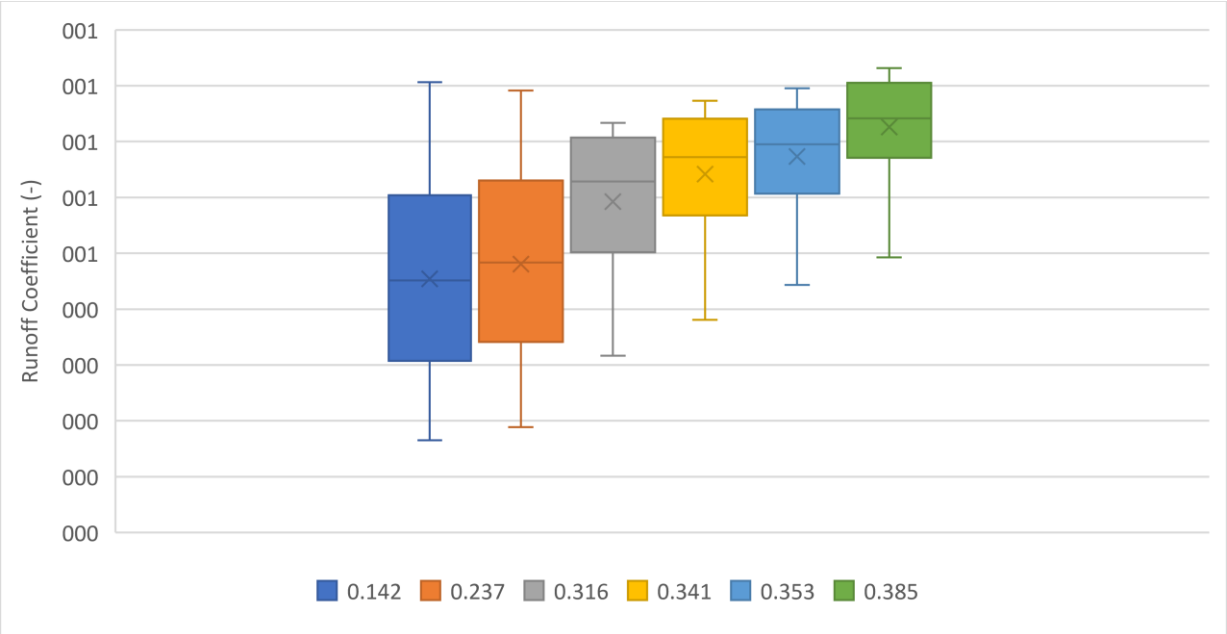

Figure 25: Box plot of the runoff coefficient with changing initial water content for Aichfeld-Murboden

4.4.2 Influence of Precipitation Intensity

Elsbethen

The three different rain events and their resulting OF based on the variation of R_i can be seen in Appendix 7.1B.1.2. The results show, that if the rain events are up and downscaled until the desired R_i is reached, the coefficient of determination equals 1. Therefore, the variation of R_i and its influence on the OF can be described as a linear function. The infiltration differences can be displayed by comparing the θ near the soil surface over time. The graph is based on the uniform precipitation event (Figure 26). Although the highest R_i induces the greatest increase of the θ, the drainage is also the highest, as an increase of θ simultaneously means an increase of k_u. It indicates that the higher the R_i, the faster θ_s is reached. Comparing the highest R_i (0.96) with the lowest (0.03) the first occurrence of OF is delayed by 20 min and the volume is decreased by 226 mm. Furthermore, the form of the Hyetograph, whether it is unimodal or multimodal, shows a similar curve form for very low R_i, where fluctuations in the θ are minor. The saturation proceeds uniformly. Figure 27 shows, that the form of the Hyetograph only has an influence on the first 5 cm of the soil profile and that further down the fluctuations of the θ are compensated. The results also show, that even if the first few cm are saturated, the θ_s is not reached throughout the profile. Therefore, the generated OF can be described as HOF.

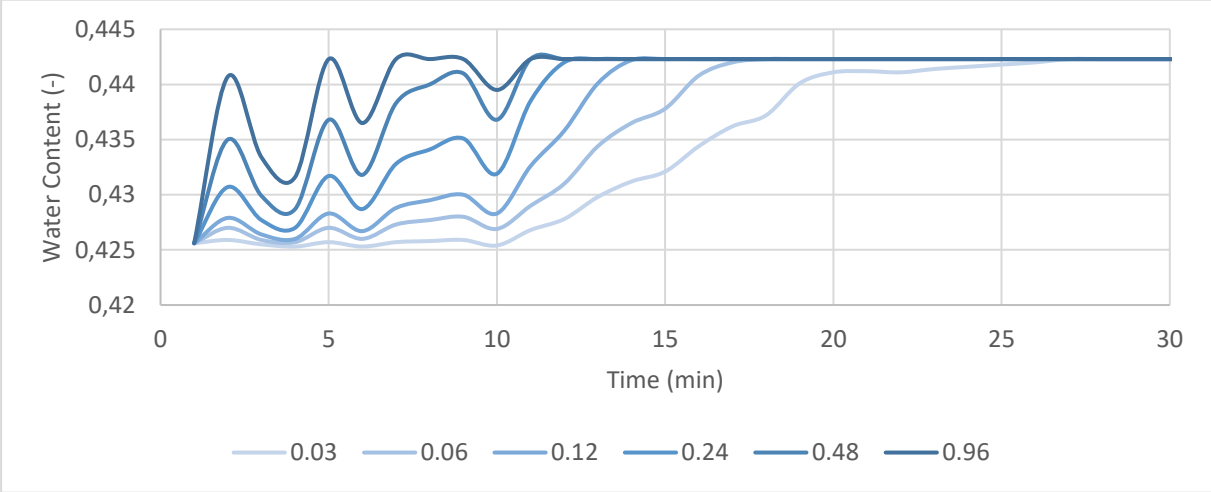

Figure 26: Water content displayed near the soil surface for different precipitation events and Ri over time for Elsbethen

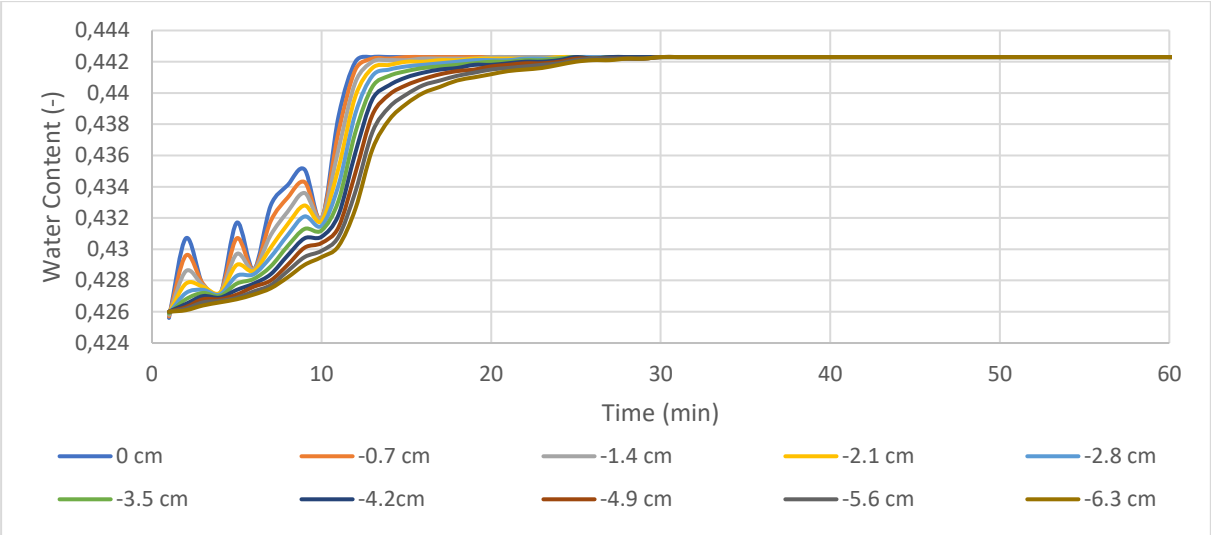

Figure 27: Water content displayed in 10 different depths near the soil surface over time for Elsbethen

Aichfeld-Murboden

The lowest R_i does not generate OF. Therefore, the difference from the highest R_i is compared to 0.06 mm/min. Again, the OF can be described as HOF, as the profile is not saturated throughout the precipitation event. Focusing on the uniform precipitation event, the occurrence of OF is only delayed by 2 min and the volume is decreased by 65.95 mm (Figure 28). The saturation process does not show high fluctuations, which compared to EL, may be due to differences in the Hyetograph. The infiltrating waterfront begins at a very steep slope for the first 2 cm of depth and continues at a slower pace in deeper horizons (Figure 29).

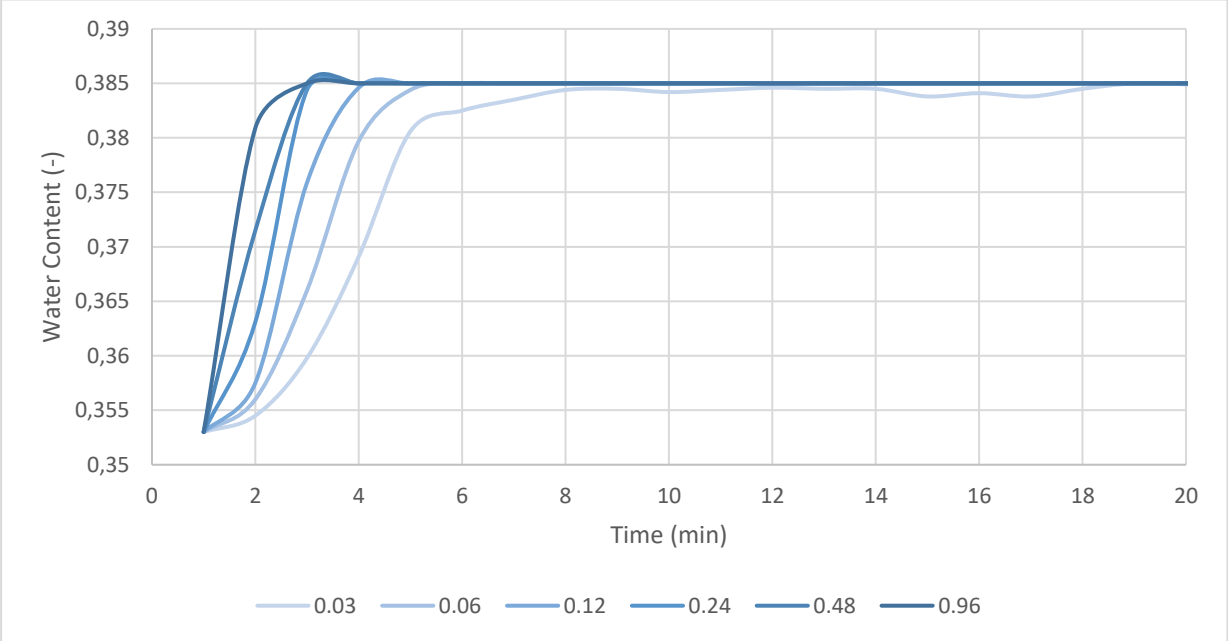

Figure 28: Water content displayed near the soil surface for different precipitation events and Ri over time for Aichfeld-Murboden

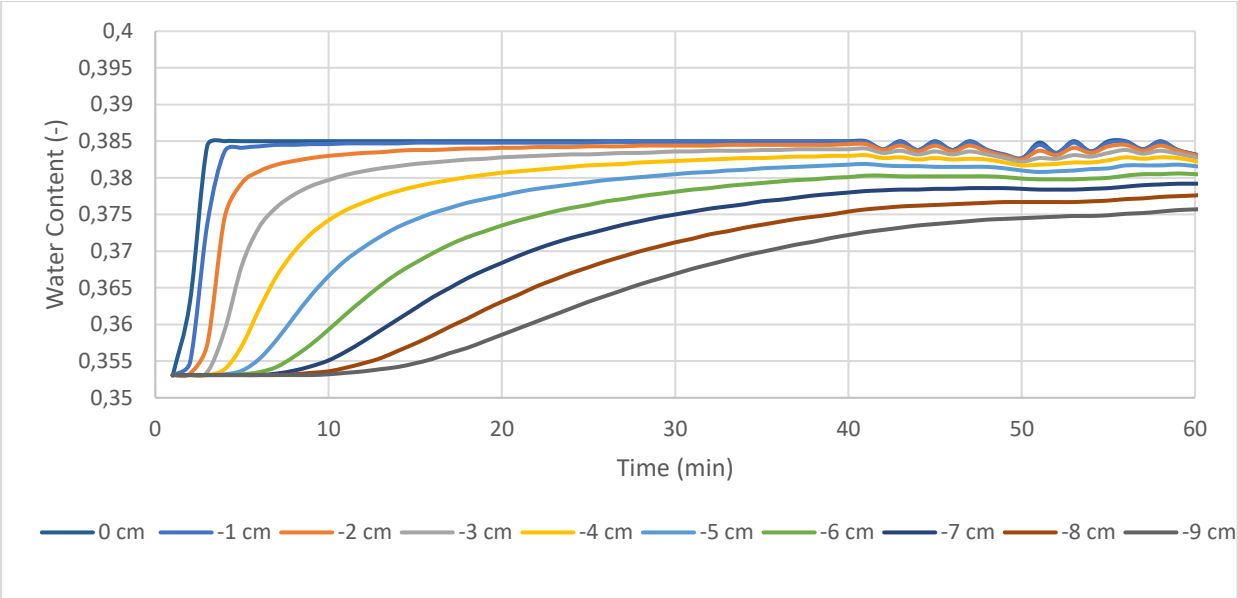

Figure 29: Water content displayed in 10 different depths near the soil surface over time for Aichfeld-Murboden

For the 10 precipitation events, without upscaling the intensity, it is still valid that the cumulated OF rises with higher R_i. The degree of determination rises (AM) with the number of events analysed. For the time resolution per minute, R^2 reaches values of 0.99 (EL) and 0.69 (AM). For the daily time resolution, R^2 reaches values of 0.95 (EL) and 0.87 (AM) (Figure 30and Figure 31).

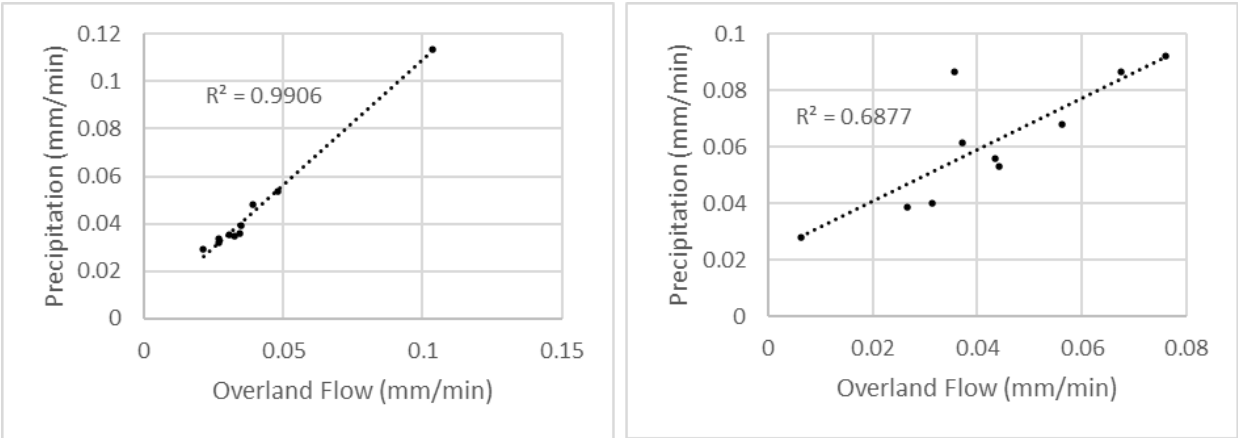

Figure 30: Influence of precipitation intensity on the generation of overland flow in a one-minute resolution. Left displays Elsbethen, right Aichfeld-Murboden

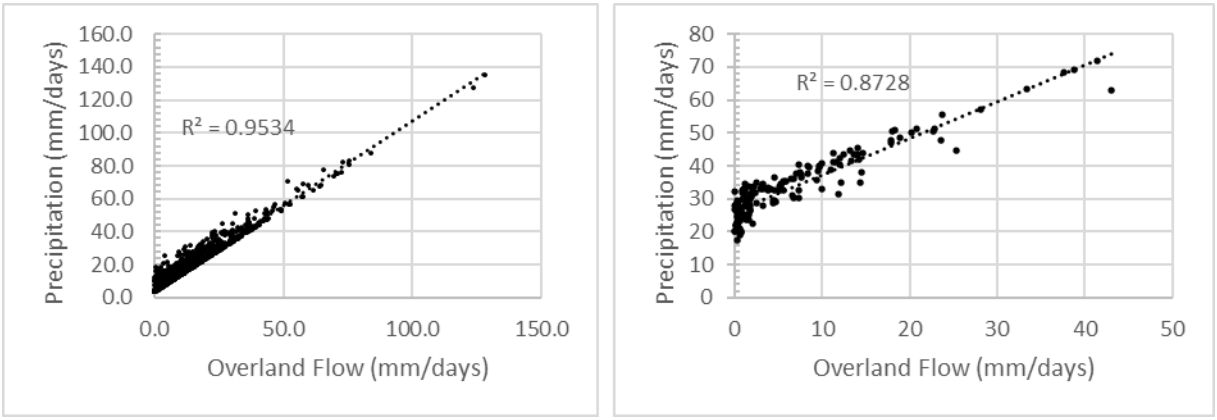

Figure 31: Influence of precipitation intensity on the generation of overland flow in a daily resolution. Left displays Elsbethen, right Aichfeld-Murboden

In both profiles, the curve describing the relation between the runoff coefficient and the R_i shows a steep increase at light and moderate R_i and aligns with nearly 1 when heavy and violent events are predominant.

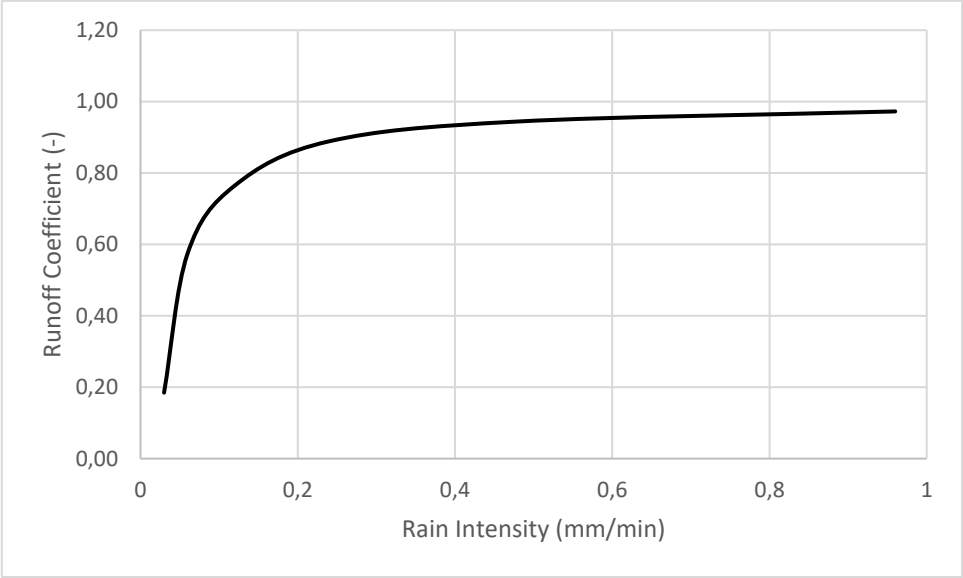

Figure 32: Runoff coefficient compared to Ri for Elsbethen

4.4.3 Influence of Slope

The deviation of OF describes the difference of the cumulated OF generated with a horizontal soil profile and the cumulated OF with an inclined soil surface. The results for EL show that the deviation with increasing slope, is almost negligible. The highest deviation is for the event on August 15, 2005 with 1.5 mm (35°). Similar results are attained with the profile in AM. Although the profiles have different soil hydraulic parameters and precipitation events, the range of the deviation is nearly identical and negligible (Figure 33). Further 2D analysis will help to prove the quality of the output function of HYDRUS-1D.

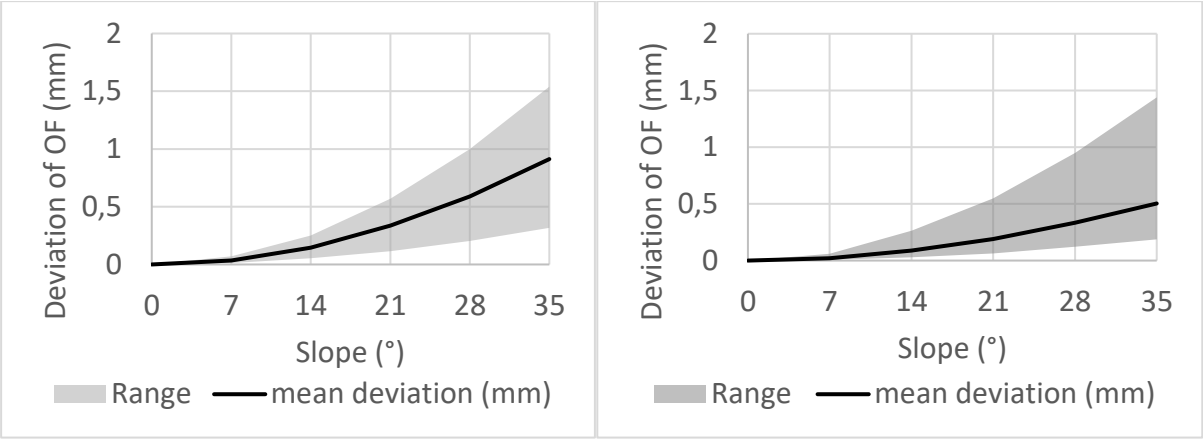

Figure 33: Deviation of cumulated overland flow depending on an increasing slope compared to a horizontal profile. Left: Elsbethen, right: Aichfeld-Murboden

4.5 Comparison of Sites

9 out of 13 profiles showed that by increasing the time resolution of the precipitation events, even profiles without any OF generation over the time period of 23 years, showed a significant response to the precipitation event with a R_i of 0.12 mm/min (Figure 34). The precipitation event with a volume of 28.9 mm caused OF in the range of 5.8 mm (Lauterach) to 26.5 mm (AM). The correlation of cumulated OF and k_s (Figure 35 left) illustrates that although there is a relation, the degree of determination is only 57 %. According to the correlation analysis, there is no interdependency of humus or clay content (Figure 35 and Figure 36) in the top layer and OF generation. Additional analysis of further precipitation events would be necessary to expand the significance of the correlation.

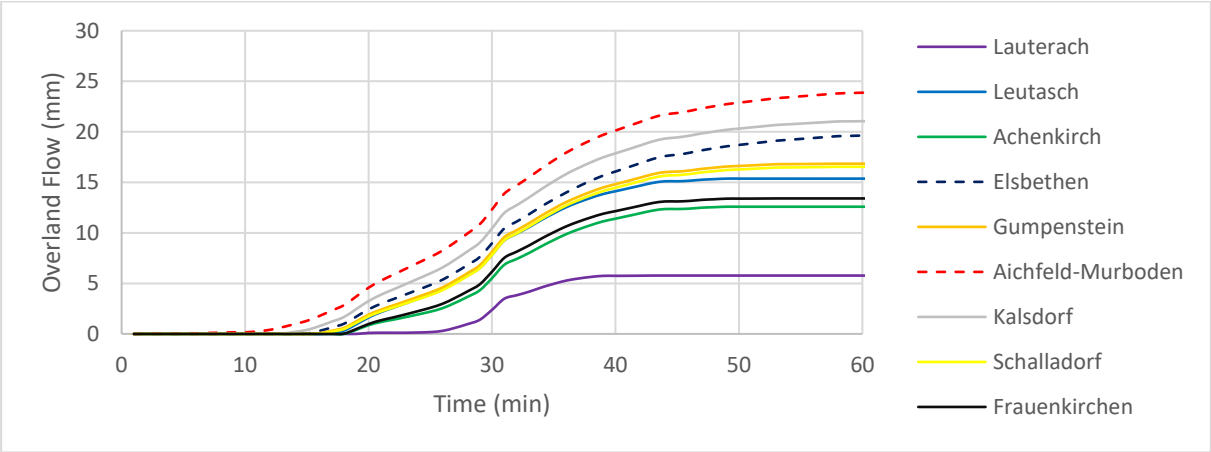

Figure 34: Overland flow generation of the sites in the first hour of simulation for a precipitation event with a Ri of 0.12 mm/min

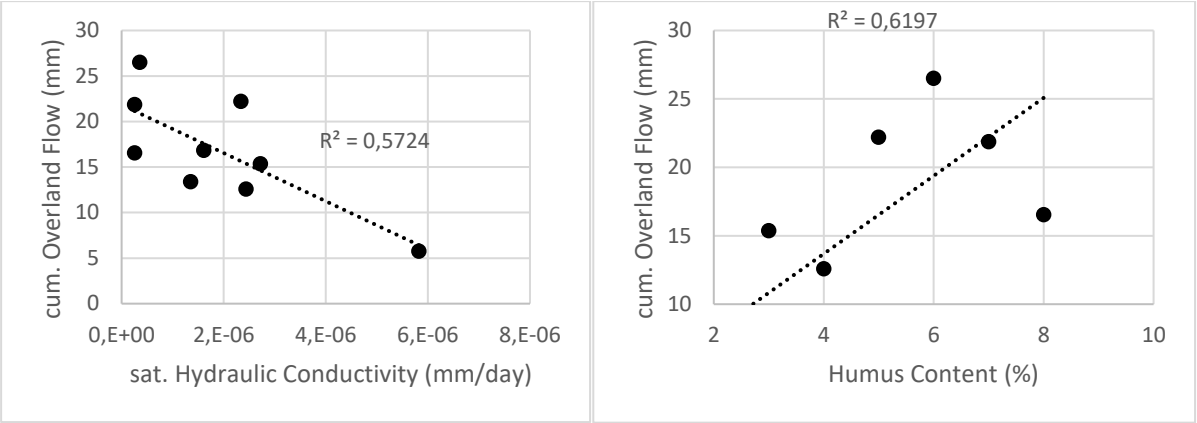

Figure 35: Cumulated overland flow and its relation to the saturated hydraulic conductivity (left) and humus content (right)

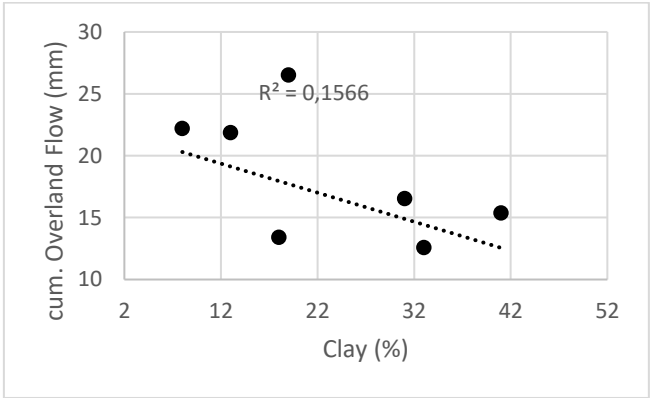

Figure 36: Cumulated overland flow related to clay content in the upper layer

4.6 Climate Scenarios

4.6.1 Elsbethen

The sum of predicted OF for the scenarios (1) very wet, (2) wet, (3) moderate and (4) dry is shown below. As the scenarios of ÖKS also include the time span from 2050 until 2075, the simulated period is expanded. As one can see in Figure 37, the cumulated OF shows high differences concerning each scenario. The range spans from 3075 mm to 42917 mm, accumulated in 50 years. The dotted line indicates the most likely course of climate change at the station. Compared to the amount of 12300 mm of OF generated within the years between 1996 until 2018, the OF would rise by at least 2.5 times in double the time (50 years). By doubling the OF from the past period, the scenarios very wet and station exceed the previous amount. Whereas the dry and moderate scenario show a similar trend, the other three indicate a steady but much higher rise.

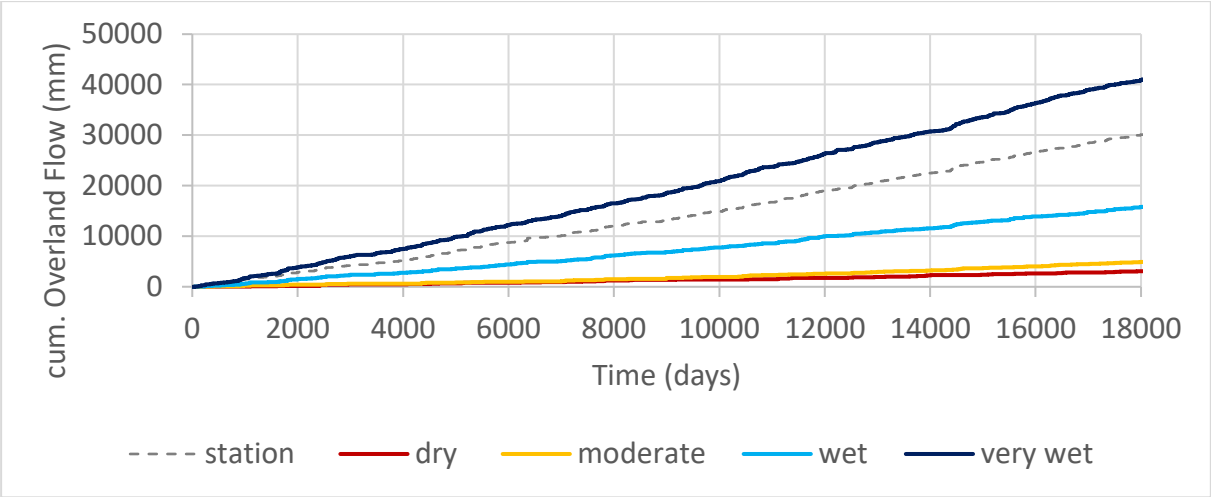

Figure 37: Cumulated overland flow for the scenarios: station, dry, moderate, wet, and very wet in Elsbethen

4.6.2 Aichfeld-Murboden

The response of the profile in AM to the different scenarios is visible in Figure 38. In contrast to EL, the range of cumulated OF spans from 1072 mm to 6870 mm. For the very wet scenario this would mean cumulative OF values considerably less than in EL. Again, under dry and moderate conditions, the output function proceeds very similar. The deviation in total amounts to 67 mm. Unlike in EL, the scenarios wet and station show a similar curve progression, with a deviation of cumulated OF of 416 mm. In contrast to the OF from the past period to the predicted scenarios, only the dry and moderate pathways would not exceed the value, if projected for 50 years.

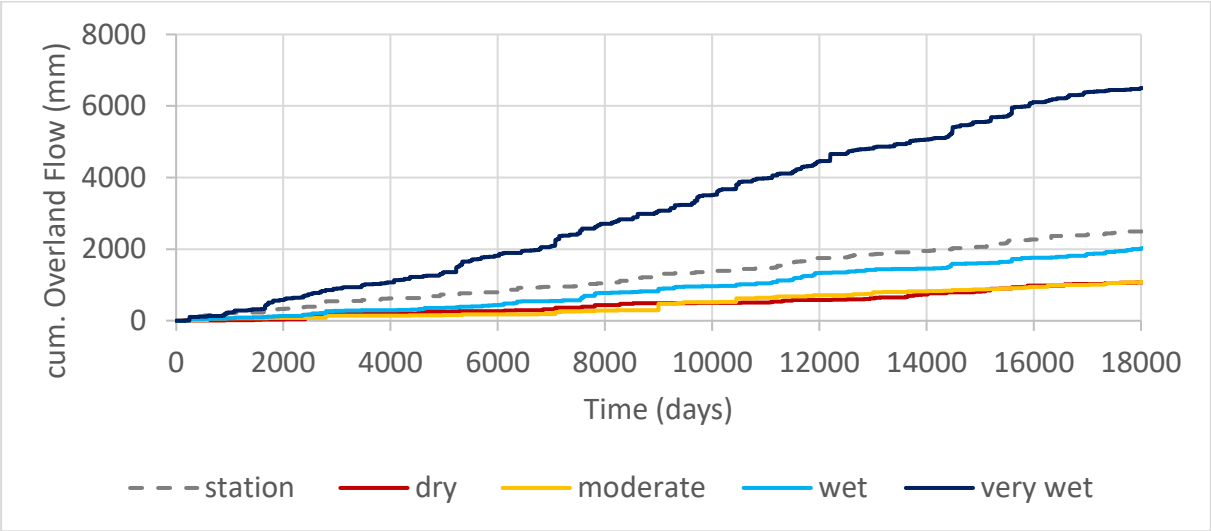

Figure 38: Cumulated overland flow for the scenarios: station, dry, moderate, wet, and very wet in Aichfeld-Murboden

The varying reaction to the scenarios for the two stations is displayed in Figure 39. The curve for AM shows an almost uniform and moderate rise, whereas EL shows a rather high increase starting from scenario 3.

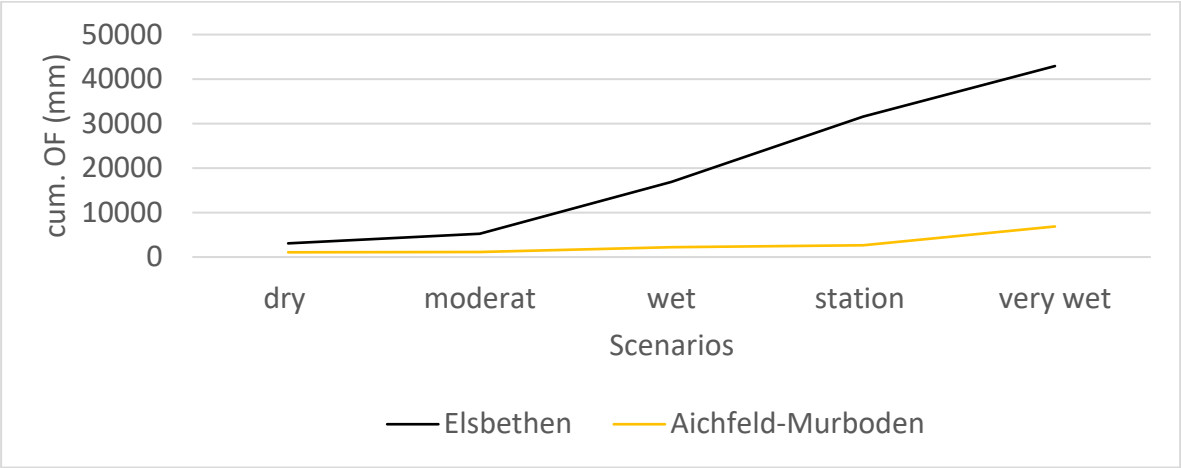

Figure 39: Comparison of the different scenarios at Elsbethen (black) and Aichfeld-Murboden (orange)

4.7 Overland Flow Analysis

The OF is displayed by the water depth over time over a length of 100 m, whereas the observation points are set at 20, 40, 60, 80 and 100 m. Figure 40 shows the water depth for the OF event from August 4, 1998 at AM at the end of the profile (100 m). The precipitation event is displayed in a time span of 200 min and the volume amounts to 524 l (at a slope of 14°) and 525 l (at a slope of 35°), as the infiltration is already abstracted from the precipitation event conducted in the previous simulation. Consequently, the average outflow of the 100 m field strip per meter is 0.0437 l/s (14°) and 0.0438 l/s (35°). As the flow velocity increases with increasing slope, the water depth declines. As a consequence of the even distribution of precipitation over the whole length, the OF at 35° is only slightly tilted to the left, as the water flows faster down the slope. However, the extension of HYDRUS-1D falls short of expectations, as the water flow can only be simulated over impervious surfaces. To further expand the simulation a two dimensional approach should be pursued, where again the infiltration processes are included.

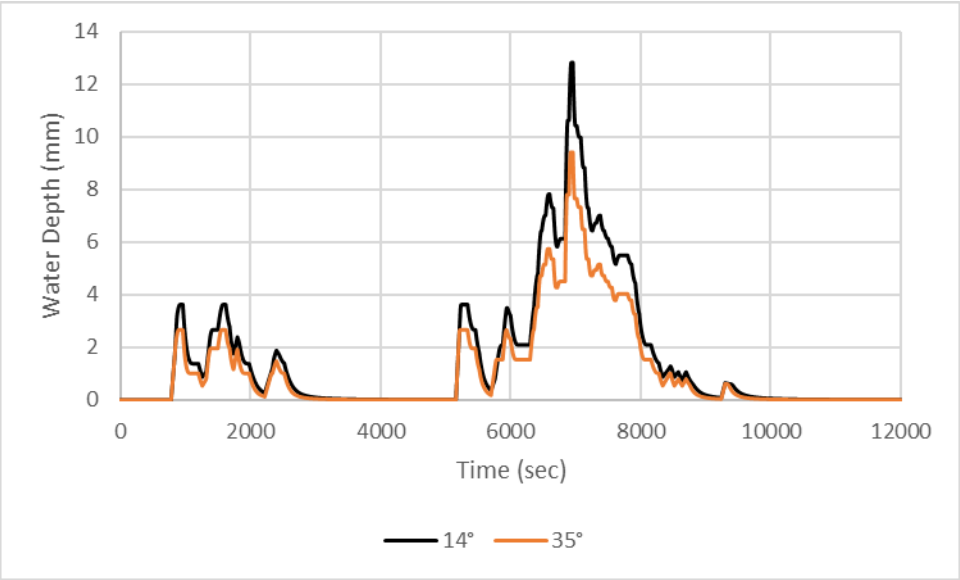

Figure 40: Water depth over time at the end of the profile (100 m) at a slope of 14° (black) and 35° (orange)

5. Discussion and Conclusion

5.1 Input data

5.1.1. Humus Content

The results of the input data evaluation show that based on different simulation approaches, the ks values indicate a wide variation, which may restrict the significance of the output function. Based on the program Rosetta, which provides data of pedotransfer functions and further estimates of WRC and HCC (Schaap et al., 2001), Kammerer (2012) derived ks values as implementation in the texture triangle Thus, as the ks values are only estimates for typical soils, it can be expected that laboratory measurements and subsequent model calibrations show decisive differences. As Rosetta does not consider humus content, which, however, is exposed to continuous changes, a possible correlation to deviations in k_s values cannot be clearly established. Humic substances exhibit hydrophobic as well as hydrophilic properties. Especially under very dry conditions and heat, hydrophobic properties become predominant (Haslmayr, 2021). Therefore, as thunderstorm season is in the summer months, the humus content should not be neglected in pluvial flood studies.

5.1.2. Temporal Resolution

Almost every site shows generation of OF for the simulated time period. The time resolution of the precipitation input data shows significant differences concerning the length of the events and thus the rain intensities. Whereas the events in Elsbethen cumulate more OF induced by events with less rain intensities, Aichfeld-Murboden cumulates again more OF, however, at greater rain intensities . Thus, the simulation with daily input data underestimates the cumulated OF at both sites. As the precipitation is summed up for daily input resolution requirements, rain intensities of short duration events are falsely displayed. The site comparison, simulated with a precipitation event with high Ri and short duration, indicate similar results, as sites with nearly no OF generation over 23 years, generate not negligible OF. A decrease in temporal resolution also results in an increase in deviations of overland flow compared to the highest resolution (Ward *et al.*, 2018). As R_i play an essential role in OF generation, high resolution data is required to sufficiently analyse the other sites. For layers which diminish the percolation, like in Elsbethen, the MIT should be set to a maximum (24 hrs) as previous precipitation events can influence the initial water content and subsequently the predominant initial hydraulic conductivity. Further studies concerning a possible relation between the MIT and the hydraulic conductivity are outstanding.

5.2 Generation of OF

5.1.3. Site Comparison

The generation of OF varies highly at the different sites, as it was expected. The lowest values occur in the east of Austria, including Frauenkirchen, Schalladorf and Pettenbach. The ks values vary, as the associated humus content shows very low values for Frauenkirchen and very high values for the other two sites. The site characteristics of Schalladorf and Pettenbach would actually indicate a rather high OF generation, because of the very low ks value and the high humus content of these two sites. However, they show one of the lowest amounts of OF. A possible explanation could be the rather low R_i for both sites. It can be expected that the R_i does not exceed the infiltration capacity. The site of Gschlössboden exhibits the highest precipitation volume (4803 cm in 23 years) and the highest Ri, however, as it also has the highest ks value, it does not show any OF generation. Overall, it can be said, that site characteristics, paired with precipitation characteristics can provide an important first assessment for the expected OF. However, laboratory measurements for the exact particle size distribution, as well as the humus content, should not be neglected, especially because eBOD data may not represent the site characteristics properly. Field measurements and further calibration of the VGM parameters are essential to display soil hydraulic properties and initial conditions. Nonetheless, (i) soil characteristics (e.g., heterotrophy, anisotropy, preferential flow paths, etc.), (ii) measurement device errors (e.g., bad calibration, installation, etc.) and (iii) measurement value errors (e.g., systematic, and stochastic errors) can falsify field measurements (Albert *et al.*, 2020). Thus, a validation is crucial. Within the project RechAUT all sites were validated in form of groundwater recharge studies. Still, a validation of OF could not be implemented, as the measurement stations do not provide corresponding measurement devices.

5.1.4. Sensitivity Analysis

For both sites – Elsbethen and Aichfeld-Murboden - the sensitivity analysis results were displayed using the runoff coefficient as comparative value.

Elsbethen

In Elsbethen, the low ks value of material two, compared to material one, decisively influences the OF generation. Results for the variation of initial water content show, that with increasing values the OF and thus the runoff coefficient increase until a certain degree of saturation is reached (Fig 24). The range of φ is highest when the waterfront starts to descend into material 2 as the different precipitation events reach the necessary saturation at different time steps. It can be said that the water content in material 2 determines the containment of possible OF events. If the mean value of φ is used, the OF will be most certainly overestimated under very dry and saturated conditions. The event with

the highest precipitation volume, reaches its maximum OF generation at a lower water content compared to the other 9 events. This could be a possible consequence of higher ponding elevations on the soil surface resulting in higher hydraulic gradient differences and consequently earlier percolation into material 2. Or as Castillo et al. (2003) states: The impact of the initial water content on the OF generation is high when R_i is low and vice-versa. The results in the variation of R_i would prove this hypothesis, as higher intensities reach similar values for φ, whereas lower R_i (0.1 – 0.3 mm/min) show a wider range. Compared with the field experiment, conducted by Mu *et al. (*2015), the generation of OF due to different R_i showed similar results. Therefore, the OF simulation of HYDRUS-1D can be considered as significant.

Infiltrating water did show fluctuations effecting only the first 3 cm of the soil profile. This implicates that the initial conditions of the first centimetres are decisive for OF generation. However, the simulation of the first centimetres of a soil profile is affected by errors, as the soil is highly influenced by erosion, compaction, anthropogenic forces, weathering etc. OF increases with increasing R_i under the same initial conditions.

The influence of slope does not show any significant results concerning differences in cumulated OF. Beside the 1D approach, the 2D expansion of HYDRUS does not deliver any significant simulation results. Although the OF is displayed over an impermeable surface, differences in water depth can be displayed and further analysed.

Aichfeld-Murboden

As both layers in Aichfeld-Murboden are characterized with a rather high permeability, the variation of initial water content led to an increase of OF. As there is no layer which hinders percolation, the results can be compared to Meißl *et al.* (2021). The deviation of φ decreases with increasing initial water content, as nearly 80 % of precipitation are derived into OF. The simplification of Markart *et al.* (2011) would overestimate the OF if applying low initial values of water content. Compared to HYDROBOD II, where very dry conditions would imply values lower than 25 % of the total measured values (= moderate at this simulation), the condition very dry and dry could be classified as one, as φ does not show significant differences. Again, the variation of R_i showed the same influence on the runoff coefficient. The layer distribution and the ks values, however, would imply a different curve form as in Elsbethen. This underlines the results, that high R_i do not depend on initial conditions or soil hydraulic properties. The increase of R_i showed again a linear increase in OF, which could be ascertained by Nassif and Wilson (1975). However, the results for the variation of slope did not show any resemblance.

Climate Scenarios

High differences in OF can be seen when analysing the four scenarios at both stations. The soil hydraulic properties of Aichfeld-Murboden indicate that even if the very wet scenario occurs, the amount of OF cumulated in 50 years would be considerably low. The expected pathway directly located at the station would still mean an increase of 1 m allocated over the years. However, compared to Elsbethen, this would still be negligibly small. Because of the nearly impermeable second layer, the

scenarios wet, station and very wet would make a huge difference of up to 42 m over a time span of 50 years. As these profiles are validated concerning groundwater studies, the results cannot be taken over directly in the context of the implementation of climate change in OF prediction studies. However, the trend directly predicted at the station, underlines the necessity of further OF analysis connected with climate change scenarios, since Elsbethen for example shows an alarming trend.

In conclusion it can be said that:

- The temporal resolution of input values, especially for precipitation, should be carefully chosen, as the parameters R_i and subsequently initial water content are heavily influenced.

- The runoff coefficient is dependent on the initial water content, but it can vary greatly in case of a nearly impermeable deeper layer. If the properties of different layers are evenly balanced, and there is no layer which diminishes percolation, the runoff coefficient increases with increasing water content and gains significance.

- The correlation of R_i and cumulated OF amounts to approximately 1. The runoff coefficient related to increasing R_i shows a significant growth. This indicates that higher R_i are less dependent on antecedent site conditions, whereas at lower R_i the knowledge of antecedent conditions is advantageous.

- Climate scenarios show an increasing trend of OF for both profiles (=station). Climate change predictions should therefore be included in OF mitigation measurements.

- As precipitation data was evaluated in a one-minute time resolution, a lack of transpiration data was a consequence. Root water uptake, however, can have a huge impact, especially if the time assessment of precipitation events is expanded. Heavy storm events often do only influence the first few centimetres of a soil profile and short duration does not always require a correct display of root water uptake.

- Humus content can have a huge impact on the hydrophobicity of the soil surface. However, soil properties were only displayed once. Therefore, possible changes in humus content are not displayed properly and soil hydraulic properties could have been changed over time.

6. Outlook

The analysis of the generation of overland flow for all profiles was conducted, in order to provide an initial classification, especially for the profiles Elsbethen and Aichfeld-Murboden. To further analyse soil physical parameters, topographical properties and precipitation characteristics and their influence on the generation of pluvial floods, the 1D approach needs to be expanded into 2D modelling simulations. Some international and national modelling approaches have already gained acknowledgement, as for example RAINMAN (Heiland *et al.*, 2020), RoGeR (Steinbrich Andreas et al., 2021), a simple code of practice (Markart *et al.*, 2011), HYDROBOD I and II (Sotier *et al.*, 2017) and many more. The results for the sensitivity analysis has shown, that simplification for the runoff coefficient introduced by Markart *et al.*, 2011 may suffice, however can sometimes overestimate the overland flow generation. Other models use the Green-Ampt-Method to display the infiltration process throughout the precipitation event. Either way, the knowledge of initial conditions, in respect to antecedent water content and slope, as well as precipitation characteristics are of utmost importance. As pluvial floods have only moved into focus recently, historical data is very rare. Therefore, to improve model validation purposes, further overland flow measurement device installation are crucial to diminish pluvial flood uncertainties.

7. Danksagung

8. References

Achleitner, S. *et al.* (2020) 'Pilotstudie Oberösterreich. Modellierung von Starkregen-Oberflächenabfluss/Hangwasser. leitfaden', pp. 1–28.

Albert, B. *et al.* (2020) 'Wasser im Boden. Sammelband zur quantitativen Erfassung und Auswertung bodenphysikalischer Größen anlässlich 25 JAhre Bodenwasserbeobachtung', *Bundesministerium für Landwirtschaft, Regionen und Tourismus*, p. 226.

Allen, R. G. *et al.* (1998) *Crop evapotranspiration - Guidlines for computing crop water requirements - FAO Irrigation and drainage paper 56*.

Austrian Standards Institute (2004a) 'ÖNORM L 1055. Probenahme von ackerbaulich genutzten Böden'.

Austrian Standards Institute (2004b) 'ÖNORM L 1056. Probenahme von Dauergrünland (inklusive Parkanlagen, sowie Zier- und Sportrasen)'.

Austrian Standards Institute (2013a) 'ÖNORM L 1061. Grundlagen zur Bodenfunktionsbewertung'.

Austrian Standards Institute (2013b) 'ÖNORM L 1076. Grundlagen zur Bodenfunktionsbewertung'.

Austrian Standards Institute (2016) 'ÖNORM L 1050. Boden als Pflanzenstandort - Begriffe und Untersuchungsverfahren'.

Becker, A. (2019) 'Extremer Niederschlag im Klimawandel - Was wissen wir?', *WasserWirtschaft*.

Bolt, G. H. *et al.* (1976) 'Soil physics terminology', in *Bull Int Sci 49*, pp. 26–35.

Bracken, L. J., Cox, N. J. and Shannon, J. (2008) 'The relationship between rainfall inputs and flood generation in south-east Spain', *Hydrological Process*, 22, pp. 683–696. doi: 10.1002/hyp.

Brooks, R. H. and Corey, T. (1964) *Hydraulic Properties of Porous Media*, *Hydrology Papers Colorado State University*.

Brunetti, G., Šimůnek, J. and Bautista, E. (2018) 'A hybrid finite volume-finite element model for the numerical analysis of furrow irrigation and fertigation', *Computers and Electronics in Agriculture*, 150(February), pp. 312–327. doi: 10.1016/j.compag.2018.05.013.

Bundesministerium für Landwirtschaf, R. und T. (2020) 'Bemessungsniederschlag 2020', p. 2021. Available at: https://ehyd.gv.at/.

Bundesministerium für Nachhaltigkeit und Tourismus (2019) *Eigenvorsorge bei Oberflächenabfluss. Leitfaden für Planung, Neubau und Anpassung*.

Carter, A. C. (1950) 'Angle of repose of noncohesive material', *Journal of Chemical Information and Modeling*.

Castillo, V. M., Gómez-Plaza, A. and Martínez-Mena, M. (2003) 'The role of antecedent soil water content in the runoff response of semiarid catchments: A simulation approach', *Journal of Hydrology*, 284(1–4), pp. 114–130. doi: 10.1016/S0022-1694(03)00264-6.

Cerdà, A. (1997) 'Seasonal changes of the infiltration rates in a mediterranean scrubland on limestone', *Journal of Hydrology*, 198(1–4), pp. 209–225. doi: 10.1016/S0022-1694(96)03295-7.

Chen, A. S. *et al.* (2010) 'An analysis of the combined consequences of pluvial and fluvial flooding', *Water Science and Technology*, 62(7), pp. 1491–1498. doi: 10.2166/wst.2010.486.

Chimani, B. *et al.* (2016) *Endbericht. ÖKS15|Klimaszenarien für Österreich. Daten-Methoden-Klimaanalyse*, *CCCA Data Centr*. doi: 10.3726/978-3-653-02922-2/2.

Chow, V. Te (1959) 'Open-Channel Hydraulics', *McGraw-Hill Civil Engineering Series*.

Dunkerley, D. (2008) 'Identifying individual rain events from pluviograph record: a review with analysis of data from an Australien dryland site', *Hydrological Process*, 22, pp. 5024–5036. doi: 10.1002/hyp.

Dunne, T. and Black, R. D. (1970) 'Partial Area Contributions to Storm Runoff in a Small New England Watershed', *Water Resources Research*, 6(5), pp. 1296–1311. doi: 10.1029/WR006i005p01296.

Eybl, J., Godina, R. and Weilguni, V. (2018) 'eHYD - Messstellen und Archivdaten der Hydrographie Österreichs', *Bundesministerium für Nachhaltigkeit und Tourismus*.

Feddes, R. A. (1980) 'Simulation of Field Water Use and Crop Yield', *Soil Science*. doi: 10.1097/00010694-198003000-00016.

Foreman-Mackey, D. *et al.* (2013) 'emcee : The MCMC Hammer ', *Publications of the Astronomical Society of the Pacific*, 125(925), pp. 306–312. doi: 10.1086/670067.

van Genuchten, M. T. (1980) 'A Closed-form Equation for Predicting the Hydraulic Conductivity of Unsaturated Soils', *Soil Science Society of America Journal*, 44(5), pp. 892–898. doi: 10.2136/sssaj1980.03615995004400050002x.

Glade, T., Mergili, M. and Sattler, K. (HG. . (2020) *ExtremA 2019. Aktueller Wissensstand zu Extremereignissen alpiner Naturgefahren in Österreich*, *Vienna University Press*. doi: 10.14220/9783737010924.

Haslmayr, D. H. (2021) *Boden im (Klima-)Wandel*.

Heiland, P. *et al.* (2020) *Policy brief. Integrating pluvial flood risk management into flood risk management plans according to the EU Floods Directive and beyond*, *Pancanaka*.

Hillel, D. (1998) *Environmental Soil Physics*.

Holden, P. A. and Fierer, N. (2005) 'Vadose Zone VADOSE ZONE | Microbial Ecology', *Encyclopedia of Soils in the Environment*, pp. 216–224.

Horton, R. E. (1932) *The role of infiltration in the hydrology cycle*, *Transactions, American Geophysical Union*.

Horton, R. E. (1945) 'Erosional development of streams and their drainage basins, hydrophysical approach to quantitive morphology', *Nihon Ringakkai Shi/Journal of the Japanese Forestry Society*, 56, pp. 275–370. doi: 10.11519/jjfs1953.37.9_417.

Hydrographischer Dienst in Österreich (2019) *Stammdatenblatt*.

Kammerer, G. (2012) 'Hydraulische Aspekte zu Gewässerschutzanlagen.', *ÖWAV Seminar Gewässerschutzanlagen für Verkehrsflächen*.

Kammerer, G. (2020) 'Bodenphysik (Vertiefung)', *Skript*, (815).

Kosugi, K. (1994) 'Three-parameter lognormal distribution model for soil water retention', *Water Resources Research*, 30(4), pp. 891–901.

Krammer, C. *et al.* (2016) 'HYDROBOD: obtaining a GIS-based hydrological soil database and a runoff coefficient calculator for Lower Austria', *Forum geografic*, XV(Suppl. 2), pp. 100–104. doi: 10.5775/fg.2016.123.s.

Land Niederösterreich (2017) *HYDROBOD 2. Dominante Abflussprozesse*. Available at: https://www.data.gv.at/katalog/dataset/hydrobod2-hydrologische-bodenkenndaten-niederosterreich-endbericht-und-rasterdaten.

Lázaro, R., Arnau, E. and Calvo-Cases, A. (2016) 'Rainfall timing and runoff: The influence of the criterion for rain event separation', *Journal of Hydrology and Hydromechanics*, 64(3), pp. 226–236. doi: 10.1515/johh-2016-0024.

Markart, G. *et al.* (2011) 'A simple Code of Practive for the Assessment of Surface Runoff Coefficients for Alpine Soil-/Vegetation Units in Torrential Rain', 2. doi: 10.13140/RG.2.1.3406.5441.

Meißl, G. *et al.* (2021) 'Brixenbach research catchment: Quantification of runoff process proportions in a small Alpine catchment depending on soil moisture states and precipitation characteristics', *Hydrological Processes*, 35(6), pp. 1–17. doi: 10.1002/hyp.14186.

Morbidelli, R. *et al.* (2018) 'Role of slope on infiltration: A review', *Journal of Hydrology*, 557, pp. 878–886. doi: 10.1016/j.jhydrol.2018.01.019.

Mu, W. *et al.* (2015) 'Effects of rainfall intensity and slope gradient on runoff and soil moisture content on different growing stages of spring maize', *Water (Switzerland)*, 7(6), pp. 2990–3008. doi: 10.3390/w7062990.

MUALEM, Y. (1976) 'A New Model for Predicting the Hydraulic Conductivity of Unsaturated Porous Media', *Water Resources Research*, 12(3), pp. 513–522.

Nassif, S. H. and Wilson, E. M. (1975) 'The influence of slope and rain intensity on runoff and infiltration', *Hydrological Sciences Bulletin*, 20(4), pp. 539–553. doi: 10.1080/02626667509491586.

Neuman, S. P., Feddes, R. and Bresler, E. (1974) 'Finite element simulation of flow in saturated-unsaturated soils considering water uptake by plants', pp. 415–417.

Österreichische Bundesrepublik (2006) *BUNDESGESETZBLATT FÜR DIE REPUBLIK ÖSTERREICH 478. Verordnung des Bundesministers für Land- und Forstwirtschaft, Umwelt und Wasserwirtschaft über die Erhebung des Wasserkreislaufes in Österreich (Wasserkreislauferhebungsverordnung – WKEV)*.

ÖWAV-Forum Klimawandel (2020) 'Klimawandelanpassung Wasserwirtschaft – Pluviales Hochwasser / Oberflächenabfluss'.

Paprotny, D. *et al.* (2021) *A probabilistic approach to estimating residential losses from different flood types*, *Natural Hazards*. Springer Netherlands. doi: 10.1007/s11069-020-04413-x.

Richards, L. A. (1931) 'Capillary conduction of liquids in porous mediums', *Physics*, 1(1907), pp. 318–333.

Romano, N. (1999) 'Water Retention and Movement in Soil', *CIGR Handbook for Agricultural Engineering, Land and Water Engineering*, (January 1999), pp. 262–284. Available at: https://elibrary.asabe.org/abstract.asp?aid=36303&t=1&redir=aid=36303&redir=[confid=cigr1999]&redirType=cigr_handbook.asp&redirType=cigr_handbook.asp.

Rosenzweig, B. R. *et al.* (2018) 'Pluvial flood risk and opportunities for resilience', *Wiley Interdisciplinary Reviews: Water*, 5(6), pp. 1–18. doi: 10.1002/wat2.1302.

Schaap, M. G., Feike, J. L. and van Genuchten, M. T. (2001) 'Rosetta: A computer program for estimating soil hydraulic parameters with hierarchical pedotransfer functions', *Journal of Hydrology*, 251, pp. 163–176. Available at: www.cals.arizona.edu/research/rosetta/download/rosetta.pdf.

Schulz, K. (2020) 'Angebot InfCapAT Modul 1+2', pp. 1–10.

Siebertz, K., Van Bebber, D. and Hochkirchen, T. (2017) *Statistische Versuchsplanung. Design of Experiments (DoE)*, *VDI-Z Integrierte Produktion*. doi: 10.3139/9783446439924.022.

Simůnek, J. *et al.* (2009) 'The HYDRUS-1D Software Package for Simulating the One-Dimensional Movement of Water, Heat, and Multiple Solutes in Variably-Saturated Media', *Environmental Sciences*, (January).

Šimůnek, J. (2015) 'Implementation of Overland Flow into HYDRUS-1D'. Available at: http://www.pc-progress.com/Downloads/Public_Lib_H1D/overland/H1D_Overland_report.pdf.

Sotier, B. *et al.* (2017) 'Hydrologische Bodenkenndaten Niederösterreich - HYDROBOD-NÖ, zweite Projektphase, Ergänzungsbericht'.

Steenhuis, T. S. *et al.* (2005) 'OVERLAND FLOW', *Encyclopedia of Soils in the Environment*, pp. 130–133. doi: 10.1007/978-90-481-3585-1_104.

Steinbrich Andreas, Leistert Hannes and Weiler Markus (2021) 'RoGer - ein bodenhydrologisches Modell für die Beantwortung einer Vielzahl hydrologischer Fragen', *Korrespondenz Wasserwirtschaft*, 14(2), pp. 94–101. doi: 10.3243/kwe2021.02.004.

Stumpp, C. (2020) 'Bodenwasser – Potentialkonzept und Wasserspannungskurve Inhalte der Vorlesung'.

Tuller, M. and Or, D. (2004) 'Water Retention and Characteristic Curve', *Encyclopedia of Soils in the Environment*, 4(January 2004), pp. 278–289. doi: 10.1016/B0-12-348530-4/00376-3.

Viessman, W. J., L.Lewis, J. G. and Knapp, J. W. (1996) 'Introduction to Hydrology', *Haper Collins College Publisher*, 4, p. 751.

Wallner, M. (2021) 'Evaluation of pedotransferfunctions for estimating soil hydraulic properties and groundwater recharge'.

Ward, H. C. *et al.* (2018) 'Impact of temporal resolution of precipitation forcing data on modelled urban-atmosphere exchanges and surface conditions', *International Journal of Climatology*, 38(2), pp. 649–662. doi: 10.1002/joc.5200.

Weather and Environmental Monitroing Directorate (2013) *MANOBS - Manual of Surface Weather Observations*. Available at: http://scholar.google.com/scholar?hl=en&btnG=Search&q=intitle:Manual+of+Surface+Weather+Observations#9.

Woolhiser, D. A., Smith, R. E. and Goodrich, D. C. (1990) 'KINEROS, a kinematic runoff and erosion

model: documentation and user manuel.', *US Department of Agriculture*.

Xue, J. and Gavin, K. (2008) 'Effect of rainfall intensity on infiltration into partly saturated slopes', *Geotechnical and Geological Engineering*, 26(2), pp. 199–209. doi: 10.1007/s10706-007-9157-0.

Yen, B. C., Te Chow, V. and Akan, A. O. (1977) 'Stormwater runoff on urban areas of steep slope', *Environmental Protection Technology Series*.

Zhang, H. *et al.* (2015) 'A surface and subsurface model for the simulation of rainfall infiltration in slopes', *IOP Conference Series: Earth and Environmental Science*, 26(1). doi: 10.1088/1755-1315/26/1/012025.

Appendix A

A.1 Profile Description

The information on different site characteristics is based on the master data collected within the project RechAUT (Hydrographischer Dienst in Österreich, 2019). Field measurement data, laboratory measurements, as well as eBOD data as additional source is placed at disposal. The pattern used to describe the soil profile for the simulation with HYDRUS-1D is as follows:

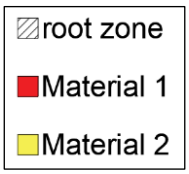

Figure 41.: Legend for the different soil profiles.

A.1.1. Lauterach

The site Lauterach (HZB-Number 394213, 414.65 m.ü.A.) is located in the Rheintal, province Vorarlberg, which also describes the related groundwater body. The double field profile is situated near the edge of the adjacent forest. The soil type is Lockersediment-Braunerde based on floating debris. It contains three horizons, namely A, Bv and BcCv, whereas all of them are summarized as one material in the simulation and are characterized as sandy loam and loamy sand throughout a depth of 80 cm, including 28 cm of root zone. The humus content of the A horizon is 4% (eBOD). The water conditions in the profile can be described as well nurtured with a moderate storage capacity and moderate permeability.

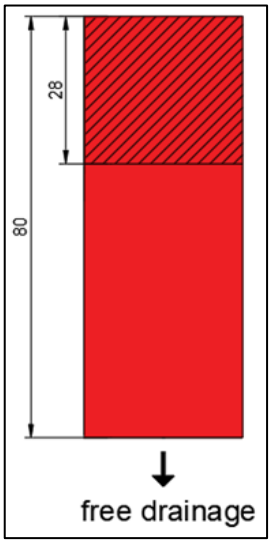

Figure 42: Soil profile of Lauterach

A.1.2. Leutasch

The village Leutasch is situated in the Northern Limestone Alps of the province Tyrol. The observed profile (HZB-Number 394023, 1150 m.ü.A.) is designed as a field profile, surrounded by Greenland and meadows. The Leutascher basin is part of the groundwater body of the Northern Limestone Alps. The soil type is Eurendsina mainly based on coarse and old gravel alluvial material. Furthermore, the natural water conditions of the soil profile are described by a moderate dryness, a moderate storage capacity and a moderate permeability. The profile is divided into three soil horizons A, AC and C. Horizons A and AC are seen as a single unit (Material 1), which stretches from a depth of 0 cm to 35 cm and consists of silt loam and loamy sand pervaded with roots to a depth of 30 cm. The C horizon (Material 2) stretches from a depth of 35cm to 150cm, which mainly consists of gravel material. The humus content of the A horizon is 9.3 %. The minimum temperature troughout the year is -20 °C in the winter months, and the maximum is 38°C in the summer months. The monthly precipitation has its highest peaks in May and August, and its minimum in December. The range of precipitation is between 130 mm/month and nearly 0 mm/month.

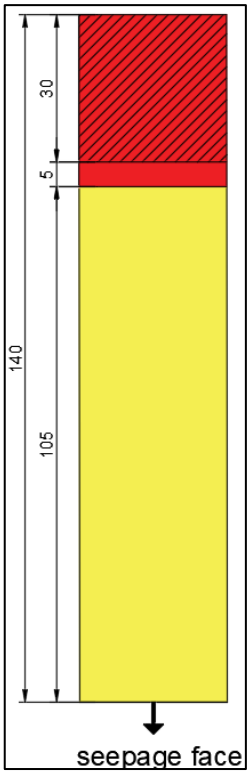

Figure 43: Soil profile of Leutasch

A.1.3. Achenkich

The profile Achenkirchen (HZB-Number 394049, 895 m.ü.A.) is situated in the province Tyrol. It is designed as a double field profile with a small Lysimeter installed. It pertains to the river basin of the Danube via the river Inn. The site is alpine, surrounded by forest. The profile is divided into two materials, material 1 stretches from 0-35 cm and material 2 from 35-140 cm. Material 1 is described as loam, material 2 as loamy sand. The root zone is 30 cm deep.

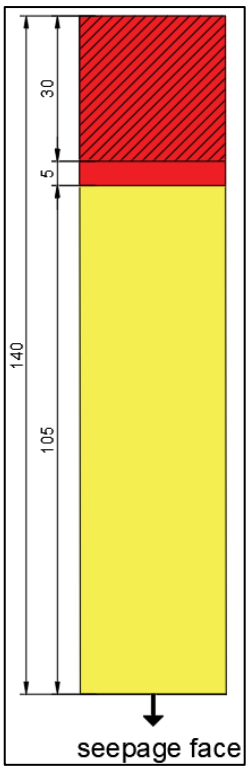

Figure 44: Soil profile of Achenkirch

A.1.4. Gschloessboden

The site Gschloessboden (HZB-Number 394478, 1737 m.ü.A.) is situated in Eastern Tyrol and is part of the 'Zentralzone Drau' groundwater body. It is located on a meadow in an alpine region. It belongs to the river basin of the Drau. The soil profile is 35 cm deep, containing one material and a root zone of 30 cm.

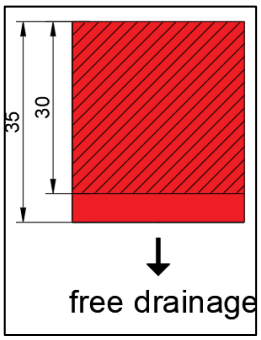

Figure 45: Soil profile of Gschloessboden

A.1.5. Sillianberger Alm

The profile Sillianberger Alm (HZB-Number 394494, 1500 m.ü.A.) is situated in Eastern Tyrol. It is again related to the river basin of Drau and the groundwater body 'Zentralzone Drau'. The profile stretches from 0-55 cm of depth, whereas 11 cm are pervaded with roots. The surrounding can be described as alpine.

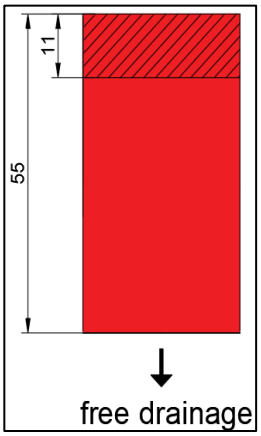

Figure 46: Soil profile of Sillianberger-Alm

A.1.6. Zettersfeld

The site Zettersfeld (HZB-Number 394098, 1990 m.ü.A.) is situated in Eastern Tyrol. It belongs to the river basin of the Drau and to the pore groundwater region of the 'Lienzer Becken'. As a double field profile, it is located in an alpine region with surrounding meadows. The profile is 60 cm deep and is described as material with a root zone of 50 cm. The humus content of the first 25 cm is 23 %.

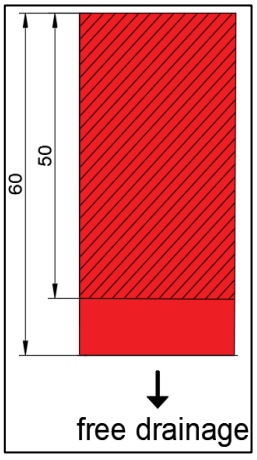

Figure 47: Soil profile of Zettersfeld

A.1.7. Elsbethen

The village Elsbethen is situated in Salzburg near the capital. The observed profile (HZB-Number 394148, 428.28 m.ü.A.) is designed as a field profile, surrounded by greenland and meadows. The profile is part of the groundwater body of 'Unteres Salzachtal'. The soil type is calcareous brown Auboden mainly based on floating debris. The natural water conditions of the soil profile are described by a well nurtured water content as a consequence of low ground water impact within the profile. The storage capacity is low, the permeability high. The profile is divided into three soil horizons A1, A2, Abv and Bvg. Horizons A 1 and A2 are seen as a single unit (Material 1), which stretches from a depth of 0 cm to 25 cm and consists of sandy silt and is pervaded with roots to a depth of 25 cm. The Abv and Bvg horizons (Material 2) stretch from a depth of 25cm to 70 cm and mainly consist of sandy silt. The humus content of the A horizon is 3.5 %. The minimum temperature throughout the year is -20 °C in winter, and the maximum is 38°C in summer. The monthly precipitation has its highest peaks in May and August, and its minimum in December. The range of precipitation is between 130 mm/month and nearly 0 mm/month.

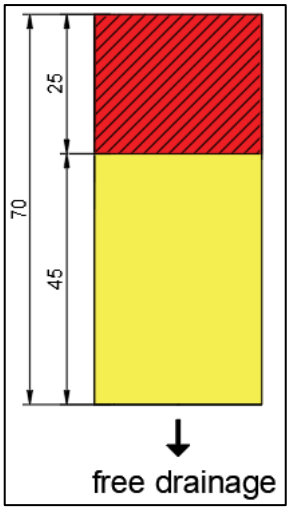

Figure 48: Soil profile of Elsbethen

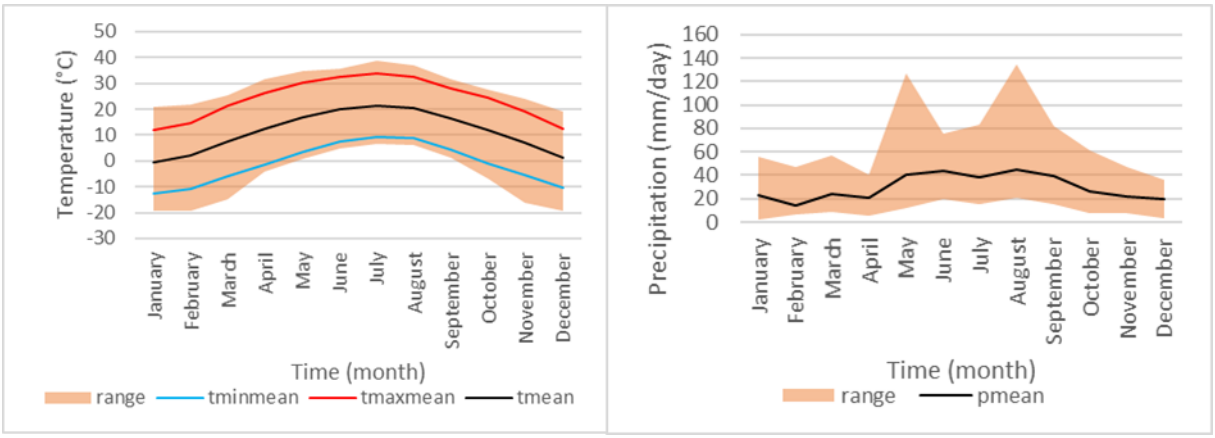

Figure 49.: Monthly temperature and precipitation for the years 1996 until 2018 for Elsebthen

A.1.8. Gumpenstein

The site Gumpenstein (HZB-Number 39421, 690 m.ü.A.) is situated in Liezen in the province of Styria. The profile is surrounded by arable land and a Lysimeter is installed. The groundwater body belongs to the group of 'Niedere Tauern', as well as to the 'Grauwackenzone'. The soil type is Braunerde. The profile is divided into A1, A2 and B horizons, however, they are all summarized as material 1. The profile is 150 cm deep, and the root zone stretches from 0 cm to 20 cm. The material can be described as sandy/loamy silt. The humus content at within the A1 horizon is 6%.

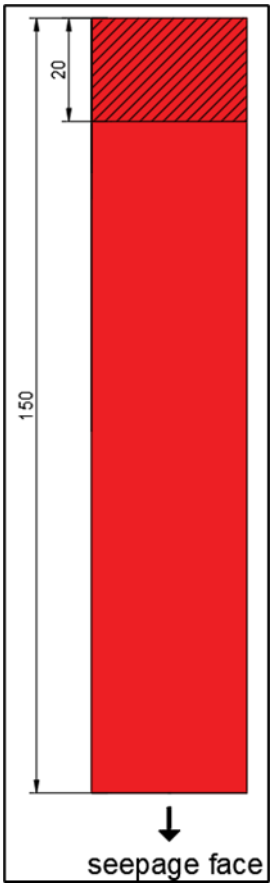

Figure 50: Soil profile of Gumpenstein

A.1.9. Aichfeld-Murboden

The site Aichfeld-Murboden (HZB-Number 394064, 668.5 m.ü.A.) is situated in the district Murtal in the province of Styria. The measurement station is a field profile surrounded by greenland and meadow within the river basin of Mur. The soil type is Lockersediment-Braunerde. The soil is divided into an Ap, AB and B horizon. Ap builds the foundation for material 1 and AB and B for material 2. Material one stretches from 0cm to 35 cm including the root zone. It is described as sandy loam. Material 2 is from 35 cm until 100 cm and consists again of sandy loam. The humus content of Ap is 3.1 %. The water content is nurtured, the profile exhibits a moderate storage capacity and a moderate permeability. The temperature shows the maximum in July with 35°C and the minimum in January with -25°C. The precipitation shows a unimodal curve, with its maximum in June (71 mm/month) and its minimum in January and December.

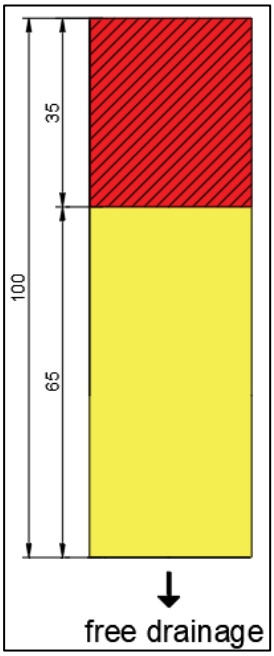

Figure 51: Soil profile of Aichfeld-Murboden

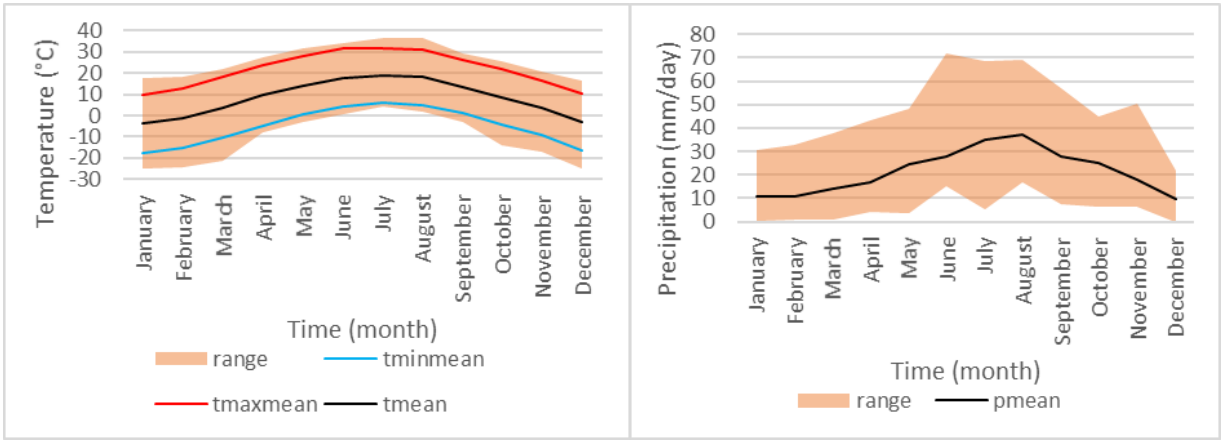

Figure 52: Monthly temperature and precipitation for the years 1996 until 2018 for Aichfeld-Murboden

A.1.10. Kalsdorf

The measurement station of Kalsdorf (HZB-Number 394072, 320 m.ü.A) is located in Styria near the capital Graz. Therefore, the groundwater body belongs to the 'Grazer Feld'. It is built as a double field profile in a greenland and meadow environment. The soil type can be described as Lockersediment-Braunerde and the horizons are divided into Ap, ABv and D. Ap is summarized in material 1, from a depth of 0 cm until 30 cm. 10 cm are pervaded with roots. ABv and D are described by material 2. Ap and ABv are described as loamy sand. The soil is rather dry with a high permeability and a low storage capacity.

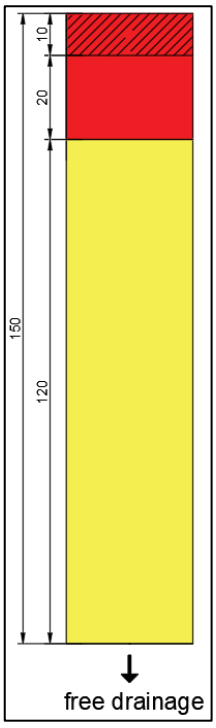

Figure 53: Soil profile of Kalsdorf

A.1.11. Pettenbach

The site Pettenbach (HZB-Number 394395, 465 m.ü.A.) is situated in Upper Austria and belongs to the river basin Traun. The profile is designed as a field profile combined with a Normlysimeter. The site is embedded in arable land and consists of Parabraunerde. The related groundwater body is 'Traun-Enns-Platte'. The soil horizons are divided into Ap, AB, B and Bg. Material one describes horizon Ap with a humus content of 2.5 % and consists of silt. Material 2 summarizes the other horizons, consisting of loamy silt. The water content is well nurtured, and the soil is characterized by a high storage capacity and a moderate permeability.

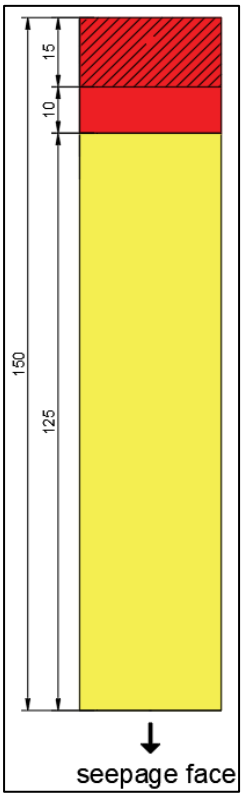

Figure 54: Soil Profile of Pettenbach

A.1.12. Schalladorf

The measurement station Schalladorf (HZB-Number 394015, 238 m.ü.A.) is situated in Hollabrunn, Lower Austria. It is a field profile surrounded by arable land. The related groundwater body is 'Gruppe Weinviertel'. The soil can be described as calcareous Feuchtschwarzerde and is divided into A1p, A2, ACg, C1g and C2g horizons. A1p is material 1 and stretches from 0 cm to 40 cm. The first 10 cm are pervaded by roots. It can be described as loam with 2.1 % of humus. The other horizons are summarized in material 2, stretching from 40 cm to 150 cm. It starts with loamy clay, over loam and finally with sandy silt. The profile is well nurtured with water, shows a high storage capacity and a moderate permeability.

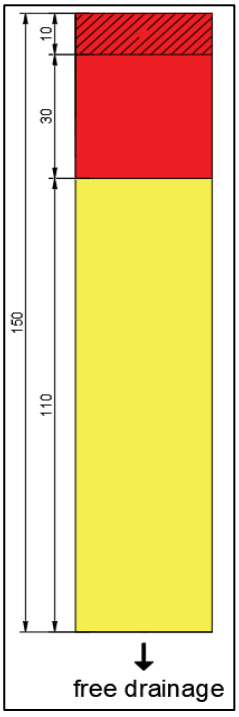

Figure 55: Soil profile of Schalladorf

A.1.13. Frauenkirchen

The profile and municipality Frauenkrichen (EZB-Number 394411, 124 m.ü.A.) is situated in Burgenland, near 'Neusiedlersee'. The measurement station is a field profile with a Lysimeter installed. It is surrounded by greenland and meadows. It belongs to the groundwater body 'Seewinkel'. The soil can be described as Chernozem. The profile is divided into four different horizons, namely A1rig, A2, AC and C, which are all combined in material 1. The depth of the profile is 145 cm and the root zone 60 cm. The humus content is 2.2 % in the upper layer. The soil is sandy loam to loamy sand. The profile can be described as dry, with a high permeability and a low storage capacity.

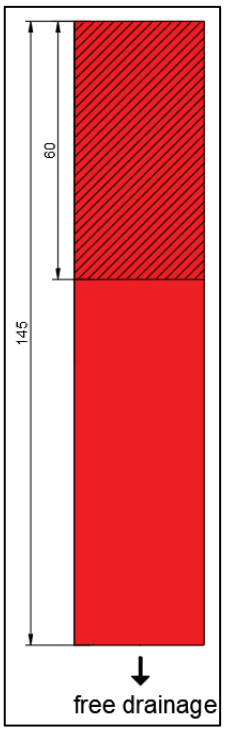

Figure 56: Soil profile of Frauenkirchen

A.2 Field Measurement Data

Table 6.: Summary of the soil horizons for the measurement stations from eBOD

Nr.	Name	Soil Type	Soil Horizon	Sand	Silt	Clay	Bulk Densitiy (g/cm³)	Humus content (%)
1	**Lauterach (Nord)**	Lockersediment-Braunerde						
	0-20		A	41	48	11	1.27	4.0
	20-65		Bv	41	43	16	1.54	0.9
	65-80		BvCv	40	35	25	1.60	0.5
2	**Leutasch**	Eurendsina						
	0-35		A	24	58	18	1.03	9.3
			AC	35	51	14	1.10	7.3
7	**Elsbethen**	Auboden						
	0-25		A1	30	63	7	1.08	8.0
			A2	36	59	5	1.23	4.6
	25-70		Abv	26	70	4	1.48	1.3
			Bvg	27	67	6	1.45	1.6
8	**Gumpenstein (Lys2)**	Braunerde						
	0-150		A1	38	53	9	1.16	6
			A2	26	63	11	1.42	2
			B	10	77	13	1.58	1
9	**Aichfeld-Murboden**	Braunerde						
	0-35		Ap	28	56	16	1.29	4
	35-100		AB	29	49	22	1.42	1.9
			B	32	45	23	1.48	1.3
10	**Kalsdorf (Grünland)**	Braunerde						
	0-30		Ap	49	42	9	1.44	2
			ABv	51	38	11	1.33	3
11	**Pettenbach (2014, Mai**	Parabraunerde						
	0-25		Ap	11	75	14	1.35	3
	25-150		AB	12	69	19	1.60	0.5
			B	11	67	22	1.64	0.3
			Bg	12	64	24	1.67	0.2
12	**Schalladorf**	Feuchtscharzerde						
	0-40		A1p	19	42	39	1.36	3
			A2	15	44	41	1.40	2
	40-150		ACg	20	42	38	1.54	0.9
			C1g	22	43	35	1.71	0.1
14	**Frauenkirchen Frei**	Tschernosem						
	0-145		A1rig	53	33	14	1.40	2
			A2	52	33	15	1.41	2
			AC	61	28	11	1.58	1
			C	64	27	9	1.60	1

A.3 Laboratory Measurement Data

Table 7.: Summary of the laboratory measurement data for the stations, including the particle size distribution

Nr.	Name	Sand	Silt	Clay	Soil Texture	Bulk Densitiy (g/cm³)	Humus content (%)
1	**Lauterach (Nord)**						
	0-20	34	45	21	sL	1.31	3.3
	20-40	31	46	23	sL	1.33	3.0
	40-80	61	25	14	lS	1.44	1.7
2	**Leutasch**						
	0-20	32	27	41	lT	0.70	31.0
3	**Achenkirch**						
	0-15	17	50	33	L	0.49	21
	15-70	44	48	8	lS		1.4
7	**Elsbethen**						
	0-25	28	64	8	sU	1.20	3.5
	25-40	53	45	2	uS	1.30	1.0
	40-55	50	49	1	uS	1.29	0.7
	55-180	48	51	1	sU	1.71	0
9	**Aichfeld-Murboden**						
	0-35	42	39	19	sL	1.45	3
	35-75	45	38	17	sL	1.53	1.2
	75-100	67	25	8	lS	1.58	1
10	**Kalsdorf (Grünland)**						
	15-30	59	28	13	lS	1.31	3.3
	30-80	87	13	0	S	1.62	0.4
	80-110	88	11	0	S	1.71	0.1
	110-200	88	12	0	S	1.71	0
11	**Pettenbach (2014, Mais)**						
	0-30	15	62	23	lU	1.37	2.5
	30-75	14	64	22	lU	1.58	1
	75-110	21	55	24	sL/lU	1.62	0.4
	110-150	24	52	24	sL	1.62	0.4
12	**Schalladorf**						
	0-50	34	35	31	L	1.49	2.1
	50-70	61	22	17	sL	1.51	1
	70-170	27	41	32	L	1.64	0
14	**Frauenkirchen Frei**						
	0-40	44	38	18	sL	1.58	2.2
	40-70	43	42	15	lS/sL	1.60	2
	70-140	56	31	13	lS	1.60	1
	140-170	81	19	0	lS	1.71	0

A.4 Inverse Calibrated VGM Parameters

Table 8.: Summary of the results from the inverse calibration within the PhD. thesis of Marleen Ambrosiu Schübl showing the Van Genuchten and Mualem parameters

Nr.	Name	Depth	θ_r (-)	θ_s (-)	α (1/cm)	n (-)	K_s (cm/day)
1	Lauterach (Nord)	0-80	0.069	0.414	0.235	1.181	50.32
2	Leutasch	0-35	0.057	0.337	0.005	1.948	23.47
		35-140	0.088	0.134	0.764	1.497	310.03
3	Achenkirch	0-15	0.092	0.562	0.014	1.734	21.06
		15-70	0.096	0.146	0.197	3.246	360.18
4	Gschlössboden	0-35	0.029	0.217	0.001	1.867	3012.48
5	Sillianberger Alm	0-55	0.018	0.474	0.336	1.063	424.83
6	Zettersfeld	0-60	0.053	0.428	0.043	1.166	61.05
7	Elsbethen	0-25	0.070	0.442	0.004	1.224	20.21
		25-70	0.040	0.389	0.004	1.550	0.28
8	Gumpenstein (Lys2)	0-150	0.102	0.337	0.012	1.321	13.93
9	Aichfeld-Murboden	0-35	0.063	0.385	0.003	1.186	3.07
		35-100	0.079	0.263	0.013	1.719	43.93
10	Kalsdorf (Grünland)	0-30	0.032	0.299	0.008	1.308	2.20
		30-150	0.077	0.349	0.028	4.236	1454.02
11	Pettenbach (2014, Mais)	0-25	0.067	0.409	0.006	1.899	37.96
		25-150	0.095	0.396	0.009	1.152	17.68
12	Schalladorf	0-40	0.094	0.462	0.009	1.588	2.20
		40-150	0.115	0.426	0.010	1.164	2.80
14	Frauenkirchen Frei	0-145	0.069	0.337	0.020	1.218	11.70

Appendix B

Appendix for functional analysis results, conducted with HYDRUS-1D and evaluated with excel and correlation analysis.

B.1 Elsbethen

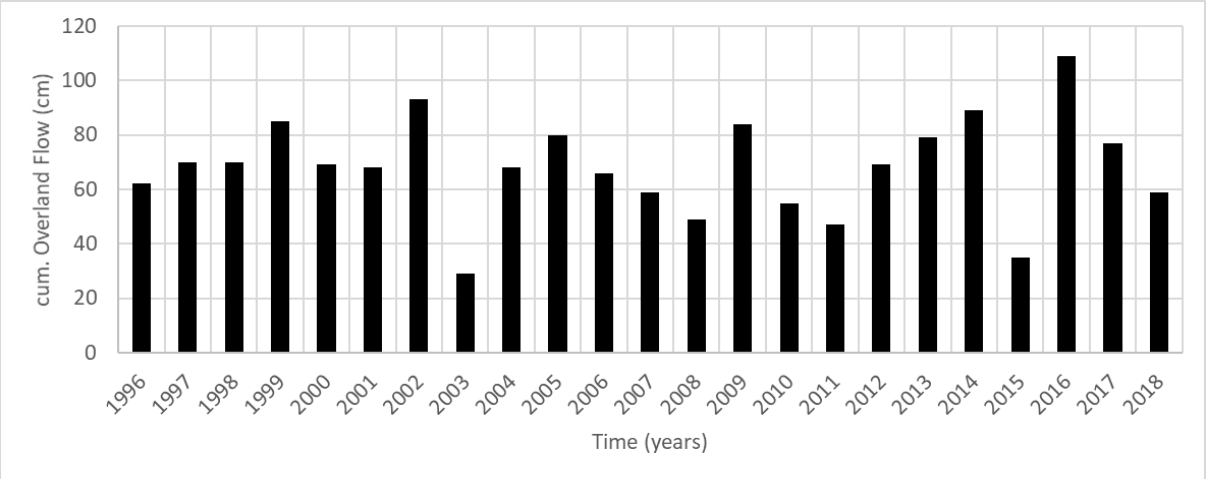

Figure 57: Annual cumulated overland flow at the station Elsbethen

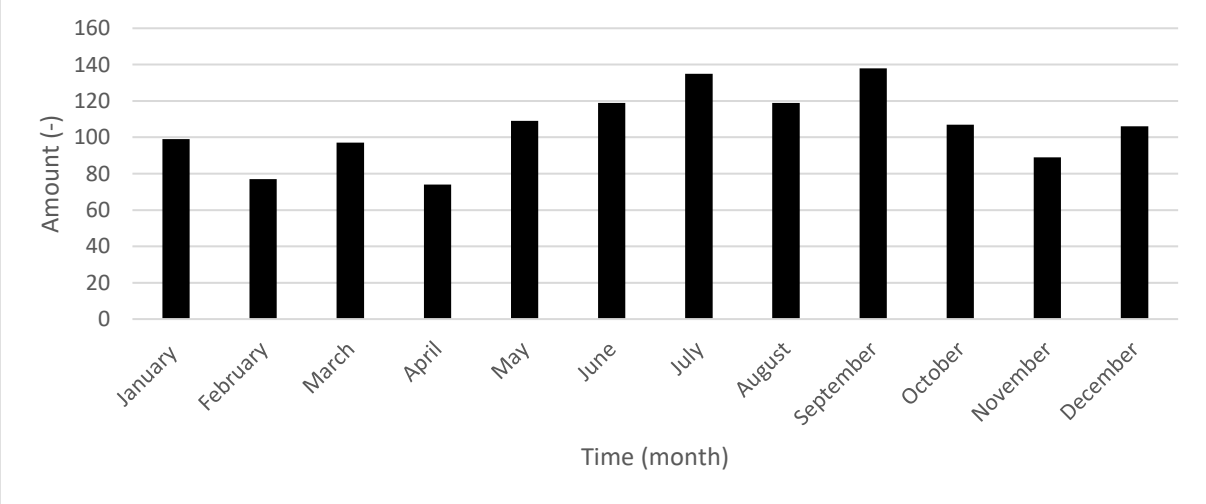

Figure 58: Monthly cumulated overland flow for the station Elsbethen

B.1.1 Input Precipitation Events

Table 9: Top 10 precipitation events generated with python with a MIT of 12 hrs and a minimum volume of 4 cm for Elsbethen

		Daily Resolution			One-Minute Resolution		
Nr.	Precipitation Event	Precipitation (cm)	Rain Intensity (mm/min)	Overland Flow (cm)	Precipitation (cm)	Rain Intensity (mm/min)	Overland Flow (cm)
1	05.07.1997	8.27	0.057	7.58	9.25	0.048	7.64
2	06.08.2002	13.50	0.094	12.87	15.83	0.054	14.185
3	11.08.2002	8.77	0.061	8.44	10.89	0.039	9.66
4	03.06.2004	7.60	0.053	7.27	12.27	0.032	10.2
5	15.08.2005	7.49	0.052	7.08	15.52	0.035	14.66
6	18.09.2006	8.19	0.057	7.33	10.59	0.036	10.09
7	23.06.2009	7.32	0.051	7.00	14.73	0.034	11.68
8	02.06.2010	7.46	0.052	7.14	7.82	0.029	5.69
9	01.06.2013	12.74	0.088	12.40	22.41	0.035	19.45
10	03.08.2014	8.07	0.056	7.57	8.1	0.113	7.43

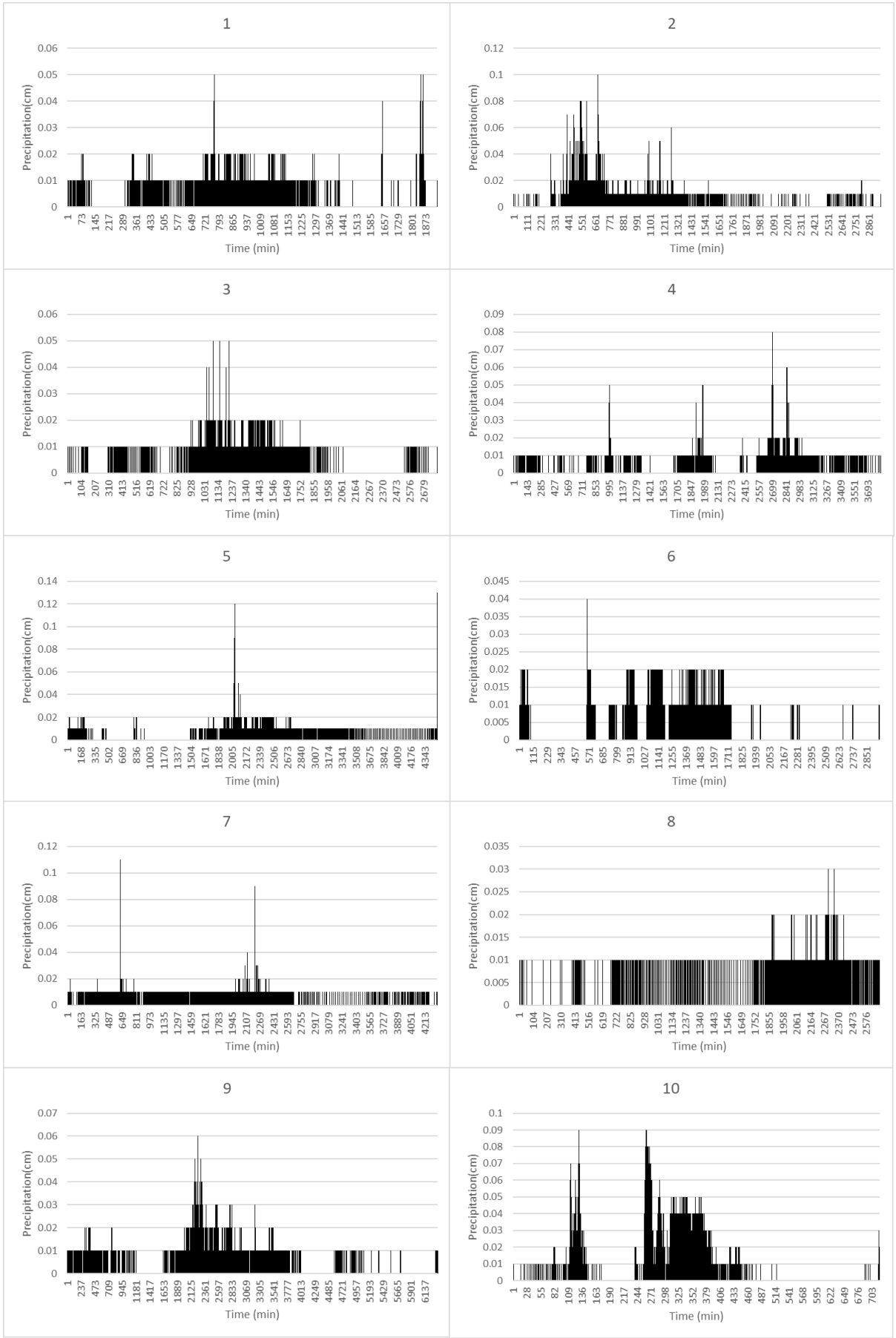

Figure 59: Hydrographs for each of the 10 precipitation events as input variables for the sensitivity analysis for Elsbethen

B.1.2 Sensitivity Analysis Data

Table 10.: Initial water content for the selected conditions in Elsbethen

condition	Material 1 θ (-)	Material 2 θ (-)
saturated	0.442	0.388
wet	0.435	0.385
median	0.426	0.375
moderate	0.415	0.355
dry	0.250	0.203
very dry	0.164	0.154

Rain Intensity

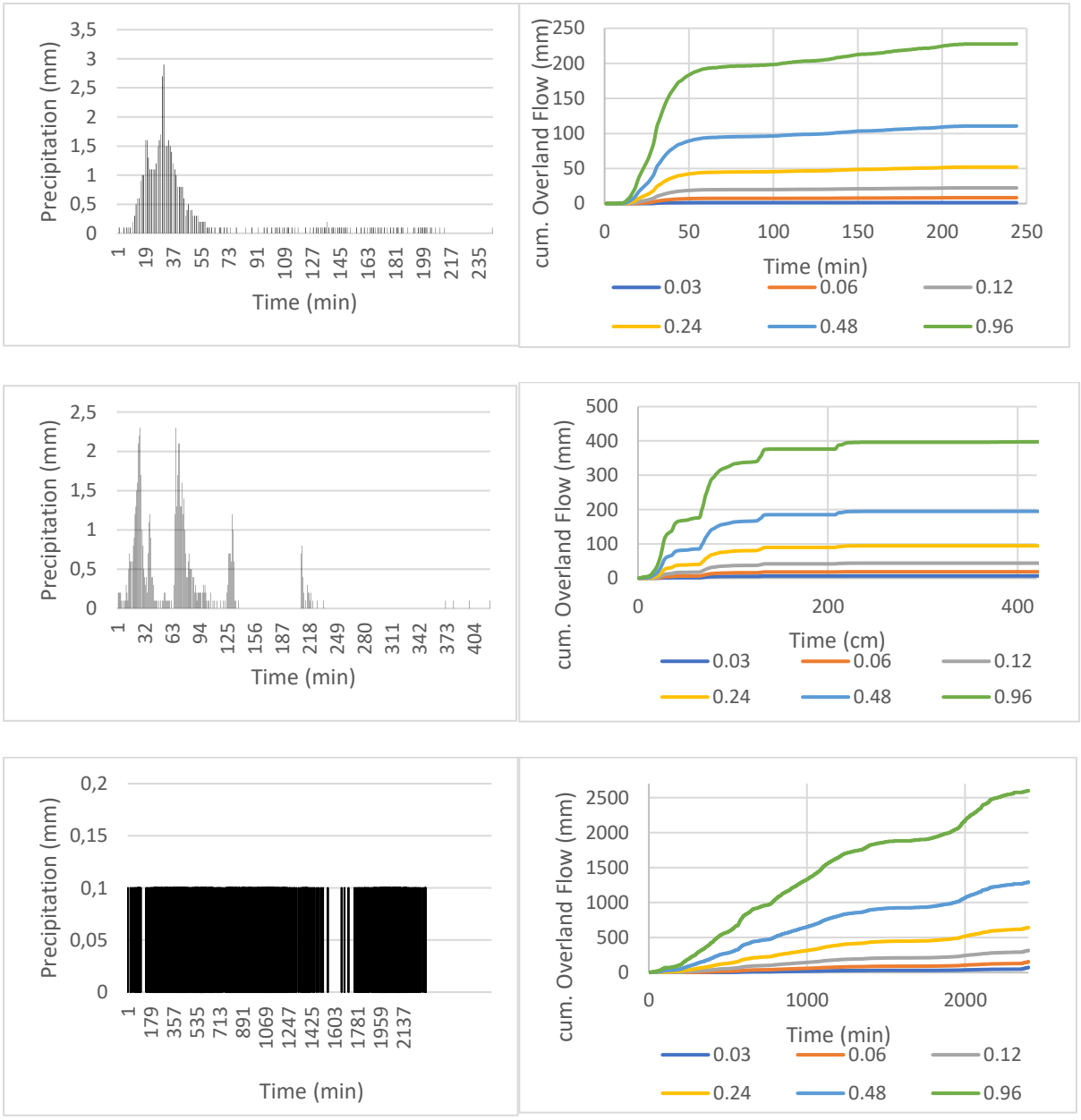

Figure 60: On the left the 3 events as input function for the R_i analysis. From the top: a uniform Hyetograph, a multi-peak Hyetograph, and an even Hyetograph. At the right: cumulated overland flow generated from the Hyetograph on the left when upscaling the R_i

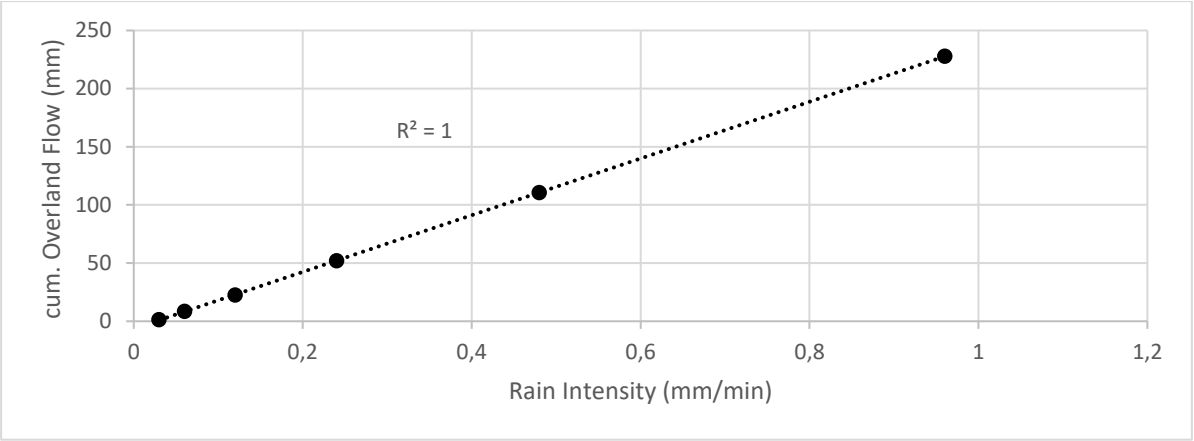

Figure 61: Correlation analysis for cumulated overland flow and Ri. Valid for all three different Hyetographs

B.1.3 Overland Flow detailed

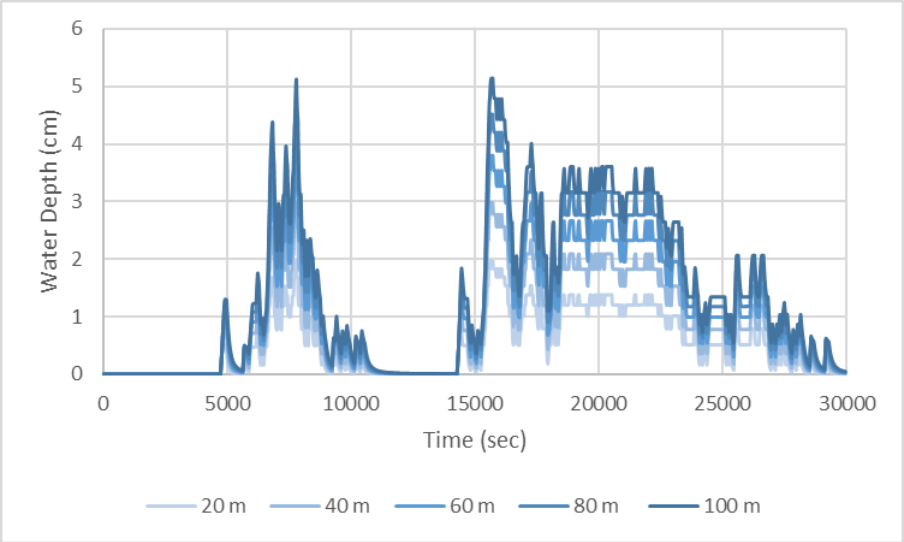

Figure 62: Overland flow for the event of the 03.08.2014 at a slope of 14° at the site of Elsbethen

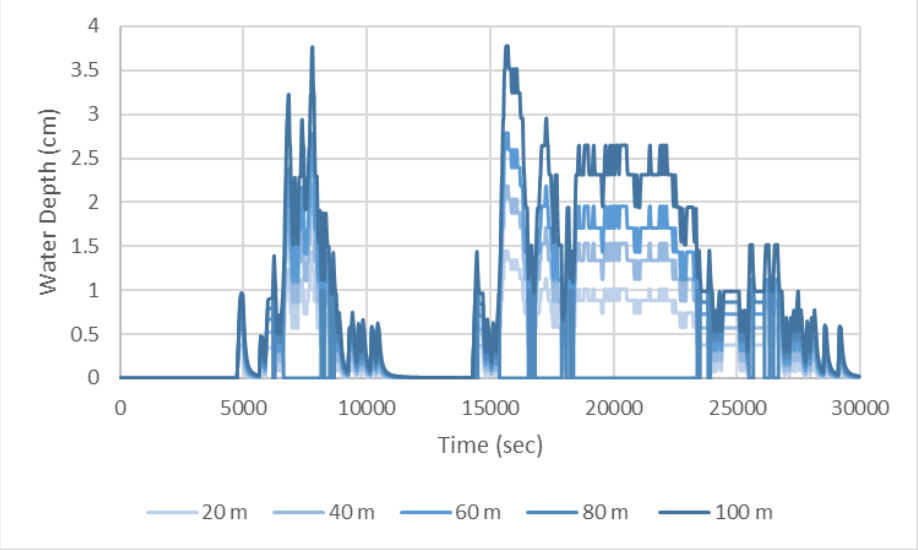

Figure 63: Overland flow for the event of the 03.08.2014 at a slope of 35° at the site of Elsbethen

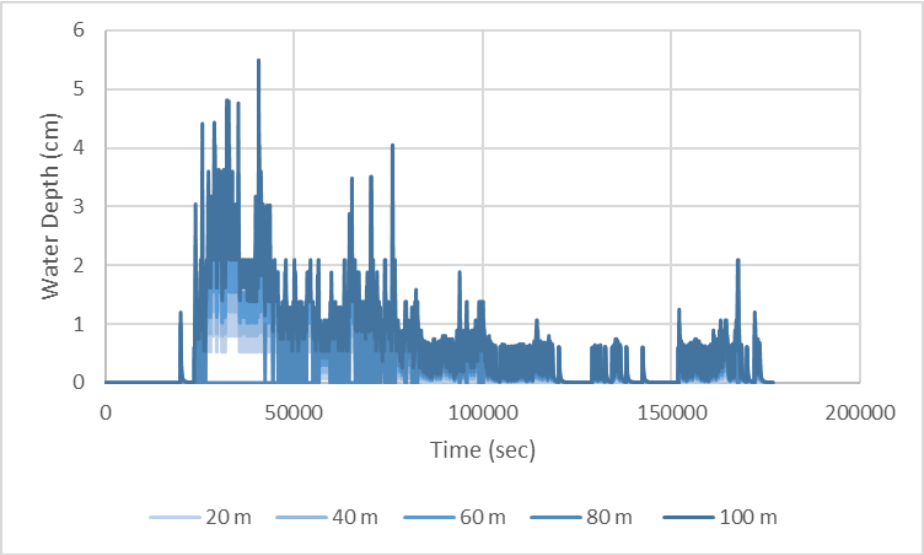

Figure 64: Overland flow for the event of the 06.08.2002 at a slope of 14° at the site of Elsbethen

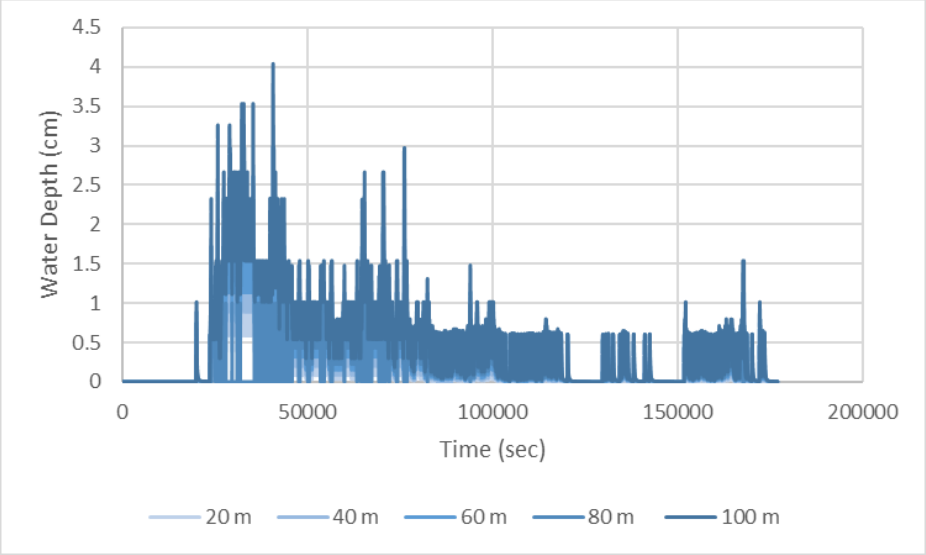

Figure 65: Overland flow for the event of the 06.08.2002 at a slope of 35° at the site of Elsbethen

B.2 Aichfeld-Murboden

B.2.1 Generated Overland Flow

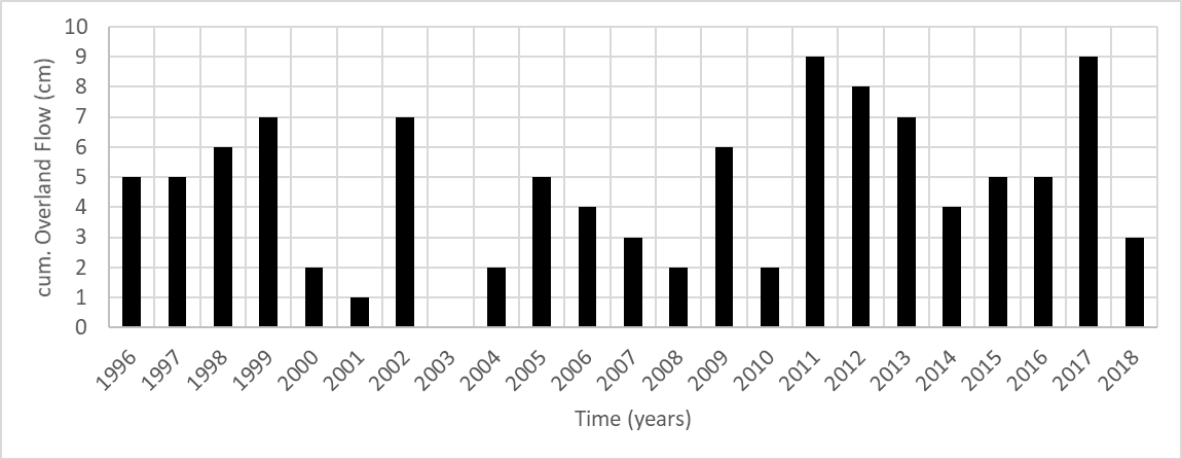

Figure 66: Annual cumulated overland flow at the station Aichfeld-Murboden

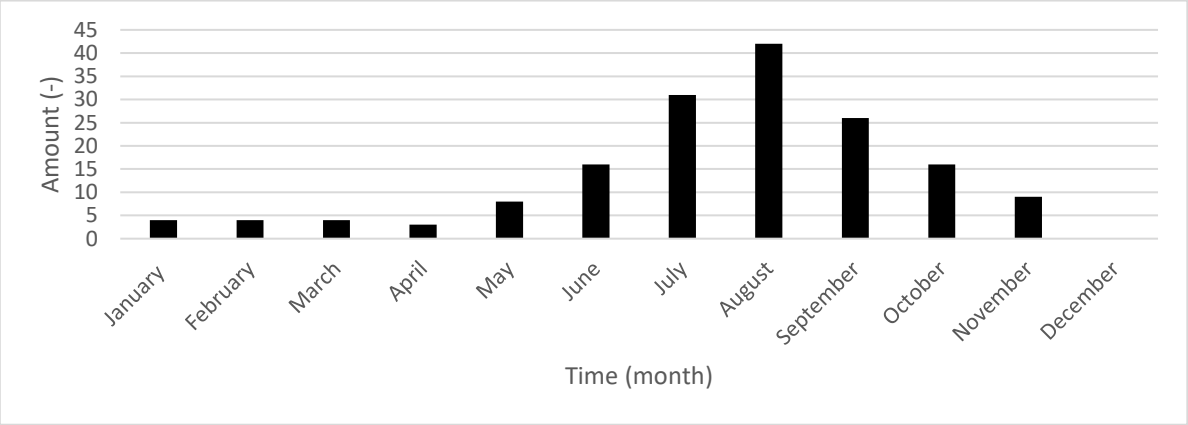

Figure 67: Monthly cumulated overland flow at the station Aichfeld-Murboden

B.2.2 Input Precipitation Events

Table 11: Top 10 precipitation events generated with python with a MIT of 12 hrs and a minimum volume of 2 cm for Aichfeld-Murboden.

		Daily Resolution			One-Minute Resolution		
Nr.	Precipitation Event	Precipitation (cm)	Rain Intensity (mm/min)	Overland Flow (cm)	Precipitation (cm)	Rain Intensity (mm/min)	Overland Flow (cm)
1	14.11.1996	4.45	0.031	2.53	4.51	0.028	2.26
2	04.08.1998	5.06	0.035	3.88	6.94	0.092	5.71
3	22.07.1999	4.56	0.032	3.33	9.79	0.053	8.09
4	15.07.2002	6.86	0.048	3.76	7.11	0.068	5.86
5	04.09.2009	5.73	0.040	2.81	5.86	0.039	4.04
6	18.06.2011	7.18	0.050	4.15	7.22	0.087	5.60
7	12.09.2012	5.56	0.039	2.37	5.56	0.062	3.35
8	31.08.2014	5.13	0.036	2.28	5.48	0.040	4.30
9	08.07.2015	2.89	0.020	2.36	4.77	0.087	1.95
10	24.07.2017	6.30	0.044	4.30	8.59	0.056	6.63

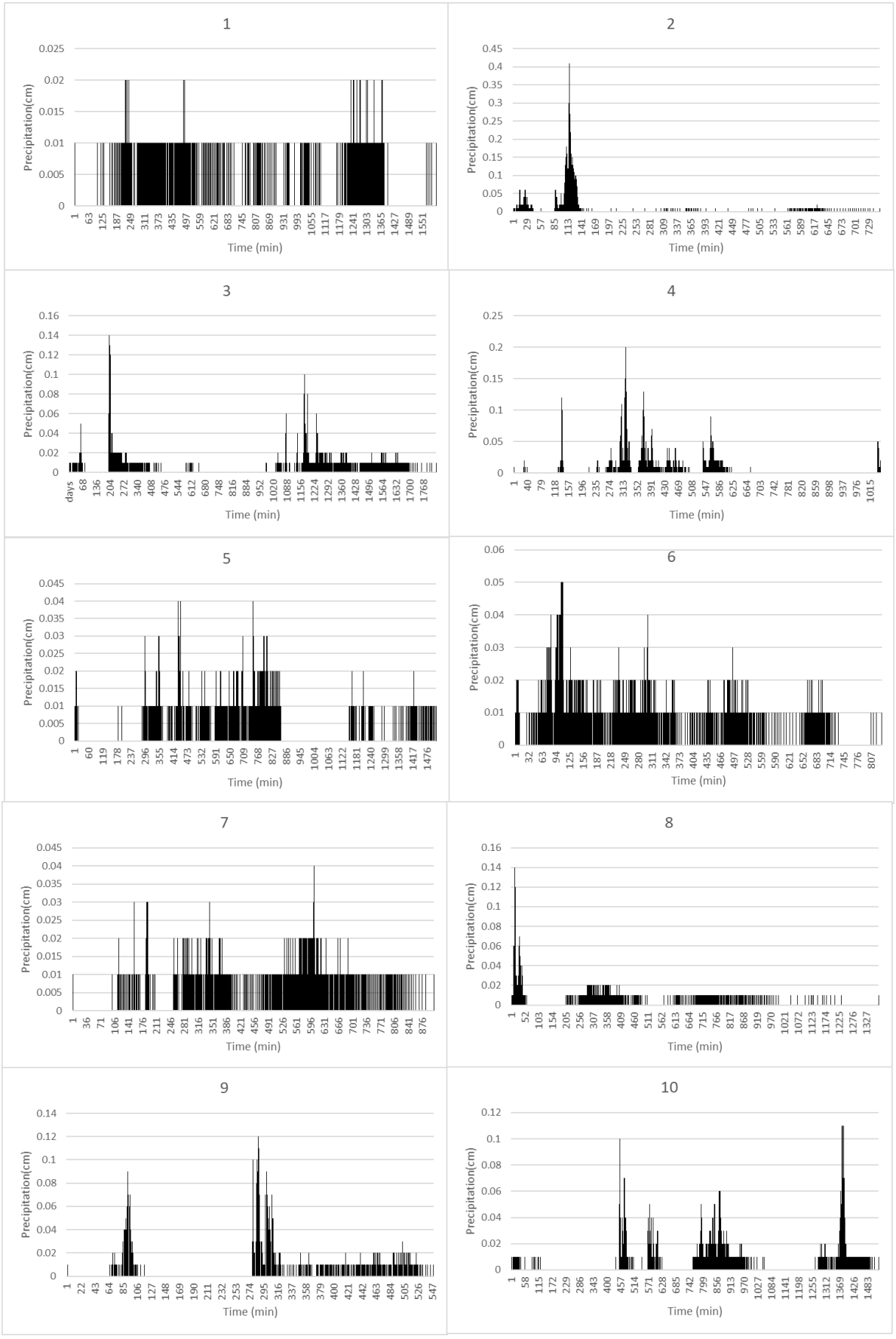

Figure 68: Hydrographs for each of the 10 precipitation events as input variables for the sensitivity analysis for Aichfeld-Murboden.

B.2.3 Sensitivity Analysis Data

Table 12.: Initial water content for the selected conditions in Aichfeld-Murboden.

condition	Material 1 θ (-)	Material 2 θ (-)
saturated	0.385	0.263
wet	0.353	0.155
median	0.341	0.141
moderat	0.316	0.122
dry	0.237	0.094
very dry	0.142	0.081

Rain Intensity

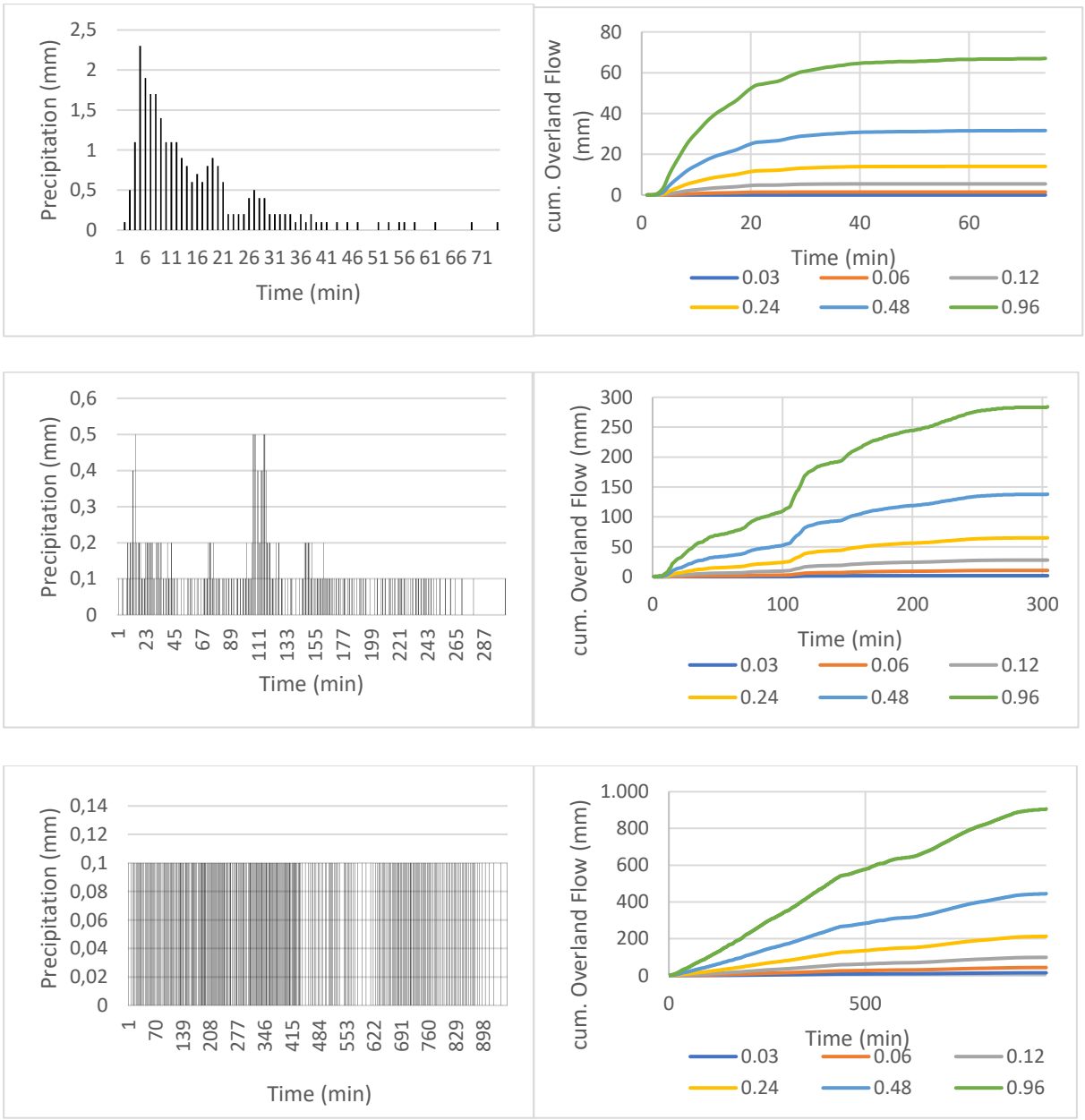

Figure 69: On the left the 3 events as input function for the R_i analysis. From the top: a uniform Hyetograph, a multi-peak Hyetograph, and an even Hyetograph. At the right: cumulated overland flow generated from the Hyetograph on the left when upscaling the R_i

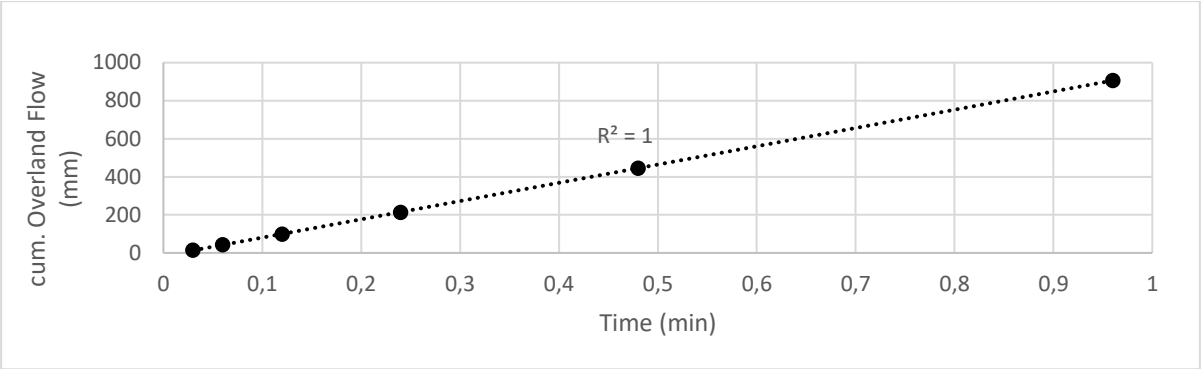

Figure 70: Correlation analysis for cumulated overland flow and Ri. Valid for all three different Hyetographs

B.2.4 Overland Flow detailed

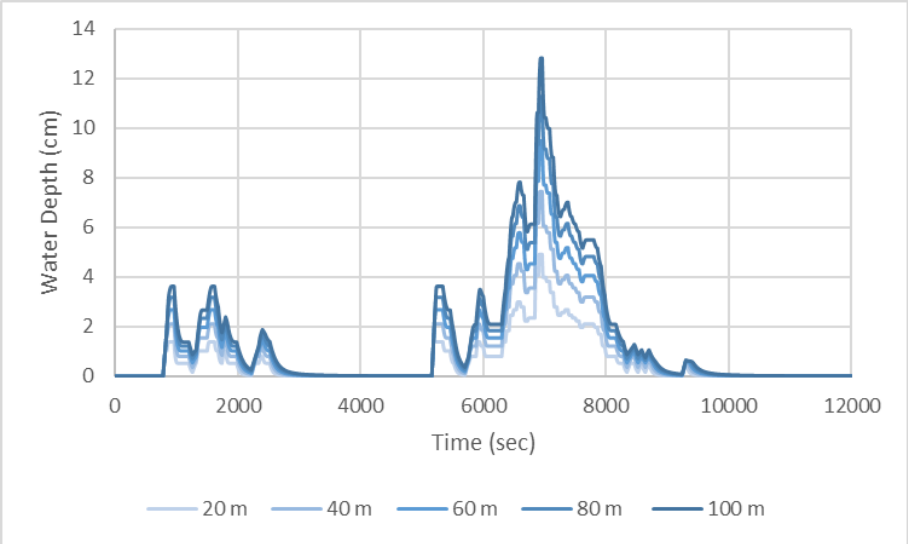

Figure 71: Overland flow for the event of the 04.08.1998 at a slope of 14° at the site of Aichfeld-Murboden

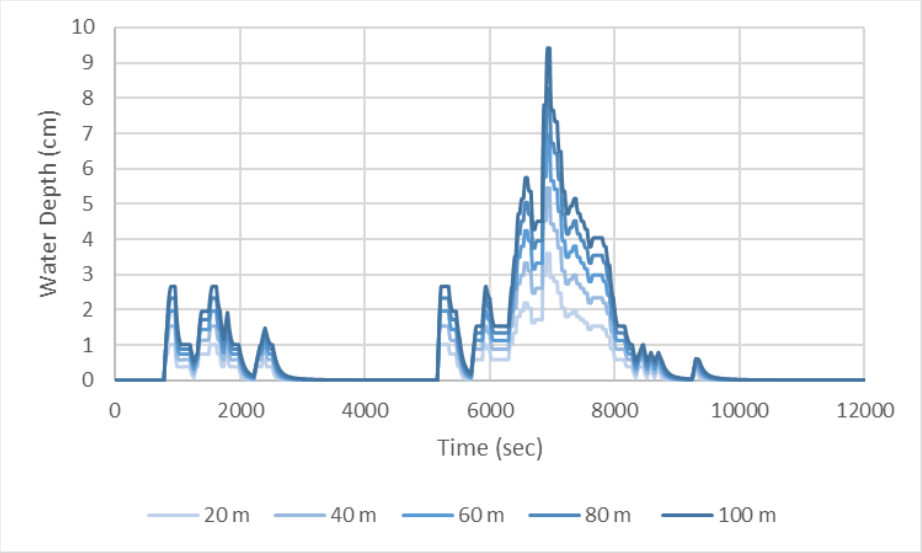

Figure 72: Overland flow for the event of the 04.08.1998 at a slope of 35° at the site of Aichfeld-Murboden

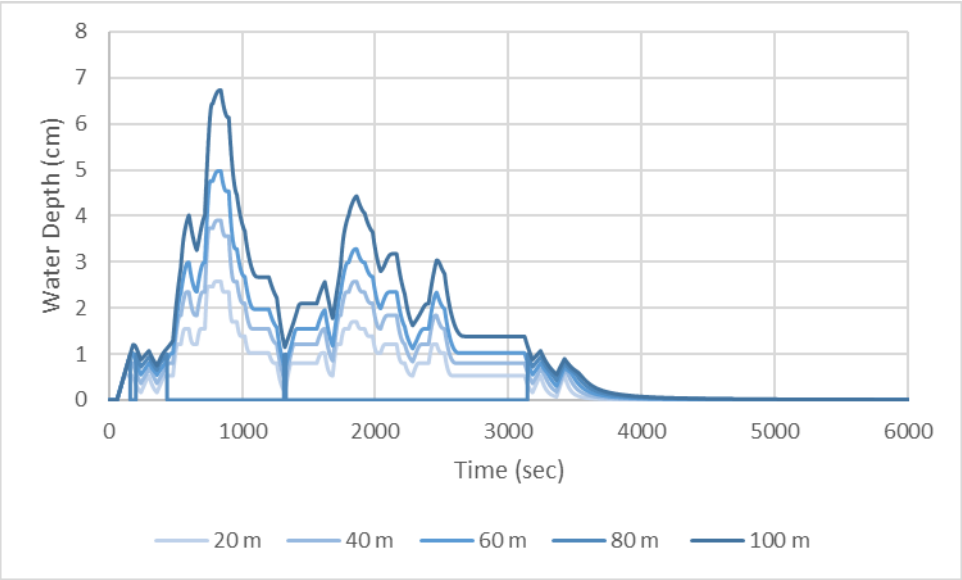

Figure 73: Overland flow for the event of the 31.08.2014 at a slope of 14° at the site of Aichfeld-Murboden

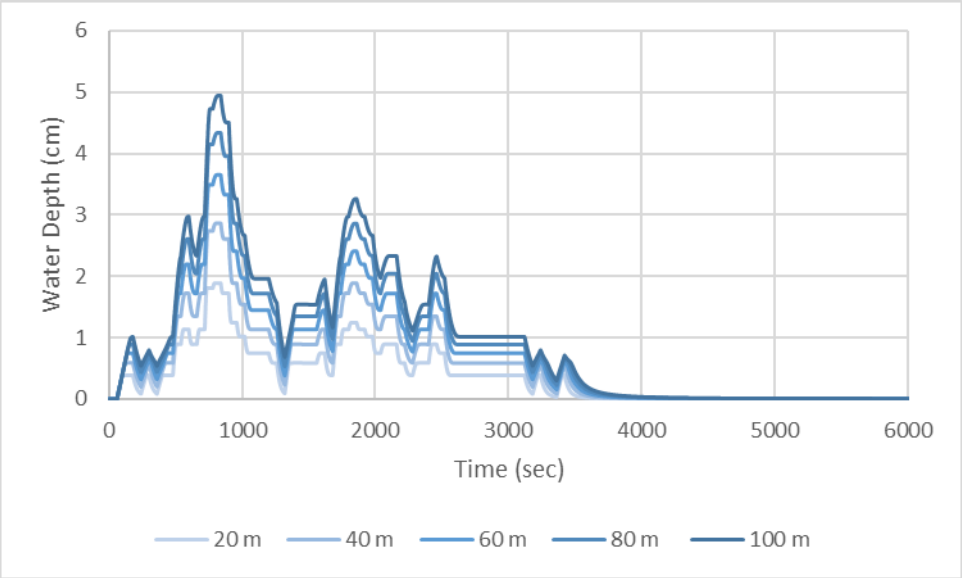

Figure 74.: Overland flow for the event of the 31.08.2014 at a slope of 35° at the site of Aichfeld-Murboden